Erik Kostson

Fatigue Crack Monitoring in Multi-Layered Aircraft Structures using Guided Ultrasonic Waves

Submitted in fulfilment

of the requirements for the degree of

Doctor of Philosophy

in the subject of

Mechanical Engineering

at University College London

I, Erik Kostson, confirm that the work presented in this thesis is my own. Where information has been derived from other sources, I confirm that this has been indicated in the thesis.

Name: .....

Date: .....

Abstract

The detection of fatigue cracks at fasteners in the sub layers of multi-layered aircraft structures can be problematic using conventional nondestructive testing methods. In this thesis the sensitivity of low frequency guided ultrasonic waves to detect these defects is studied. Guided ultrasonic waves typically have energy distributed through the thickness of such structures and allow for defect detection in all sub-layers, but have wavelengths larger than commonly used in bulk wave ultrasonic testing.

The model aerospace multi-layered structure investigated consists of two aluminium plate strips adhesively bonded using a paste adhesive with a fastener hole. Guided waves were excited by placing piezoelectric (PZT) transducers on the surface of the structure. Experimentally the wave propagation and scattering was measured using a laser interferometer. The wave propagation was studied numerically using Semi-Analytical Finite-Element (SAFE) calculations and 3D Finite Element (FE) simulations.

Thickness and width mode shapes of the guided waves were identified from the SAFE simulations. By placing PZT discs across the width of the structure the excited flexural wave modes could be controlled to an extent. The thickness mode shapes of these waves are similar to those in a large multi-layered plate structure. 3D FE simulations predict a similar amplitude change due to a defect in these structures. Fatigue crack growth monitoring on tensile specimens was realized, measuring the amplitude at a single point. The measured changes in the amplitude of the ultrasonic signal due to a defect agree well with 3D FE simulations.

These investigations found that using low frequency guided ultrasonic waves defects through the thickness of a hidden sub layer can be detected from measurements on the undamaged, accessible layer.

Acknowledgements

I would like to thank the people whose efforts made this study possible:

First of all, my parents Konstantinos and Maria Anestiou for all of their sacrifices, my brother Georgios Anestiou for inspiring and motivating me throughout the course of this work and my wife for her patience, support and understanding.

Paul Fromme, my supervisor, for his excellent supervision, for providing me with an excellent research environment and for his revision of this work.

The Engineering and Physical Sciences Research Council (EPSRC) and the industrial sponsor AIRBUS UK, for the financial support.

Nader Saffari, my second supervisor, for the many interesting discussions and his valuable comments on the transfer thesis.

Chee (Kostas) Tam, the LaTeX and Adobe® guru and my best man, who helped in putting this thesis together. Colleagues whom I would like to thank for their friendship are, Sergey Martynov, Alexandra McCredie, Rochana Propainop, Emad Ghandourah, Bernard Masserey and Andrea Sanfilippo.

Contents

List of Figures

List of symbols

Symbol and acronym	Description
α	Shortest distance between nodes
c_p	Phase velocity
c_g	Group velocity
δ	Skin depth
$\Delta\psi$	Phase difference
Δt	Time of flight
ΔT	Time step
ϵ	Electrical permeability
E	Modulus of elasticity
f	Frequency
h	Plate thickness
k	Wavenumber
K_t	Stress concentration factor
λ	Wavelength
Λ	Beatlength
L	Element side
L_{notch}	Notch length
μ	Magnetic permeability
N	Number of point forces
ν	Poisson's ratio
r_o	Hole radius
r	Radius
R	Stress ratio
ρ	Density
σ	Electrical conductivity
SD	Standard deviation
ϕ	Angle
x, y, z	Cartesian coordinates
Δx	Distance between two points along the x-coordinate
ω	Angular frequency

Chapter 1

Introduction

Aircraft structures are subject to various types of loading conditions, mainly during take-off, landing, and manoeuvring. Such operating conditions can lead to the development of fatigue cracks in the aircraft structure. Due to the stress concentration fatigue cracks often initiate at the fasteners connecting multiple metallic layers. Because of their ability to propagate over long distances, guided waves offer an efficient way for the Non-Destructive Evaluation (NDE) and Structural Health Monitoring (SHM) of large areas. Low frequency guided ultrasonic waves, e.g., a flexural mode similar to the A_0 mode, have been shown to be sensitive to fatigue cracks at fasteners in a single metallic layer [1]. In a multi-layered structure this type of mode would have energy distributed through the thickness of the structure. This would allow in principle for the detection of defects in all of the layers. The topic of the PhD thesis is a preliminary study of the application of low frequency guided ultrasonic waves for the monitoring of fatigue crack growth at fastener holes in the different layers of multi-layered aircraft structures.

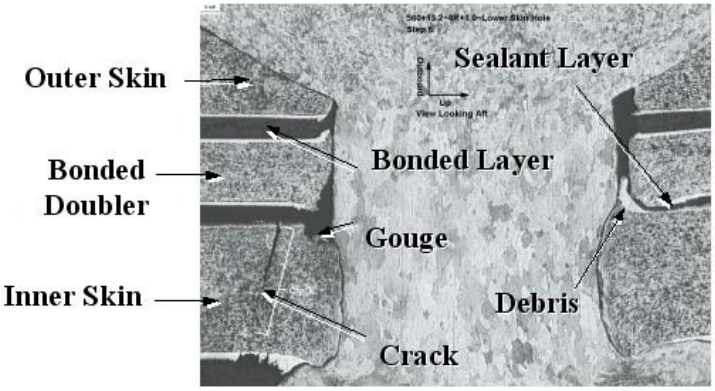

Figure 1.1: Microscopy of the cross section of rivet hole in a lap joint [4].

1.1 Motivation

Ensuring aircraft safety, while controlling operating costs, is one of the primary objectives for aircraft companies. A report from AIRBUS [2] stresses this fact, saying that operating costs such as fuel have little potential for further reduction, while the maintenance costs can be further reduced in the future. Maintenance costs could also become a major concern for airlines with aging aircraft fleet, as the manpower required for inspection is increasing with the aircraft's life. Numbers given by Sampath indicate that the man-hours required for inspecting and repairing the damage of an EF-111A fighter increased by 400% during ten years [3]. Holes for fasteners and rivets connecting multiple metallic layers in aircraft structure are some of the locations where damage like fatigue cracking often appears due to the stress concentration (figure 1.1). The outcome of a major airframe fatigue test performed on a Tornado fighter aircraft showed that 70% of the damage on this aircraft resulted from fatigue cracking in the different structural layers, occurring mostly at fastener holes, joints, rivets and bolts [5]. Some of the current inspection techniques used for aircraft maintenance involve time consuming and complex procedures. This can make such techniques very labour intensive and expensive. Many aircraft structures require removal of multiple structural components to detect flaws in the internal layers of the structure [6] by visual inspection. This procedure for the inspection of multi-layered

aircraft structures is fairly cumbersome, resulting in significant downtime for aircrafts. Studies by the aircraft industry have demonstrated that an aircraft SHM system could result in considerable maintenance cost and downtime reduction [7, 8]. For this reason the PhD thesis investigates the sensitivity of guided ultrasonic waves to detect such defects, as it could be used in SHM of aircraft structures.

1.2 Non-Destructive Testing (NDT) techniques for future SHM systems

A brief description of some current NDT techniques for the detection of sub-layer defects in multi-layered aircraft structure is presented in this section. The aim here is to show their defect detection capability and to briefly discuss their suitability for future SHM systems in aircrafts.

The adaptation and integration of current NDT techniques for SHM at damage critical locations is one way to potentially reduce inspection time and cost [5]. Some of the most common NDT techniques used for aircraft inspection are ultrasonic testing (UT) and eddy currents [9]. Other techniques used for the NDT of aircrafts are vibrational techniques, thermal wave imaging, guided waves, x-rays, and acoustic emission. According to Boller, of the NDT techniques mentioned above, only a few were considered to be mature for being used in a SHM system [5]. Two of the NDT techniques which could potentially be used for SHM in aircrafts are UT and guided waves. Another NDT technique which can be used in future SHM systems are eddy currents [2]. One of the requirements for future SHM systems is that they need to be able to detect defects in the sub-layers of multi-layered aircraft structures [10].

1.2.1 Eddy currents

An eddy current is an electrical phenomenon generated through electromagnetic induction [11]. An alternating current in a conductor, such as a coil will create a magnetic field in and around itself. If the coil is brought close to another conductor, the alternating magnetic field will induce small currents (eddy currents) in that material. Eddy currents concentrate near the surface adjacent to an excitation coil and their strength decreases with distance from the excitation. This phenomenon is known as the skin effect. The depth from the surface of the conductor where the current density decreases to 37% from its value on the surface is called skin depth (δ) and can be estimated using the following equation [1]:

$$\delta = \frac{1}{\sqrt{\pi f \mu \sigma}}, \tag{1.1}$$

where μ is the magnetic permeability, σ is the electrical conductivity of an isotropic material and f is the frequency of the alternating current in the coil.

Currently high frequency eddy currents are used for the detection of surface cracks in aircrafts with a minimum detectable size (corner crack at fastener holes) of 0.030 inches (0.76 mm) in aluminium, titanium and steel layers [9, 12]. While high frequency eddy currents are sensitive to detect surface defects, their detection capability for buried cracks in thick structures is limited because of the skin depth which decreases with increasing frequency [13]. By using low frequency eddy currents the penetration depth can be increased (equation 1.1), making it possible to detect deep buried cracks in thick structures and in the 2^{nd} layer of a multi-layered structure [9]. On the other hand low frequency eddy currents can have difficulties detecting smaller defects. Recent advances in sensor technology, e.g. the development of giant magnetoresistive (GMR) sensors, has given an extended sensitivity to low frequency applications [14]. An inspection method using this type of sensors could detect

[1] The equation is valid for conductors (e.g. steel and aluminium) with $\sigma \gg \omega \epsilon$ (ϵ is the electric permeability and ω is the angular frequency) [11].

narrow slots (6.3 mm long) in the lowest layer of a stack of three aluminium plates with a total thickness of 25 mm [15]. These sensors can be quite large, making them probably inappropriate for SHM purposes on aircrafts. Eddy currents are restricted to monitor damage only locally e.g. at fastener holes. Because of the large number of fastener holes in an aircraft a future SHM system based entirely on eddy currents could be very expensive.

1.2.2 Ultrasonic testing

In conventional UT (bulk wave), high frequency (0.1 - 10 MHz) sound waves (longitudinal or shear waves) are utilized for flaw detection/evaluation, dimensional measurements and material characterization. The most common UT techniques are pulse-echo and pitch-catch measurements. In pulse-echo measurements, the transmitter generating the ultrasonic sound waves which propagate through the thickness of the structure, is also receiving the reflected waves from e.g. flaws or geometrical boundaries. For pitch-catch measurements one transducer is emitting ultrasonic sound waves and another transducer is receiving the sound waves [16].

UT on aircrafts (pulse-echo) have a proven track record of detecting cracks [9]. The use of conventional ultrasonic testing techniques for the inspection of a multi-layered structure requires the presence of a sealant/adhesive between the layers. A sealant or an adhesive functions as couplant for the ultrasonic energy to propagate from one layer to the other. Under laboratory conditions and with the presence of a sealant layer, very small defects (0.64 mm long notch) have been detected [17] for thickness values up to 120 mm. Past studies have investigated the possibility of detecting fatigue damage in the 2^{nd} layer of a multi-layered structure using similar UT techniques. Komsky and Achenbach used bulk shear waves for the inspection of a bolted DC10 spar-cap/strap connection [18]. Later a group at QinetiQ developed an inspection technique for 2^{nd} layer detection [19]. However, 2^{nd} layer defect detection using conventional UT techniques can be problematic if a coupling medium between

the layers at the fastener hole is inadequate or missing [12, 19]. Similar to eddy currents, an SHM system based on conventional bulk wave UT has the disadvantage that only local damage monitoring can be achieved. This would require a dense transducer distribution for the monitoring/inspection of large areas, making a SHM system based on these two NDT techniques very expensive. Using eddy currents and conventional UT at damage critical locations in combination with other techniques is a more realistic approach in a future SHM system [2].

1.2.3 Guided ultrasonic waves

Guided waves[2] are able to propagate along the plane of a plate thus inspecting an area of such a structure. This technique is offering potential benefits for the monitoring/inspection of large areas compared to other more localized techniques. A general review of the guided wave capabilities for inspection which includes aging aircraft inspection has been given by Rose [20]. One of the discussed aging aircraft applications is the inspection of adhesively bonded components.

The usage of adhesives in order to bond metallic structures together created a requirement for the inspection of the bond quality between the bonded metallic structures. As the testing of large areas using conventional UT techniques can be very time consuming, guided waves offered an efficient way of inspecting bond qualities over large areas. Rokhlin [21] et al., Pilarski [22], Nagy [23] and others have investigated the usage of guided and interface waves for inspecting the strength of adhesive bonds. Since then more research has been done on the inspection of adhesive bonds [24] in multi-layered aircraft structure using guided waves. On the other hand very little work has been done for the detection of fatigue damage in multi-layered aircraft structures using guided waves.

The understanding of the scattering of guided waves around fastener holes with and without defects in plate-like aircraft structures can be very important, e.g., for determining the sensitivity of these waves to defects of different size. This type of

[2]A review of guided ultrasonic waves is presented in chapter 4.

studies have been performed mostly on large single layer plate-like structure. These studies will be reviewed in detail in chapter 6, where the scattering in large single and multi-layered plates is investigated. The following paragraph reviews some work done on the possibility of detecting defects at fastener holes in multi-layered structure.

Komsky and Achenbach [18] have investigated the possibility of detecting defects at holes in multi-layered structures using high frequency guided ultrasonic waves. Later Quarry [25] investigated how guided waves can be used for detecting 2^{nd} layer defects in multi-layered structures. The results from these investigations show that a notch can be detected with this method, but no further investigations were made to detect defects at fastener holes, where fatigue damage usually develops. The possibility of detecting fatigue defects at fastener holes in multi-layered structures using high frequency guided ultrasonic waves (5 MHz) has been investigated by Lindgren et al. [26]. The results from their work show that defects can be detected, but the sensitivity for detecting them depends on the interface conditions between the different layers. For this reason it could be very important to study and identify guided waves which are insensitive to interface conditions, but on the other hand are sensitive to eventual defects such as fatigue cracks. The authors also noted that high frequency guided ultrasonic waves will be attenuated if a material, such as an adhesive, is present between the metallic layers, thus making it very difficult to monitor large areas. The selection of appropriate modes is very important in order to minimize the attenuation of the guided waves for large area inspection in multi-layered structure. According to Dalton et al., potential modes for large area inspection of double-layered metallic fuselage structures should have frequencies below 2 MHz [27]. Guided wave modes are damped out very fast at high frequencies, making it difficult to inspect large areas.

As mentioned earlier a flexural mode similar to the A_0 mode, has energy distributed through the thickness of the multi-layered structure, making it possible to detect defects in all of its layers. This flexural mode is also not very sensitive to changes in the material properties and thickness of the adhesive layer [24]. Utilizing

such a mode in the low frequency regime could overcome difficulties such as missing sealant and attenuation. Working at lower frequencies decreases also the number of propagating modes, thus making it significantly easier to interpret the received signal [28]. Measuring the guided wave at a few points on the surface of the structure, rather than measuring with a dense distribution of eddy current sensors or UT transducers, might offer a way to detect defects in large areas. Guided waves have wavelengths significantly larger than commonly used in conventional UT techniques. Regarding this, the wave propagation characteristics of these waves and their sensitivity for the detection of fatigue cracks in multi-layered structures needs to be ascertained. This project studies the possibility of using low frequency guided ultrasonic waves for detecting and sizing fatigue cracks at fastener holes in multi-layered aircraft structures.

1.3 Objectives

The aim of the research project in collaboration with Airbus UK was to develop a novel NDT methodology and to demonstrate the application of guided ultrasonic waves for SHM applications in complex, multi-layered structures, such as aircraft wings. The further aim would be to tackle the real NDT problem in aerospace industry of the detection and monitoring of fatigue cracks in the sub-layers of multi-layered aircraft structures and to demonstrate the proposed novel SHM technology for aerospace industry.

This PhD thesis studies the sensitivity of guided waves to real fatigue cracks in multi-layered structures. The specimens used consist of two adhesively bonded aluminium plate strips with a single fastener hole. The geometry and lay up of these specimens is locally similar to multi-layered structures with fastener holes found in aircrafts (e.g., at wings, around windows and doors). In order to study the sensitivity of guided waves to fatigue cracks in multi-layered tensile specimen, fatigue crack growth during cyclic loading was monitored. Because of the size and capacity of

the fatigue machine the model structure was restricted. The type of defect that was examined was a fatigue crack which grew at a fastener hole in the opposite layer from where the monitoring was performed (hidden layer).

For these experiments to be successful appropriate excitation and measurement equipment for guided waves in multi-layered tensile specimens had to be developed. In order to do this it was important to study and understand the wave propagation in single and multi-layered tensile specimens. Because of the finite width of these specimens (additional width modes), the wave propagation is more complicated compared to large plates. The course of these investigations began by studying the wave propagation in the single layer specimen before moving on to the more complicated multi-layered specimen. Different excitation configurations were tried during these studies in order to excite a single mode. The final setup used for the fatigue experiments excited and measured low frequency bending modes similar to the flexural mode in a large multi-layered plate.

For studying the sensitivity of the waves to fatigue cracks, it is important to understand the interaction of guided waves in these structures with a fastener hole with or without any fatigue cracks present. Initially the scattering at a fastener hole in a single layer plate was studied. Having understood the physics behind this, the scattering in a large multi-layered plate with the same lay up as in the tensile specimen was investigated. This work was compared to the scattering from the multi-layered tensile specimens. Fatigue experiments were carried out investigating the sensitivity and the possibility of sizing defects in multi-layered tensile specimens using guided ultrasonic waves.

1.4 Outline of the thesis

The objectives of this research project have been investigated and are presented in the order given below.

Chapter 2

In this part of the thesis the general experimental setup used for studying the wave propagation and scattering is shown. Specimen geometries for the single and multi-layered aluminium plates and aluminium tensile specimens are presented here. Measurements procedures for the wave propagation in tensile specimens and for investigating the scattering at a fastener hole in plates and tensile specimens is explained. A description of the fatigue experiments and the on-line fatigue crack growth monitoring in multi-layered tensile specimens is given.

Chapter 3

The next chapter describes the Finite-Element (FE) methodology used in this project. The Matlab program which generates the (FE) mesh and the input files used by the FE software (ABAQUS [29]) is explained. Important features in this program such as the Cartesian mesh, meshing of the fastener hole and defect (notch and crack) are explained in more detail. A general overview is also given for the evaluation procedure of the obtained results. A brief description of a Semi-Analytical Finite-Element (SAFE) code which was used to study the wave propagation in the single and multi-layered tensile specimens is given.

Chapter 4

The main aim of the studies presented here was to understand the wave propagation in single and multi-layered plate-like structure. Theoretical studies were made on a single layer plate in order to understand the different wave types that can exist in such a wave guide. The dispersion curves for the single layer plate are compared to

the dispersion curves for a multi-layered infinite plate. Dispersion curves and mode shapes for the single and multi-layered tensile-specimens obtained with the SAFE code are presented, compared and discussed.

Chapter 5

The experimental results obtained from studies of the wave propagation in the tensile specimens are shown and described here. The objective of these studies was to excite the lowest flexural mode, which would produce a uniform incident wave field. Three different methodologies were examined for isolating this mode in the tensile specimens. The excitation used for the fatigue experiments in the multi-layered specimens is described here.

Chapter 6

Results from the scattering at a fastener hole in large plates are presented and compared to FE simulations. The aim of these studies is to understand the scattering in these structures. Initially the scattering at a fastener hole with and without a defect in a single layer plate is studied experimentally and numerically (FE). Similar studies are carried out for a multi-layered plate. These results are compared to the scattering in the multi-layered tensile specimen.

Chapter 7

The aim here was to study the sensitivity of guided waves to real fatigue cracks. In this chapter results from three sets of experiments involving fatigue crack growth monitoring in multi-layered tensile specimens are shown and discussed. The first set of experiments is a preliminary study for monitoring fatigue crack growth and for studying the influence of fatigue cracks on the scattered field in multi-layered tensile specimens. For studying the repeatability of these measurements a second set of experiments was performed. The results from the fatigue crack monitoring on 3

specimens are compared to FE simulations. Similar to the first set of measurements, a study on the influence of a fatigue crack on the scattered field around a fastener hole is presented. The same investigations are carried out in the third set of experiments, but this time the excitation setup is slightly changed compared to the previous set of fatigue experiments in order to simulate only single sided access to the structure.

Chapter 8

Results from the guided wave propagation and the scattering are summarized and future work described to continue from this thesis.

Chapter 2

Experimental methods

The aim of the experiments was to investigate and understand the wave propagation and scattering at a single fastener hole with or without defects in single and multi-layered structures. Experiments were also carried out to monitor fatigue crack growth using guided ultrasonic waves in multi-layered tensile specimens. In this chapter the specimens, excitation setup and measurement procedures used are presented.

The experimental description for the different investigations is presented here in the same order as the results presented in this thesis. The first part of this chapter gives a brief description of the general experimental setup [1, 30] used during all of the experimental studies performed as part of this work. This is followed by a more detailed description on the setup used to study the wave propagation in the tensile specimens. A similar description is given for the larger plates which were used to study the scattering of guided ultrasonic waves at a fastener hole with and without a defect. In the last part of this chapter the methodology used during the fatigue experiments is explained. A detail description of the fatigue, excitation and measurement setup used in these investigations is given.

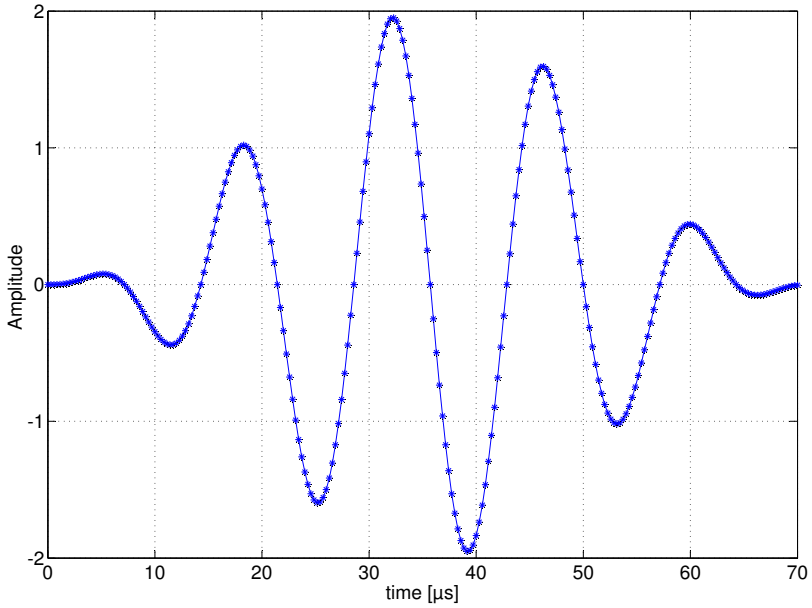

Figure 2.1: Typical multi-cycled excitation signal with a centre frequency of 70kHz.

2.1 General experimental information

The phase and group velocities of guided waves are not the same for different frequencies (dispersion) causing signal distortion as the signal propagates along the plate. In order to avoid extensive signal distortion a narrowband signal can be applied, where most of the energy is concentrated around the centre frequency of the signal. The signal used for the excitation of the flexural waves in the structures used in this thesis was a narrowband 5 cycle sinusoidal in a Hanning window (figure 2.1). The excitation frequency (35 - 115 kHz) depended on the desired mode of excitation and the experiments performed. The signal was defined in Labview and generated as a voltage signal from a function generator (Aglient 3322 OA) (figure 2.2), which also sends a trigger signal to the oscilloscope. The signal was amplified (Krohn-Hite 7602 M) and transfered via cable to the excitation transducers, which generated the guided waves. Guided waves can be generated by different methods. Wedge transducers and air-coupled transducers are often used to generate guided waves [31]. Although these transducers have been used with success for the generation of guided ultrasonic waves, PZT discs and plates were found to be the the most convenient

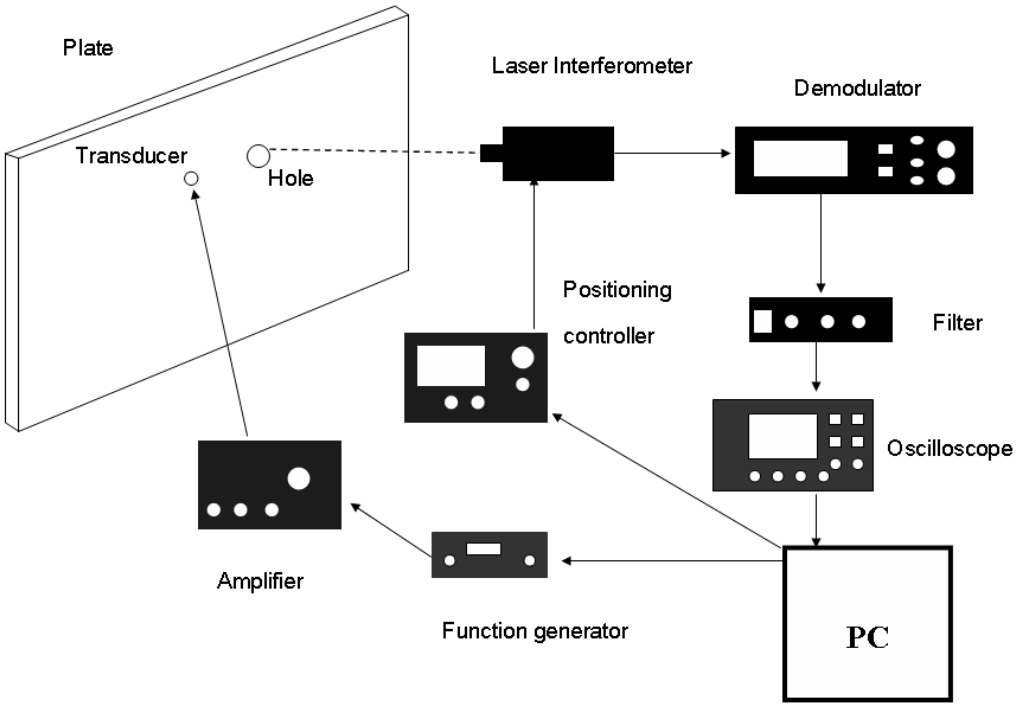

Figure 2.2: Schematic view of experimental setup

for the excitation of low frequency guided ultrasonic waves. These transducers have the advantage that their geometrical properties can easily be chosen depending on the experiment performed and the type of structure and they can be permanently attached to the structure. The discs were bonded on the surface of the plates or the tensile specimens using a fast curing two component epoxy based adhesive (Bondmaster Double Bubble).

The wave generated by the transducer propagates along the plate, but is also scattered at obstacles (fastener holes, defects and boundaries). The incident and scattered waves were measured using a heterodyne laser interferometer (Polytec). The laser beam generated by the sensor head (Polytec OFV-505) had an output power of less than 1mW. The beam diameter was below 50 μm, allowing for pointwise measurements of the scattered field. The laser interferometer is moved parallel to the specimen on a scanning rig, allowing e.g. for the measurement of the scattered field in the vicinity of the defect or for measuring the wave propagation along and across the tensile specimen. The laser was connected to a demodulator (Polytec

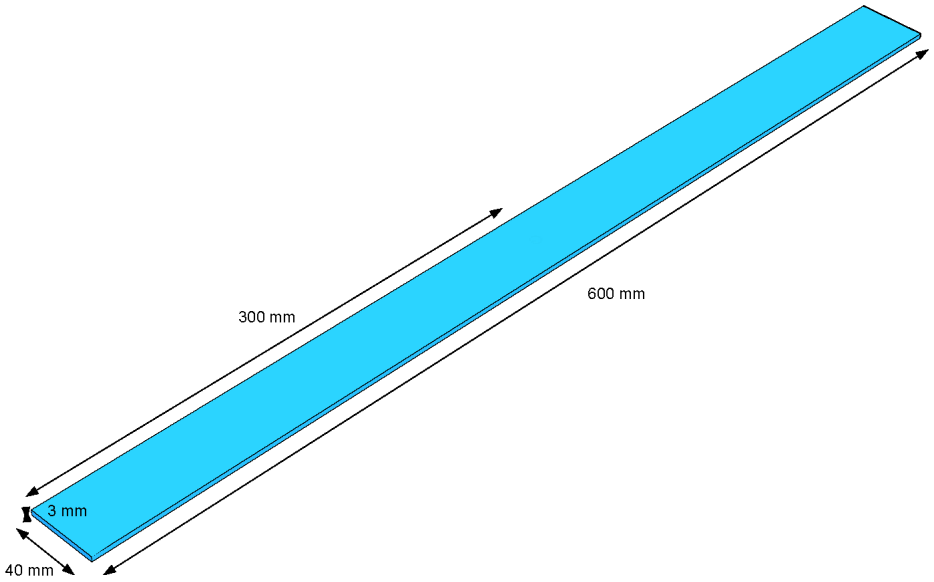

Figure 2.3: Single layer aluminium tensile specimen.

OFV-5000 Vibrometer Controller) which processes the measured velocity. The output signal from the demodulator is a voltage signal with an amplitude proportional to the out-of-plane velocity component of the surface at the measurement point. The voltage signal from the demodulator was then bandpass filtered (Krohn-Hite 3988) around its centre frequency (for 35 kHz: 10 - 60 kHz; for 115 kHz: 80 - 150 kHz). The signal was averaged (20 - 30 times) and stored in an oscilloscope (LeCroy 9304), with a maximum sampling frequency of 100 MHz. Finally the signal was transfered to a PC for further evaluation.

2.2 Wave propagation in tensile specimen

2.2.1 Tensile specimen

Measurements were performed on single and multi-layered tensile specimens in order to study the wave propagation in these structures. The tensile specimens used for these studies were 40 mm wide, 600 mm long and 3 mm thick. The material of the specimens was an 2014-T6 aluminium alloy, with a modulus of elasticity (E) of 72 GPa, Poisson's ratio (ν) of 0.33 and density (ρ) of 2700$\frac{kg}{m^3}$. These plate strips were also used for manufacturing the multi-layered tensile specimens. The

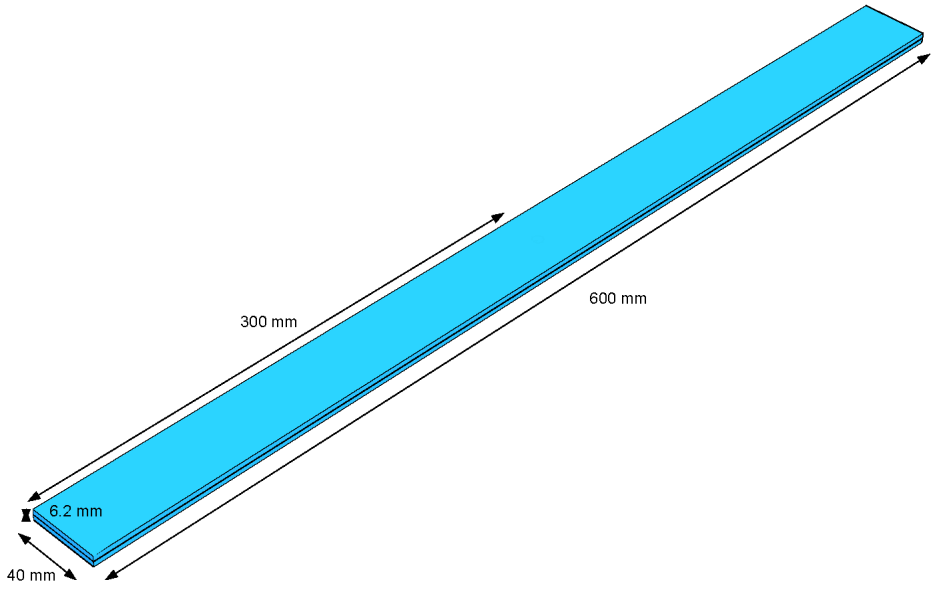

Figure 2.4: Multi-layered tensile specimen.

multi-layered tensile specimen (600 mm x 40 mm x 6.2 mm) shown in figure 2.4 consists of two single layer tensile specimen, bonded together with an epoxy based adhesive (HYSOL-9394 EA, E = 4.2 GPa; $\nu = 0.37$; $\rho = 1360\ \frac{kg}{m^3}$) [32].

Different manufacturing methods were tried out during the course of this work. In general all of the specimens were surface treated using sandpaper (600 grit). Before applying the paste adhesive the surfaces were cleaned using acetone and ethanol. After the paste adhesive had been applied on both of the surfaces to be bonded, a pressure load was applied. This pressure load was retained during the whole curing period, which according to the specifications was performed at room temperature. The load was applied by clamping the tensile specimens between two thick steel plates of similar dimensions. Six ties were used across the length of this steel plates in order to apply the pressure on the tensile specimens. In the first stage of the manufacturing process, the specimens were manufactured without the use of spacers to control the thickness of the adhesive layer. Instead the amount of adhesive needed to obtain the desired layer thickness (0.2 mm) was calculated and applied on the specimens (specimen 1 - 3). This manufacturing method proved to be inadequate of producing adhesive layers with the same thickness for different

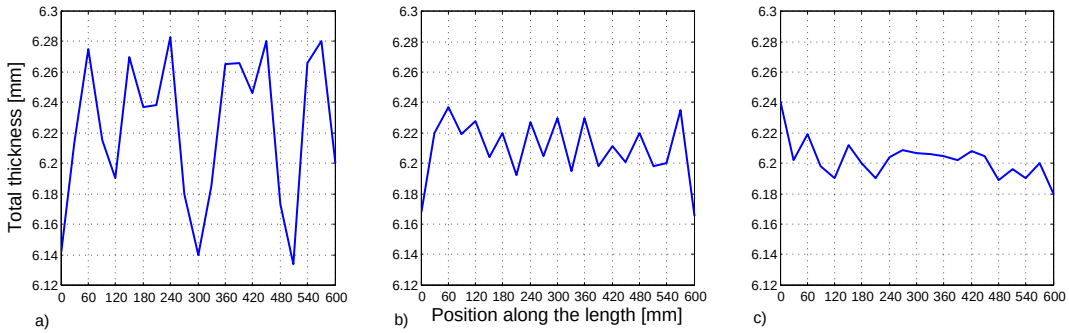

Figure 2.5: Thickness for three multi-layered tensile specimens; (a) specimen 4; (b) specimen 6; (c) specimen 14.

specimens and was therefore changed. To overcome the problem with the adhesive layer thickness spacers were introduced in the adhesive layer between the tensile specimen (specimen 4 - 6). Steel wires 0.22 mm thick and about 45 mm wide were placed across the width and approximately 60 mm away from each other along the length of the specimen. For one manufactured specimen (specimen 4) the adhesive did not cure well, so the thickness at the centre (300 mm) was much smaller than in the rest of the specimens (figure 2.5a). This was probably caused by the fact that the adhesive was mixed at this location on the specimen. For the remaining specimens the adhesive was prepared on a separate specimen. For specimens 5 and 6 it was observed that the thickness at the location of the wires (every 60 mm along the length of the specimen) was slightly larger than in the rest of the specimen. This lead to a periodical thickness variation along the length of the specimen (figure 2.5b). It was also seen that the ends of the specimen showed the largest difference compared to the centre, where a more uniform layer was observed. This was most probably caused by the fact that the amount of adhesive applied at this location was smaller than in the centre of the specimen. For the remaining specimens to be manufactured, the wires were cut in to smaller pieces ($\sim$ 3 mm long) and distributed randomly along the length and width of the specimens. From figure 2.5c (specimen 14) it can be seen that this method resulted in less thickness variation compared to the previous method (figure 2.5b). For specimens (7 - 14) which were manufactured according to this method the measured total thickness (averaged along the centre

of the specimens) was between 6.202 mm (SD: 0.012 mm, spec.14) and 6.266 mm (SD: 0.044 mm, spec.12). These specimens were used during the fatigue experiments which are presented in chapter 7.

Even though the obtained adhesive layers did not vary to much, the possibility of using spacer beads for controlling the thickness of the adhesive layer was investigated. Spacer beads (Ballotini ^{TM}) were used in the specimens which were used during the last set of fatigue experiments (specimen 15, 16, 17 and 18). The amount of spacer beads ($\sim$ 0.2 mm diameter) used was about 1% of the amount of adhesive applied on the specimens. This method produced repeatable adhesive layers with similar thickness variation to the specimens using pieces of thin wires as spacers. The average thickness taken along the centre of the specimens was in this case between 6.21 mm (SD: 0.008 mm, spec.15) and 6.225 mm (SD: 0.006 mm, spec.18).

2.2.2 Excitation

In the first part of these investigations PZT plates were used for the excitation of the guided waves in the single layer tensile specimen. The material of the PZT plate selected was a Ferroperm piezoceramic (Pz27) polarized in the thickness direction. The PZT plates were 40 mm wide (same as tensile specimens), 5 mm long and 1 mm thick. In the experiments the PZT plates were placed across the width of the specimen and 190 - 250 mm away from one end of the specimen. The excitation signal used in these studies had a centre frequency of 35 kHz.

Multiple PZT discs were also tried out as excitation. The PZT discs used for the excitation of guided waves in these structures were of the same material as the PZT plates (Pz27) with a diameter and thickness of 5 mm and 2 mm respectively. The PZT transducers were glued to the plate using the epoxy based adhesive (2.1). For the excitation frequencies used in this thesis (35 kHz, 100 kHz and 115 kHz), the discs are contracting and expanding with an applied voltage, producing a force normal to the surface under the PZT disc. Previous studies on large plates have

shown that for similar frequencies which are used in this study, the energy transferred to the longitudinal mode and the shear-horizontal mode is negligible [1]. The PZT discs used here will mostly excite the first anti-symmetric guided wave mode since the operating frequency is well below the cut-off for any higher order thickness modes for the large plates. In the specimens studied here, this anti-symmetric propagating wave mode is initially cylindrical, but because of the finite width of these specimens the wave is undergoing multiple reflections from the sides.

The different excitation setups investigated used initially one, three and five PZT discs. The single PZT disc was placed 190 mm away from one end of the specimen and in the centre of the single layer specimen (right in figure 2.6). The three PZT discs were placed 190 mm away from one end. Two of the discs were placed symmetrically 4 mm from the sides (black discs in centre figure 2.6), while the third disc was placed like the single disc in the centre of the specimen between (black dashed circle in centre figure 2.6) the two discs. For the setup using five PZT discs, another two discs were added to these three PZT discs. These two discs were placed 12 mm away from each side respectively.

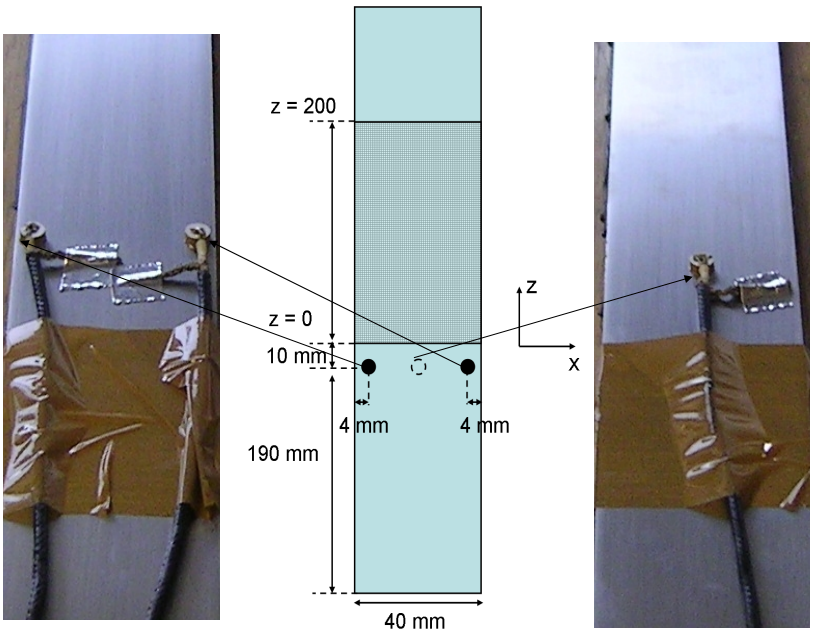

Figure 2.6: Left: excitation configuration on one side; centre: schematic view of excitation and measurement grid; right: excitation on opposite layer.

For the last experiments on the tensile specimen, two discs were placed at the nodes of the unwanted mode ($Fx1$, figure 4.7) in order to suppress it. The two PZT discs were placed symmetrically 9 mm away from the sides of the specimen. This approach of suppressing unwanted modes ($T, T1$ and $Fx1, Fx2$, figure 4.9) was also investigated in the multi-layered tensile specimens.

Two different excitation setups were used in the multi-layered specimens. The excitation frequency used in this part of the investigations was 115 kHz. The excitation setup shown in figure 2.6 gave the most repeatable wave propagation. This setup consists of three PZT discs permanently bonded 190 mm from the end of the specimen. Two of the discs (black dots in centre figure 2.6) were placed symmetrically 4 mm from the side on the top layer (left figure 2.6) and one disc was placed in the centre of the opposite layer (right figure 2.6). This type of excitation was used in almost all of the specimens for the first set of fatigue experiments (Chapter 7), except of specimen 7 which used a PZT plate (excited at 40 kHz). The same excitation was used in the second set of fatigue experiments. In the last part of the wave propagation measurements, the single disc placed in the centre of one layer was removed (right figure 2.6), leaving only the two discs on the same layer (left figure 2.6). This excitation setup was used in the third set of fatigue experiments (single sided access).

2.2.3 Measurements

Laser measurements of the guided ultrasonic wave field were taken to study the wave propagation in single and multi-layered tensile specimens. Measurements were taken following the experimental procedure described in the beginning of this chapter. Pointwise measurements of the ultrasonic guided wave field propagating in the z-direction (length direction) were taken on a Cartesian grid (centre, figure 2.6) every 1 mm in the x-direction (width direction) and 2 mm in the z-direction. Measurements started 5 - 10 mm away from the excitation and covered 180 - 300 mm for the single

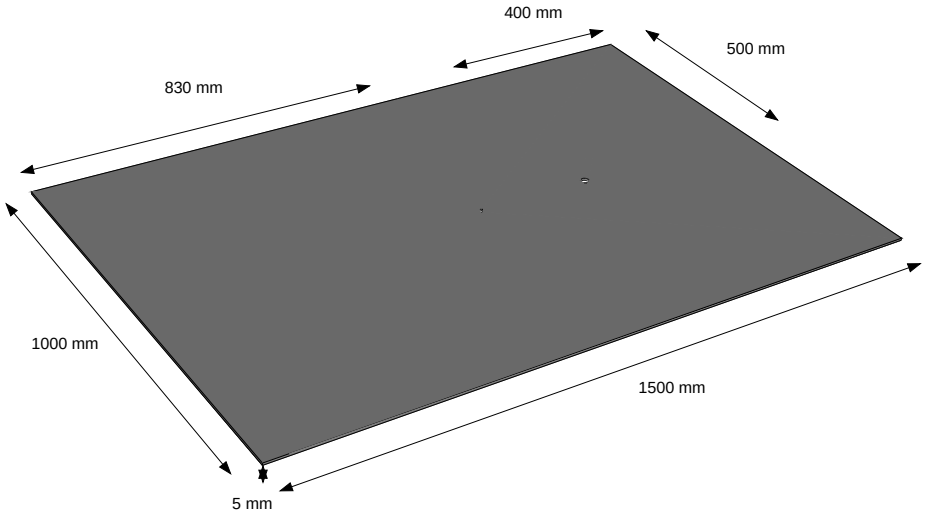

Figure 2.7: Single layer aluminium plate.

layer and 200 mm for the multi-layered specimen. The measured time series was transferred to the PC and evaluated using Matlab. Using Fast Fourier Transform (FFT), amplitude values at the centre frequency of the excitation signal are extracted for each measurement point. In order to investigate the modes which propagate these amplitude patterns were analysed further. The location of the fastener hole for the first set of fatigue experiments was 100 mm away from the excitation. The fastener hole had a diameter of 6 mm and this was kept constant throughout the investigations. The fastener holes were drilled in steps of 1 mm starting from 3 mm in diameter up to the final size. In the second set of fatigue experiments the fastener hole was placed 110 mm away from the excitation. In the last set of fatigue experiments the fastener hole was placed 30 mm away from the excitation.

2.3 Scattering in plates

Measurements were performed on large single and multi-layered plates in order to study the scattering at a fastener hole with and without a defect.

2.3.1 Single and multi-layered plates

The first set of experiments measured the scattered field around a fastener hole with and without defects. These measurements were carried out on a single layer aluminium-alloy plate (figure 2.7). The size of the plate was 1500 mm x 1000 mm with a thickness of 5 mm. Later a fastener hole (20 mm diameter) and a slot through the thickness of the plate (described in section 2.3.4) were introduced in order to study the influence of a defect on the scattered field around the fastener hole (figure 2.7).

The large multi-layered plate used in these investigations, consists of two 3 mm thick aluminium alloy (2014-T6) plates (750 mm square), bonded together with the same adhesive used for the multi-layered tensile specimens. Spacer beads were used to control the thickness of the adhesive layer. The amount of adhesive used was calculated to obtain an adhesive layer of about 0.2 mm. Some extra adhesive was added because part of it would squeeze out from the sides of the plate. Controlling the thickness of the adhesive layer was not as easy as for the tensile specimens which were clamped between two steel plates of comparable size. Because of the size of the plates it was not possible to do the same as for the tensile specimens. In the absence of an alternative such as an autoclave or a large press, the pressure load was applied by placing several weights (20 kg) directly on one plate. Because of the plate size it was difficult to quantify the quality or thickness of the adhesive layer. It was observed that at the edges and extending about 50 - 100 mm into the plate, the adhesive was inadequate or missing. In order to quantify the quality and thickness of the adhesive layer away from the edges, the plate was taken apart after the measurements. The thickness was measured in the centre of the plate. At the measurement locations for the wave propagation (between excitation and fastener hole) the adhesive layer thickness was found to be between 0.4 - 0.6 mm, which is thicker than the desired layer thickness. The reason for the thicker adhesive layer close to the fastener hole (6 mm diameter) and the excitation, is because the amount

of adhesive applied in the centre of the plate was larger than the amount on the edges. This and the fact that very little of this adhesive squeezed out towards the sides, resulted in a very thick layer at this location. At the measurement area for the scattering experiments around the fastener hole, the thickness variation of the adhesive layer was between 0.5 - 0.6 mm.

2.3.2 Excitation

A single PZT disc was used for the generation of the guided ultrasonic waves in the large plates. The PZT disc used for the excitation of guided waves in the structure was of the same type as the PZT discs used in the tensile specimens. In these measurements a backing mass (10 mm long brass cylinder, 5 mm in diameter) was glued on one face of the disc (5 mm in diameter and 2 mm thick). The same excitation transducer was used in the large multi-layered plate. The disc was placed 270 mm away from the centre of the fastener hole in the single layer plate (figure 2.7). Because of the bad quality of the adhesive layer away from the fastener hole and attenuation, the excitation transducer was placed closer to the fastener hole (110 mm from centre of hole, same as for tensile specimens 10 - 14) in the multi-layered plate. The excitation signal was 100 kHz in the single layer plate and 115 kHz in the multi-layered plate. In both cases the excitation frequencies were well below the cut-off frequency for any higher order thickness modes for the single and multi-layered plate (figures 4.1 and 4.2 respectively). At the working frequencies a propagating cylindrical wave is generated. In addition, if the radius of the fastener hole is much smaller than the distance between the excitation and fastener hole, the wave fronts of the generated wave can be assumed to be straight at the fastener hole.

2.3.3 Phase and group velocity measurements

The investigation of single mode propagation in the large plates involved phase velocity measurements. These velocity measurements may be compared to theory making it possible to identify the different modes. The wave field was measured at

two different locations on the plate separated by a small distance from each other ($\Delta x = 1$ mm). By taking the FFT of the two measured signals, the phase velocity (c_p) could be evaluated according to the following equation:

$$c_p(f) = 2\pi\Delta x \frac{f}{\Delta\psi}, \tag{2.1}$$

where $\Delta\psi$ is the phase difference between the two time signals for a certain frequency f. It must be said here that this equation is only valid when the phase is a linear function of the propagation distance (x), like in one dimensional wave propagation or at large distances from the excitation in cylindrical wave propagation in plates.

It is also possible to identify different modes by considering their group velocities. Group velocity was measured by taking the time Δt it takes for the signal to travel between two points were the signals are being measured. The distance between the two points ($\Delta x = 200$ mm) was known. By measuring the time of flight for the signal envelope from one point to the other, the group velocity (c_g) could be calculated:

$$c_g = \frac{\Delta x}{\Delta t}. \tag{2.2}$$

2.3.4 Scattering measurements

For the scattering around a fastener hole with or without a defect in the large single layer plate, measurements were taken pointwise on a radial grid around the hole every 5^o and every 0.5 mm in the radial direction (r = 10.5 mm to 32.5 mm). To investigate the sensitivity to various defects a 2 mm long notch was initially cut through the thickness of the plate using a hand-held cutter. Using the same cutting equipment the length of the notch was increased to 4 mm.

In the large multi-layered plate the measurements were taken on a smaller grid compared to the single layer plate every 5^o and every 1 mm in the radial direction (r = 4 mm to 15 mm). The defects introduced in the plate were machined with a thin cutter (1 mm diameter). The machined notch was about 1 mm wide and had a

length and depth of 2.25 mm, extending partly through one of the layers. Later the size of the notch was increased to a length of 5.25 mm and through one layer. The scattered field was measured on the undamaged layer when defects were present in one of the layers.

2.3.5 Initial scattering measurements on a tensile specimen

Similar measurements were done for a tensile specimen with and without a defect. Measurements were taken before and after a 6 mm long fatigue crack had grown through one of the layers and on the opposite layer (undamaged) from where the crack was located. The scattered field was monitored on a radial grid around the 6 mm diameter fastener hole, every 5^o and every 1 mm in the radial direction (r = 4 mm to 10 mm). The results from these measurements were either displayed on a circle around the hole or as a colour-coded surface around the hole. Through these measurements a good understanding of the geometry of the scattered wave and the influence of a notch or a crack can be gained. The characteristics of the scattered field around a hole are described in more detail in chapter 6. To study the influence of a defect on the scattered field in more detail, measurements were made before and after a notch was cut. The Fourier transformed signals from these measurements were later subtracted, giving information about the change in the amplitude pattern caused by the defect. To study the additional wave scattered at the defect, the complex amplitude difference between the damaged and undamaged case can be taken [1]. From this study the propagation characteristics of the wave scattered at the notch can be obtained.

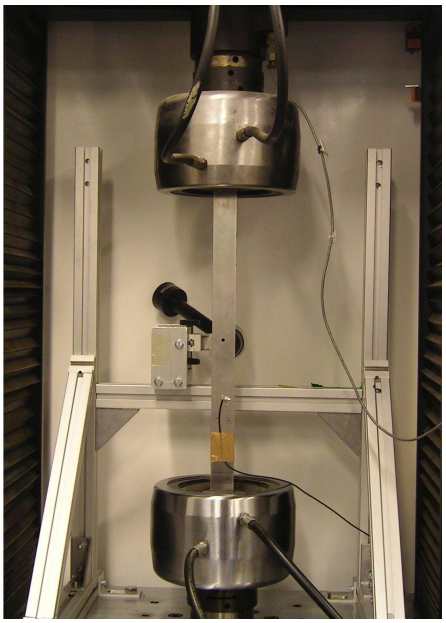

Figure 2.8: Fatigue setup with specimen in hydraulic clamps and microscope visible.

2.4 Fatigue crack growth monitoring

2.4.1 Fatigue setup

The aim of this work was to look at real fatigue cracks for the defect detection using guided ultrasonic waves. For this reason fatigue experiments had to be performed in order to generate these defects. An important design factor for the geometry of the tensile specimens investigated in this thesis was the size of the hydraulic clamps. The maximum specimen width, length and thickness which could be fatigued in this fatigue machine (Instron, figure 2.8) was about 70 mm, 700 mm and 15 mm respectively. For the fatigue experiments the multi-layered tensile specimens (2.2.1) were subjected to cyclic tensile loading. A maximum load of 30 kN was selected so that the maximum stress in the vicinity of the hole is about 90 % of the yield limit (stress concentration factor $K_t \approx 3.1$), in order to remain in the range of elastic deformation. The cyclic loading was performed with a stress ratio of R = 0.1 and cycling frequency of 10 Hz. A small starter notch, approximately 0.2 - 0.4 mm long,

was placed at the corner of the hole at the free surface of the bottom layer to control the crack location. For the first set of fatigue experiments, the crack length was measured on the surface of the bottom layer optically using a digital microscope (resolution: 200 pixels per mm), while applying the maximum load to make the crack more visible. In the second and third set of fatigue experiments the crack length was measured both inside the fastener hole (crack depth) and on the surface. After the crack dimensions had been measured and under this static load a measurement of the ultrasonic wave field was taken at the monitoring location at the fastener hole. The crack length was measured by transfering the images captured from the microscope to PC for further analysis. The measurement of the crack depth which was initially (second set of fatigue experiments) carried out by inserting into the fastener a cylindrical rod with a 45^o end where a mirror film was glued. A digital image of the fastener was then taken. This proved to be acceptable to measure the crack depth when it was almost through one layer, but very difficult to detect the initiation of fatigue crack growth. For this reason a 45^o angle mirror was glued on to one end of the rod (third set of fatigue experiments). This gave a much clearer view of the cracks compared to the mirror film which gave a more diffuse view because of the surface condition of the film.

2.4.2 Excitation and monitoring

For the first set of fatigue experiments the excitation setup consisted of one PZT plate, excited at 40 kHz (specimen 7). This frequency proved to be too low to detect fatigue cracks which were about 5 mm long (figure 7.1b) and was therefore changed. The excitation frequency was increased to 115 kHz for the next measurement (specimen 8), using the excitation setup with the three PZT discs (figure 2.6).

For all of the three specimens fatigued successfully in the second set of fatigue experiments the excitation setup consisted of three PZT discs (figure 2.6). In the last set of fatigue experiments the piezoelectric disc on the centre of one layer was

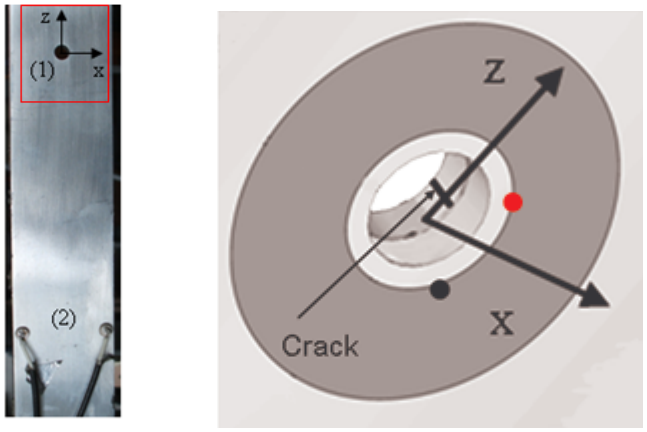

(a) (b)

Figure 2.9: (a) Tensile specimen with fastener hole (1) and excitation (2); red rectangle is enlarged and shown in figure (b); (b) schematic view of fastener hole and fatigue crack location on specimen; measurement grid (dark gray area), measurement point for single point monitoring during the first set of experiments (red dot) and second/third set of experiments (black dot); wave propagation in z-direction, used coordinate system marked.

removed. The excitation setup used in these experiments is described in more detail in a previous section (2.2.2).

In the first set of fatigue experiments crack initiation was monitored initially every 10 000 cycles. To monitor the influence of fatigue crack growth on the amplitude of the ultrasonic wave field the cyclic loading was stopped every 1 000 cycles (after a crack had become visible), the maximum tensile loading (30 kN) was applied to the specimens to hold the crack and a measurement taken at a single point. For specimen 7 the monitoring point was on the top layer close to the fastener hole and in front of the crack (bottom layer). The ultrasonic wave field amplitude was measured behind the crack (red dot at z = 2 mm and x = 5.5 mm in figure 2.9b) for specimen 8. After every measurement a digital image of the crack was taken on the surface of the damaged bottom layer. With this methodology specimens 7 and 8 were fatigued successfully.

Because the initial measurement of the crack length on specimen 8 was done after the crack had grown significantly, in the second set of fatigue experiments (specimen 10, 13 and 14) crack initiation was monitored initially after 10 000 cycles

and there after every 5 000 cycles. At these points a digital image of the crack (bottom layer) was taken and the ultrasonic wave field was measured on the top layer in front of the crack (black dot at z = -3 mm and x = 3 mm in figure 2.9b). The shortest measured crack length and depth was about 0.6 mm. After crack initiation the cyclic loading was stopped every 1 000 cycles, an image of the crack was taken followed by a measurement of the ultrasonic wave field taken at the single monitoring point. In order to get an estimate of the variation (noise) in these experiments, more measurements were taken prior to crack initiation in the third set of fatigue experiments. A measurement of the ultrasonic wave field was taken every 1 000 cycles at the same point as in the second set of fatigue experiments from the start of the fatigue experiments. Digital images of the crack were initially taken every 5 000 cycles and every 1 000 cycles after a crack was visible.

2.4.3 Scattering in tensile specimens

Before the start of the fatigue experiments measurements of the scattered field were taken around the fastener hole under static tensile loading (30 kN). The same measurements were performed when a fatigue crack had grown through one of the layers.

Because of the laser head, which was locked at one position, the wave field could only be monitored at a single point in the first set of fatigue experiments. For studying the influence of a bottom layer fatigue defect on the scattered field (top layer) around the fastener hole, the tensile specimen (specimen 8) was removed and brought to a machine which applied a static tensile load to avoid crack closure. Under this tensile loading measurements were taken on a radial grid (dark gray area in figure 2.9b) on the surface of the opposite layer from where the crack was located, every 5^o in the angular direction and every 1 mm in the radial direction (r = 4 mm to r = 12 mm). The evaluation procedure used in these investigations to study the scattering was the same as for the large plates described earlier.

For the second and third set of fatigue experiments a modification was done on the monitoring setup used for studying the defect influence (bottom layer) on the scattered field around the fastener hole. A scanning rig for the laser was set up close to the fatigue machine, allowing for the scanning of the specimens while clamped. Before fatiguing, measurements were performed while the maximum tensile load was applied to the specimens (30 kN). Measurements of the ultrasonic wave field were taken on a radial grid (dark area in figure 2.9) every 5^o in the angular direction and every 1 mm in the radial direction (r = 4 mm to r = 15 mm) on the surface of the undamaged top layer. These measurements were repeated after a crack had grown in the bottom layer.

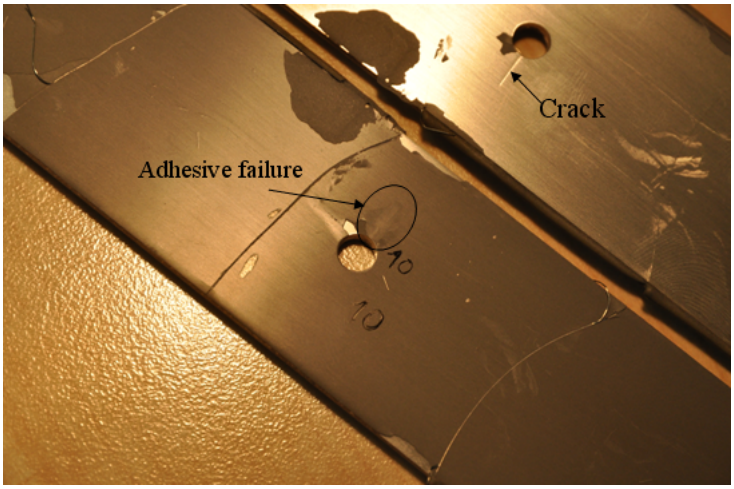

Figure 2.10: Digital image of a multi-layered tensile specimen (specimen 10) taken apart after the fatigue experiments. The image shows a 6 mm long crack at the fastener which grew in one layer and an area of possible adhesive damage (black ellipse) on the opposite layer.

2.5 Visual inspection of adhesive layer after fatigue testing

After carrying out the fatigue experiments some of the specimens were opened for a visual inspection of the adhesive layer. By eye it could be seen that there was some evidence of changes in the adhesive layer (black ellipse in figure 2.10) at the

crack location in one of the specimens (spec.10). An optical microscope was used to study the adhesive around the fastener hole in more detail. The optical microscope revealed a crack like damage ($\sim$ 2 mm long) in the adhesive and at the edge of the fastener (slightly visible in figure 2.10). The rest of this area did not show this type of damage. Instead it showed a void like surface pattern which was different from the surface conditions in the rest of the specimen. This pattern (dark patch inside black ellipse in figure 2.10) has about the same length as the defect (indicated in figure 2.10) suggesting that this change might have been caused due to the stress concentration close to the crack-tip.

Chapter 3

Finite-Element (FE) analysis

In many engineering and research situations one finds it necessary to get approximate numerical solutions to various problems when analytical solutions do not exist. As no analytical solution exists for the wave propagation and scattering of guided waves in multi-layered structure, it was chosen to use ABAQUS [29], a commercial FE software package for the numerical study of the guided wave propagation and scattering in these structures. This FE package has been successfully used to study guided wave propagation by other research groups (e.g. Imperial College NDE Group) and is together with two other FE packages (ANSYS and COMSOL), the most used for these type of studies. Other approximate numerical analysis methods which have been used for this type of guided wave propagation studies in plate structures over the years are the Finite-Difference [1] and Boundary-Element method. These methods have not been extended in a commercial software package to a very large degree for guided wave propagation problems. In the first part of this chapter the main features of the FE model used in this thesis are presented and discussed. For obtaining the wave propagation characteristics for the single and multi-layered tensile specimens a Semi-Analytical Finite-Element (SAFE) code was used [33].

3.1 Matlab code for FE model

During the course of this thesis a large number of FE simulations were performed, studying the guided wave propagation in tensile specimens and the scattering at a fastener hole in a large plate. For this reason it was important to automate and reduce the time to run the simulations. This was done by using a Matlab program to generate the input files automatically (text files containing the FE mesh, excitation and monitoring points), instead of using the more time consuming graphical interface (ABAQUS/CAE [29]) to generate these files. Different to the graphical interface which generates an irregular mesh for the type of structure studied here, the Matlab code can generate a Cartesian mesh. An advantage of this constant mesh is the obtained control over the node numbers which makes it easy to generate defects (notch, crack), but also to place monitoring points at the desired locations.

By giving input parameters, e.g., the element size, the diameter of the fastener hole and the length of the crack, the Matlab code can very quickly create different FE models. In the program, the dimensions of the plate, the size and location of the fastener hole, the size of defect and the size of the elements are defined. The defect can be modelled as a notch, by giving its width, length and depth. Later the code was changed so a zero width crack through one layer could be modelled. The monitoring areas, the excitation and the type of analysis performed are defined in the program, which writes this information to an input file using specific commands (input file commands, [29]). A similar Matlab based code was developed to automatically post-process the results obtained from the FE solver (ABAQUS/Explicit). The main features of the FE model such as mesh, excitation and evaluation procedure are described here next.

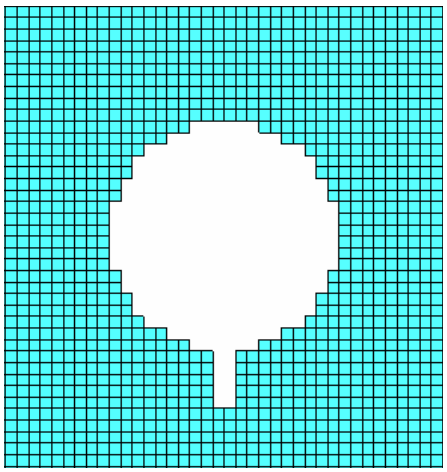

Figure 3.1: Cartesian mesh for a plate with a hole and a notch.

3.2 FE mesh

Meshing structures like the tensile specimen presented in chapter 2 using the graphical interface can often result in an irregular mesh. A disadvantage with such a mesh is the lack of control of the element size which can result in numerical dispersion (phase velocity variations caused by an inadequate mesh), if the elements are too large compared to the wavelength of the guided waves or if the time step used is too large for some elements. The irregular node numbering could also make the positioning of monitoring nodes e.g., on a circle for monitoring the scattered field around a fastener hole very difficult. The geometry of the studied structure was approximated by a Cartesian mesh (figure 3.1). A Cartesian approximation of a fastener hole has been used successfully by other authors [1] for similar studies to those presented in this thesis. From these investigations it was observed that if a sufficient number of elements are used across the diameter then this approximation is adequate. The resulting node distribution gave complete control of the node numbering, allowing e.g., for positioning of monitoring points at the desired locations. The element size which is determined by the input parameters gave complete control over the dimension of the elements, allowing for the simple calculation of the time step needed for a convergent solution [34].

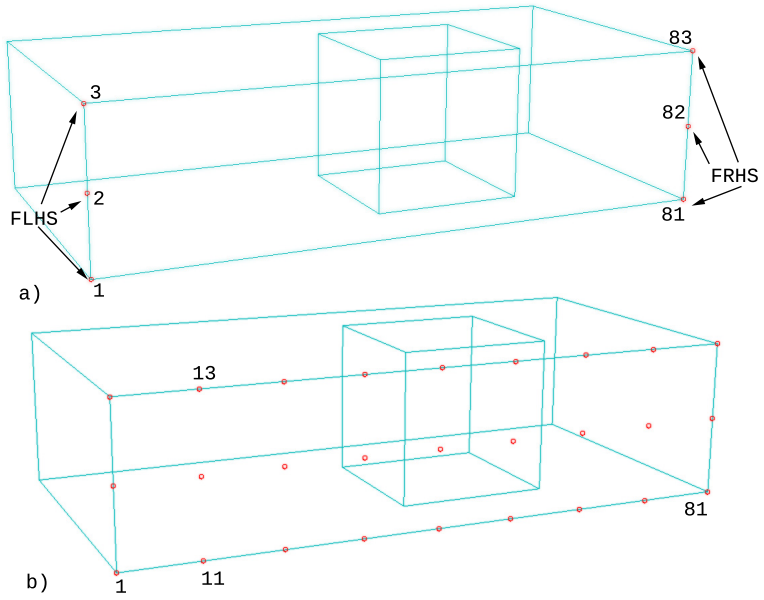

Figure 3.2: (a) Location of side nodes and their node numbers (FLHS and FRHS) on a single layer specimen; (b) nodes located on the front face of a single layer specimen.

3.2.1 Node generation

A very simple geometry is used in the following example aiming to describe the node and mesh generation used during the course of this thesis. After the input parameters (length, width and thickness of the structure and element size) have been given, the program generates equidistant nodes which are written out in the input file. Node number 1 was always placed at the origin (FLHS, figure 3.2a). In the thickness direction the node numbers were increasing by one. Nodes were defined on the same face, but on the opposite side at the right corner (node 81 to 83 FRHS 3.2a). Similar to the front face (figure 3.2b) of the specimen the corner nodes were defined for the rear face. The front and rear face could be populated with nodes (figure 3.2b) after the sides (FRHS, FLHS 3.2a) had been defined. The remaining nodes were generated by filling the area separating the front face and the rear face (figure 3.3). In this way all of the nodes were generated for one layer. For the multi-layered structure, this procedure was repeated for the adhesive layer and the second layer. The main advantage of the method used here is that the node number increment is known in each direction, thus making it very easy to calculate the node number at a certain location.

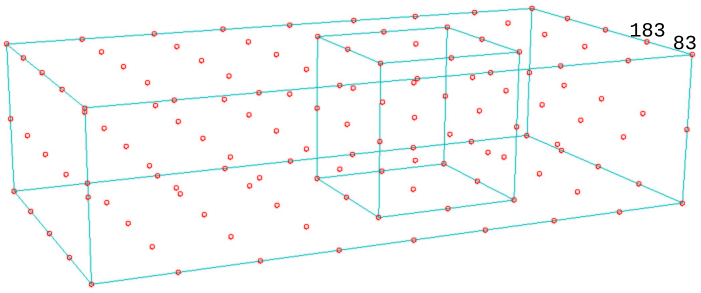

Figure 3.3: Nodes of the Cartesian 3D-mesh for a plate with a square hole.

3.2.2 Element generation

After the nodes had been generated it was possible to define the mesh. The Cartesian mesh which was used for the simulations throughout this project consisted of linear, 8-node, 3D rectangular elements (C3D8R, [29]). In the example shown here, which aims to illustrate how the meshing was carried out, a very simple geometry is used. The initial steps of the meshing involve the plate regions which is to the left of the fastener hole (figure 3.4). The meshing of this part of the structure was done by initially defining a single element (element 1 for the left part in figure 3.4) and by thereafter automatically meshing the region up to the left boundary of the hole. The part to the right of the fastener hole was also meshed. For the multi-layered structure elements were also created for the adhesive layer and the second layer. In this way three different parts were defined in the FE model. These parts were connected by tying their nodes together on the interface of the connected parts.

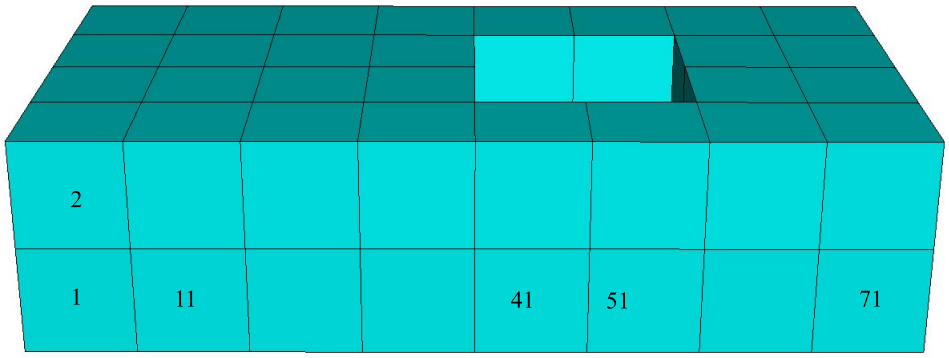

Figure 3.4: Cartesian 3D-mesh for a simple plate with a square hole.

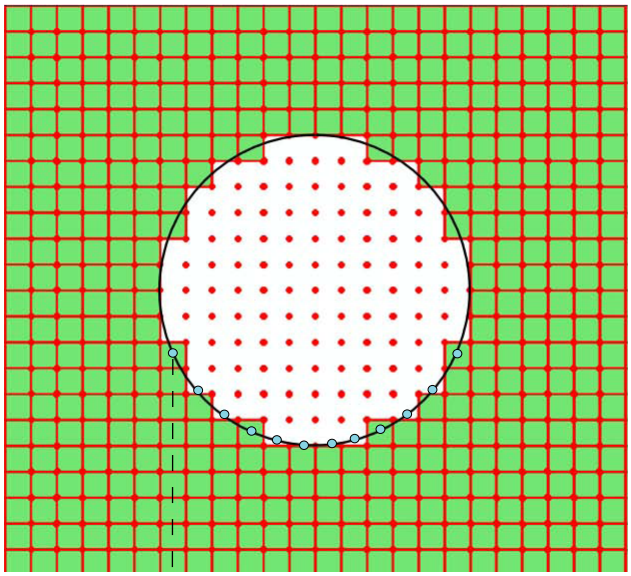

Figure 3.5: Cartesian mesh and nodes (red dots) at a fastener hole (r_o = 6 mm) in a single layer tensile specimen; points (blue dots) on the real boundary of the hole (black circle) used for calculating the number of elements (0.5 mm x 0.5 mm x 0.75 mm) needed for the Cartesian approximation of the fastener hole.

3.2.3 Meshing of fastener hole and notch

After the mesh at both sides of the hole has been constructed, the program generates the mesh for the part with the fastener hole. To illustrate this, a different structure than the plate with the square hole (figure 3.4) is presented in this section. The structure is the single layer tensile specimen (600 mm x 40 mm x 3 mm, chapter 2), with a 6 mm diameter fastener hole in the middle of the plate (300 mm, 20 mm). The fastener hole (black circle figure 3.5) for this specimen is approximated by the Cartesian mesh (figure 3.5). For the tensile specimen 12 elements (0.5 mm x 0.5 mm x 0.75 mm) were used across the diameter of the fastener hole. The number of elements needed from the bottom edge of the plate up to the approximated hole boundary are obtained by calculating the vertical distance (dashed black line in figure 3.5) from the bottom of the plate to the blue points on the black circle in figure 3.5 which illustrates the physical hole boundary. This was done across the diameter of the fastener hole. In the case of a notch, elements were removed from the mesh at the location of the fastener hole (figure 3.1). Only a notch perpendicular to the grid direction could be modelled with this code.

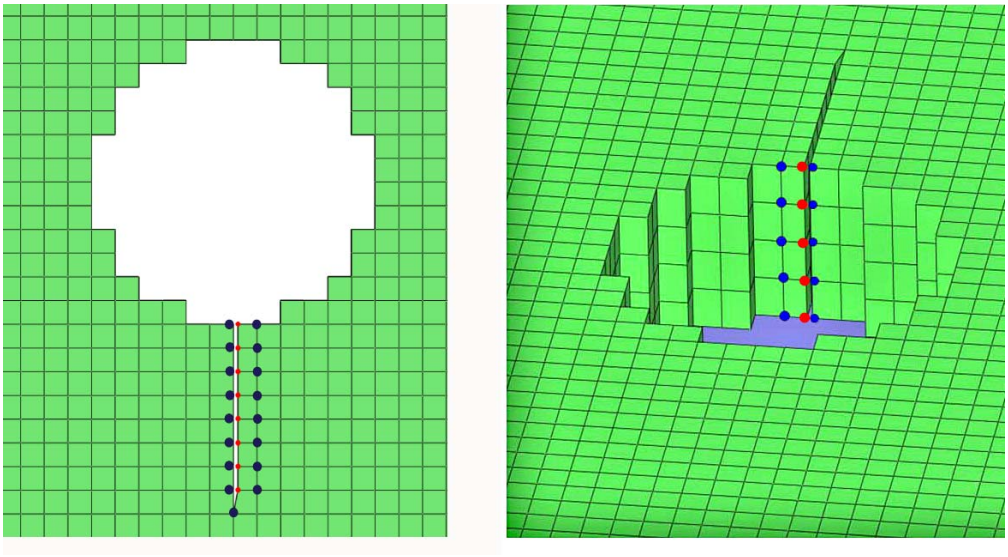

Figure 3.6: Cartesian mesh of fastener hole ($r_o = 6$ mm) and crack; initially generated nodes (blue dots) and extra nodes for constructing the crack (red dots); (a) top view; (b) side view; only a single column of extra nodes is seen on the inner hole surface.

3.2.4 Modelling of crack

This code is built on the previous code which generated the notch by removing elements. Input parameters such as the width and length of the crack are given in the Matlab code. Having specified these parameters the code will generate the crack automatically. Seen in figure 3.6 is a 4 mm long, 0.2 mm wide through crack in the single layer tensile specimen. The crack was generated by initially introducing extra nodes (small red dots in figure 3.6) at a certain distance (depending on crack width) from the previous notch boundaries (large blue dots in figure 3.6 a and b). Elements were generated, connecting only to one side of the initial notch. With this code it was possible to model a zero width crack. For the multi-layered specimen the crack was only modelled completely through one layer (figure 3.6 b). The element size was not changed at the crack tip which might miss the stress concentration at this location.

3.3 Excitation

Input parameters for the excitation are the coordinates, the direction and magnitude of the excitation force which are defined at the end of the code for different types of excitations. The PZT discs used in the experiments were modelled as out-of-plane point forces. For the large plates, which used one PZT disc, a single point force was used. This had previously been shown to be a good model for large plates [1]. In the fatigue experiments the three PZT discs used for the excitation (centre figure 2.6), were modelled by two forces with the same phase and amplitude at the location of the two discs on one layer (left figure 2.6) and with one point force of the same amplitude, but 180 degrees out-of phase at the centre of the opposite layer (right figure 2.6).

3.4 Monitoring

In the investigations of the wave propagation on the tensile specimen, nodes were monitored on the surface area of the specimen. The nodes were placed on lines spaced equidistant across the width of the specimen. The spacing between nodes on the lines and the spacing between the lines could be defined as required. The measurement grid used in these studies was the same as in the experiments (section 2.2.3). For studying the scattering, monitoring points were located on a circle around a fastener hole (figure 3.7). The centre of the circle, its radius and the number of monitoring points around the circle (white dots figure 3.7) could be defined. The number of monitoring points depended on the required resolution. For the comparison of the scattered field obtained from the FE simulations to the experiments, monitoring points had to be placed on a concentric circle around the hole. These points do not normally coincide with a node in the FE mesh. For this reason in order to evaluate the displacement at each monitoring point (figure 3.7), the four closest nodes (red dots figure 3.7) were calculated. In figure 3.7 it is possible to see that these four

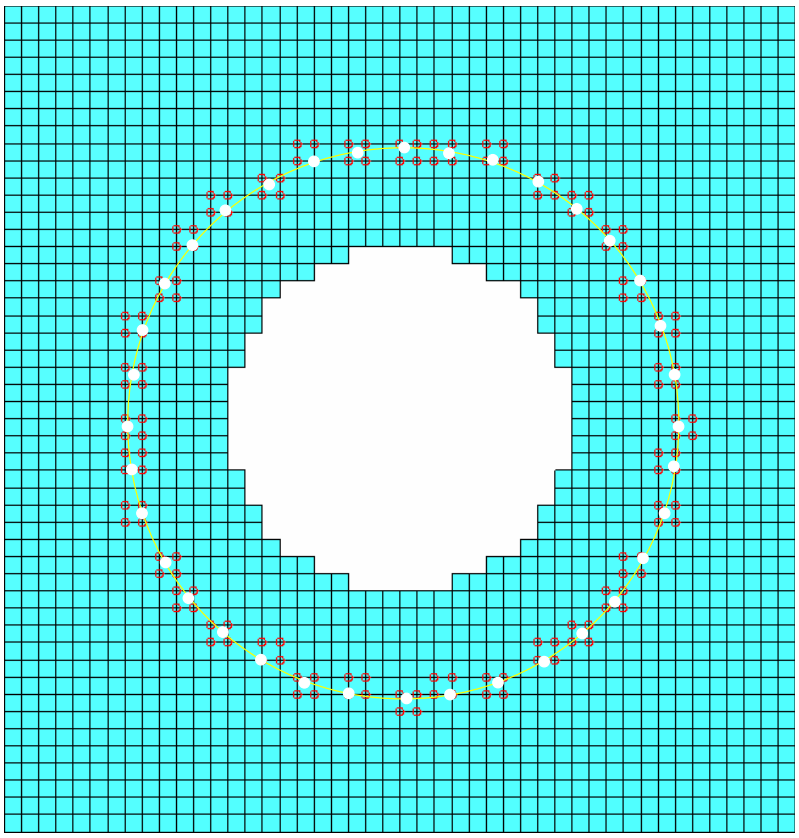

Figure 3.7: Monitoring nodes for a circle around a fastener hole.

nodes that are being monitored during the simulations form a square containing the monitoring point on the circle. The out-of-plane displacements of all of these nodes in the FE mesh were monitored throughout the simulations. The obtained results were then Fourier transformed. The amplitude for the four nodes was evaluated at the excitation frequency and bilinear interpolation was used for the calculation of the amplitude at the monitoring point. These steps were repeated for all of the monitoring points around a circle in order to obtain the total scattered field on a circle around a hole. The total scattered field around the hole could be obtained by repeating this procedure for circles with increasing radii, forming a radial grid similar to the experiments (2.3.4). All of the evaluations were carried out automatically using a Matlab program.

3.5 Element size and time step in FE simulations

This section discusses the element size and time step criteria used in the FE simulations which were carried out during this thesis.

3.5.1 Spatial stability

8-node rectangular elements were used in the FE-simulations presented here. In all cases the element size was determined from the shortest wavelength within the bandwidth of the excitation. A rule of thumb which has been used by other authors [35, 36] for FE simulations and which ensures accurate modelling (FE) is as follows:

$$\frac{\lambda}{8} \geq L. \tag{3.1}$$

This condition states that the smallest number of elements needed to approximate the shortest wavelength within a bandwidth is about 8. This criterion gives an element side (L) of about 2.5 mm for the single layer plate and about 2 mm for the multi-layered plate and tensile specimen. The sides of the elements used of the FE simulations were 1 mm x 1 mm x 1.25 mm for the single layer plate, 0.75 mm (cubic) in the large multi-layered plate, and 0.5 mm x 0.5 mm x 0.75 mm were used for the multi-layered tensile specimen. This can seem a bit too small, requiring unnecessary computation time, but an acceptable approximation of the fastener hole needs small enough elements. In the multi-layered tensile specimen 12 elements were placed across the diameter of the fastener hole. For the large multi-layered plates 8 elements were used across the fastener hole. Finally, for the single layer plate, 20 elements were placed across the fastener hole. The number of elements placed across the diameter of the fastener proved to modell the interaction of the guided waves with the fastener hole quite accurately (see chapter 6). More details about the mesh (e.g. element size in adhesive) in these structures is given in chapter 6, where the results from these simulations are presented.

3.5.2 Temporal stability

To ensure that the explicit algorithm is stable [29] the time step used must satisfy the stability criterion stated e.g., by Cook [34]. To be on the safe side, 80 % of that criterion was used:

$$\Delta T \leq \frac{0.8\alpha}{c_p}. \tag{3.2}$$

The stability criterion states that the time step (ΔT) must be smaller than the time it takes for the fastest wave to cross the shortest distance between adjacent nodes (α), where c_p is the phase velocity of the fastest propagating wave [29, 34]. The time step used for the calculations with 1 mm elements (large single layer plate) was 10^{-7}s and 10^{-8}s for elements with 0.5 and 0.75 mm sides (multi-layered). This time step satisfies also the stability criterion in the adhesive layer, where the smallest distance between nodes in the adhesive layer elements (thickness) is 0.1 mm, but the speed of the fastest wave is smaller than in the adherents. The required stability limit in this case is about $7 \cdot 10^{-7}$s.

3.6 Influence of element size on phase and group velocity calculations in FE simulations

It is known that the element size in FE calculations influences the phase and group velocities of the guided waves. For this reason simulations were performed in order to study how the element size is influencing the accuracy of the calculated phase and group velocities.

The case of study was the first anti-symmetrical guided wave mode (A_0), which is similar to a flexural mode, in a 10 mm thick steel plate. The elements used here where 3D brick elements (cubic, 1 mm). The plate was 500 mm (square) and boundary conditions were used on the side of the plate allowing only in plane motion that is motion parallel to the side surface (symmetry boundary conditions). The excitation signal was a five cycle sinusoidal signal in a Hanning window. The

Element size	c_p	c_g	Rela. error c_p	Rel. error c_g
5 mm $\sim \lambda/5$	1.030 m/ms	2.08 m/ms	56 %	35 %
2.5 mm $\sim \lambda/10$	2.335 m/ms	3.07 m/ms	0.8 %	4 %
1 mm $\sim \lambda/24$	2.346 m/ms	3.10 m/ms	0.4 %	3 %
0.5 mm $\sim \lambda/47$	2.349 m/ms	3.14 m/ms	0.34 %	1.5 %

Table 3.1: Phase and group velocities for different element sizes.

excitation frequency was 100 kHz, which gives a frequency thickness of 1 MHz mm. Theoretical values of the phase and the group velocity for this frequency thickness are 2.36 m/ms and 3.20 m/ms respectively. The velocities of the guided ultrasonic waves were measured according to the procedure described in section 2.3. The time step was held constant through the simulations. The magnitude of the time step was chosen as $10^{-8}s$, which is enough to fulfill the stability criterion for all of the element sizes. The results obtained were very close to the theoretical values for both the phase and group velocity. By increasing the number of elements, the evaluated velocity tends toward the theoretical value. This fact indicates that the solution is converging to the real solution [34]. Using a very small element size requires more computational power and longer computational times. Regarding this it is convenient to use elements that are approximating the geometry well and that produce accurate results, but without increasing the computational times significantly.

3.7 Semi-Analytical Finite-Element (SAFE) calculations

The aim of the SAFE calculations was to study the wave propagation characteristics of the guided waves propagating in a structure with a rectangular cross section (tensile specimens).

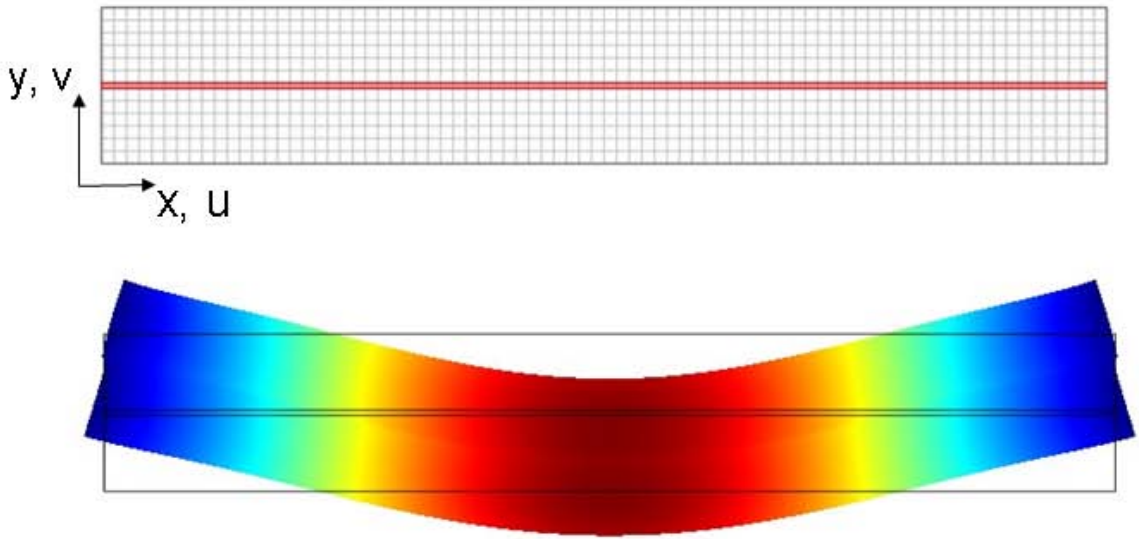

Figure 3.8: Top: 2D FE mesh of cross section (40 mm x 6.2 mm) for the multi-layered tensile specimen used in the SAFE-code; element size: 0.5 mm x 0.5 mm (alum.), 0.2 mm x 0.5 mm (adh.); bottom: flexural mode ($Fx1$, chapter 4) at 115 kHz obtained from SAFE calculations; geometry (black lines), deformed shape (colour plot).

3.7.1 Previous work

Most of the early theoretical work of guided waves in plates of finite width was done by Morse, Mindlin and Fox. Morse [37] studied the propagation of longitudinal waves in isotropic rods with a rectangular cross section, while Mindlin and Fox [38] studied the flexural waves that can propagate through an isotropic bar of rectangular cross section. Other early work on the wave propagation in this kind of structure was carried out by Nigro [39] and Aalami [40]. Most of the work mentioned above was carried out on structures with fairly simple shapes of the cross section. Since the theoretical analysis of the wave propagation in more complicated structures is often very difficult, a new technique called the SAFE method was developed [41]. With this methodology it is possible to analyse the wave propagation in a structure with complex cross section. In SAFE a 3D wave problem is simplified to an equivalent 2D problem by assuming a wave propagation along one direction. The cross section, i.e, the section normal to the direction of wave propagation, can then be discretized using 2D FE elements (top figure 3.8). From the numerical solution of the eigenvalue problem for the 2D cross section, the corresponding wavenumbers and mode shapes

are calculated for each frequency. Work on the propagation of guided waves in plates with rectangular or arbitrary cross section based on SAFE methods was done by Taweel et al. [42], Hayashi and Rose [43] and Mukdadi et al. [44]. Mukdadi's work which is closely related to parts of the work presented in this thesis (wave propagation in multi-layered bars) was based on such a SAFE model applicable to an arbitrary number of layers. The work done in this thesis for calculating the dispersion curves is based on a similar SAFE model.

3.7.2 SAFE code

The dispersion diagrams and mode shapes for single and multi-layered tensile specimen were obtained using a SAFE code developed at the University of Bordeaux [33]. The authors used a commercial FE software (COMSOL) with a similar eigenvalue formulation and modified the governing equations to agree with the formulation used in the FE software. In this way they could express the coefficients of the eigenvalue equations in the FE software in terms of the known density and complex elastic constants. By numerically solving the eigenvalue problem for the 2D cross section, the corresponding wavenumbers and mode shapes are calculated for each frequency.

For calculating the dispersion curves of the single and multi-layered structure the 2D mesh was created in COSMOL (top figure 3.8). In the single layer tensile specimen (3 mm thick, 40 mm wide) 4-node square linear elements were used (0.5 mm x 0.5 mm). The same elements were used in the adherents (aluminium) of the multi-layered specimens, while due to the smaller thickness, the element used in the adhesive layer were 0.2 mm thick and 0.5 mm wide. Smaller elements were tried through the thickness (0.1 mm), but no significant improvement of the accuracy of the results was seen. After the geometry and mesh of the specimen had been defined it could be imported in to the SAFE code which calculated automatically the dispersion curves and mode shapes (bottom figure 3.8) for these structures by numerically solving the eigenvalue problem for the 2D mesh and the corresponding

wavenumbers and mode shapes are calculated for each frequency. For distinguishing the different mode types a Matlab based code was developed during the course of this thesis. This code evaluated the displacements at different locations of the specimen and depending on their magnitudes and directions different mode types were identified. In the next chapter results from the wave propagation in single and multi-layered tensile specimens using this SAFE code are presented and discussed.

Chapter 4

Guided waves in single and multi-layered plates

In the first part of this chapter the dispersion curves for a single layer aluminium plate are presented. After the theory of guided waves in a single layer plate has been discussed, the wave propagation in a multi-layered infinite plate is analysed. Dispersion curves and mode shapes are shown for a multi-layered plate, which are later compared to the results obtained for the single layer aluminium plate. In the last part of this thesis the wave propagation in single and multi-layered tensile specimens is presented and analysed.

4.1 Large plates

A waveguide is a component with two or more parallel boundaries which "guide", e.g. sound waves in the direction of the waveguide layer. Some of the earliest work on guided waves is from Pochhammer [45] who studied the wave propagation in a rod. Later Rayleigh [46] and Lamb [47] derived the theory for guided waves propagating in an isotropic plate of infinite extent. Early studies of the wave propagation in multi-layered structures were carried out by Thomson [48] who studied the wave propagation in multi-layered media for seismological applications. Later Knopoff

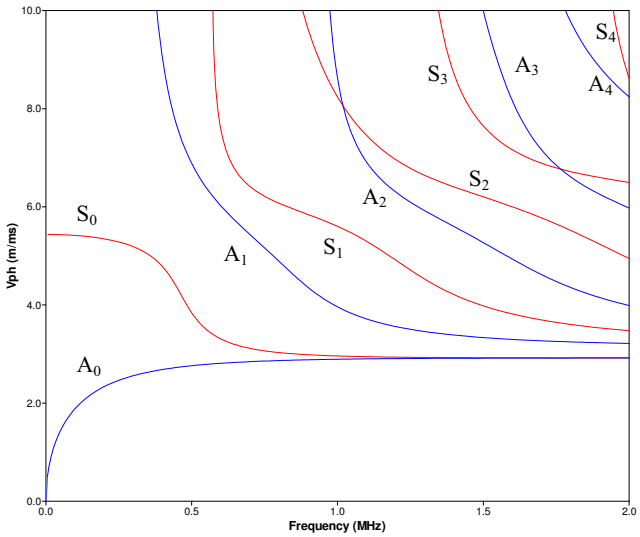

Figure 4.1: Dispersion curves for a 5 mm thick 2014-T6 aluminium plate.

[49] developed the global matrix method for elastic wave problems in multi-layered media, in which a large single matrix is assembled. Modal solutions of the single matrix describe the properties of the wave propagation in the multi-layered structure that is being studied. A review of general matrix methods for calculating dispersion curves in multi-layered structures with particular interest to ultrasonic applications has been presented by Lowe [50]. Basic physics and wave mechanics including the calculation of dispersion curves of guided waves in single and multi-layered plate structure can be found in a textbook published by Rose [51].

4.1.1 Single layer plate

During the PhD studies a commercial programme (Disperse) [52] was used to derive dispersion curves for single and multi-layered plates of infinite extent. This program has been developed at Imperial College and is based on matrix methods. Initially dispersion curves were obtained for a 5 mm thick aluminium plate (section 2.3). The red curves obtained from Disperse are the symmetrical modes, while the blue curves are the anti-symmetrical curves (figure 4.1). The lowest modes propagating in this structure are the lowest anti-symmetrical (A_0) and symmetrical modes (S_0). The

rest of the curves correspond to higher order symmetric and anti-symmetric modes. In chapter 6 the detection of defects in a single layer plate was investigated using the first anti-symmetrical mode A_0 at a frequency thickness (0.5 MHz mm) region below the cut-off for higher order modes. The dominant displacement of the A_0 mode is a motion in the thickness direction of the plate. For low frequencies the out-of-plane motion of the A_0 mode becomes a pure bending wave, while for higher frequencies rotary inertia and shear motion become important [53]. In the next section some results will be presented of a study made on the wave propagation of guided waves in a multi-layered plate.

4.1.2 Multi-layered plate

The multi-layered plate studied, had a total thickness of 6.2 mm and consists of two 3 mm thick aluminium adherents (2014-T6) bonded by a less stiff 0.2 mm thick adhesive layer (HYSOL [32]). The dispersion curves in figure 4.2a show similar characteristics to those for a single layer plate (figure 4.1), with symmetric and anti-symmetric propagating modes. In an infinite multi-layered plate, consisting of two metallic plates with a weaker adhesive or sealant layer, a bending mode similar to the A_0 mode exists. For frequencies close to the used frequency (115 kHz, frequency thickness: $\sim$ 0.7 MHz mm) the dominant out-of-plane displacement of this A_0-like bending mode does not vary much through the thickness (figure 4.3b), similar to the A_0 mode. Due to the lower stiffness of the adhesive there is a strong shear motion in the bond layer for higher frequencies (figure 4.3b). Figure 4.2b compares the dispersion curves for the A_0-like mode in a multi-layered plate (solid, figure 4.2b) with the A_0 mode in a single layer plate with the same thickness (3 mm) as one of the adherents (dashed, figure 4.2b) and a single layer plate with a thickness (6.2 mm) equal to the total thickness of the multi-layered plate (dotted, figure 4.2b). From this figure one can see that the A_0-like mode for the multi-layered plate and the A_0 mode in a single layer plate which has the same total thickness as the multi-layered plate, agree well with

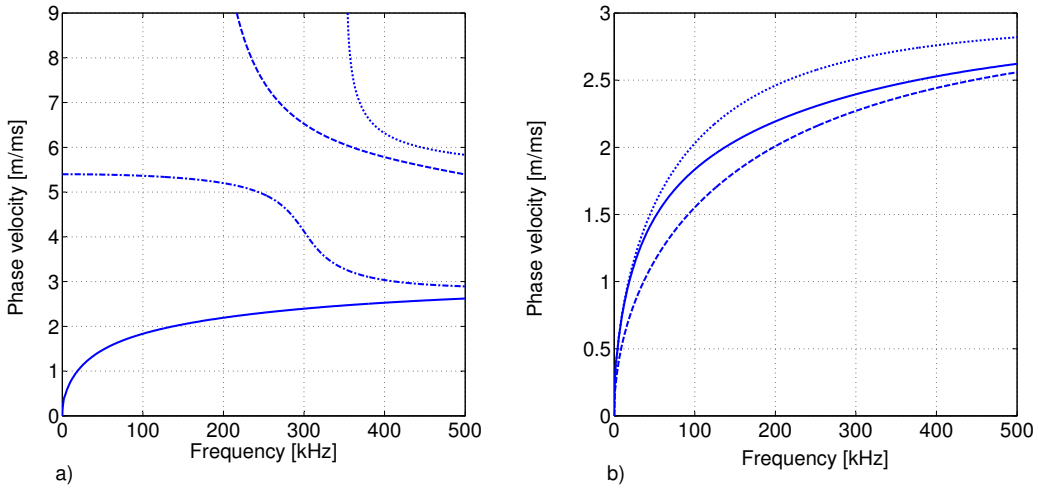

Figure 4.2: (a) Dispersion curves for an infinite multi-layered plate obtained with Disperse; A_0-like mode (solid), S_0-like mode (dash-dotted), A_1-like mode (dashed), S_1-like mode (dotted); (b) dispersion curves for the lowest flexural modes in multi- and single layer plates; A_0-like mode (solid), A_0 mode in 3 mm thick alu. plate (dashed), A_0 mode 6.2 mm thick plate (dotted).

each other for low frequencies (below 50 kHz). The mode shapes (20 kHz) for the multi-layered plate and the 6.2 mm thick single layer plate are shown in figure 4.3a. It can be seen that both in-plane and out-of-plane displacements agree very well at this frequency, suggesting that this type of multi-layered plate is bending similar to a single layer plate (same thickness). The dispersion curve of the A_0-like mode in the multi-layered plate and the A_0 mode in a 3 mm thick single layer plate show good agreement for higher frequencies [54]. Good agreement is found in the out-of-plane mode shapes (500 kHz) in the adherents for the A_0-like mode and the A_0 mode in a single layer plate with the same thickness as one of the metallic layers (figure 4.3c). Because of the resistance caused by the adhesive layer, the in-plane motion at the interface between the adhesive and the adherent in the multi-layered plate (figure 4.3c) is slightly smaller than the corresponding motion in a single layer (figure 4.3c). Overall there is a good agreement for the motion for these two structures suggesting that the wave propagation in a multi-layered structure at high frequencies is similar to the guided wave propagating in a single layer plate with the same thickness as one of the adherents.

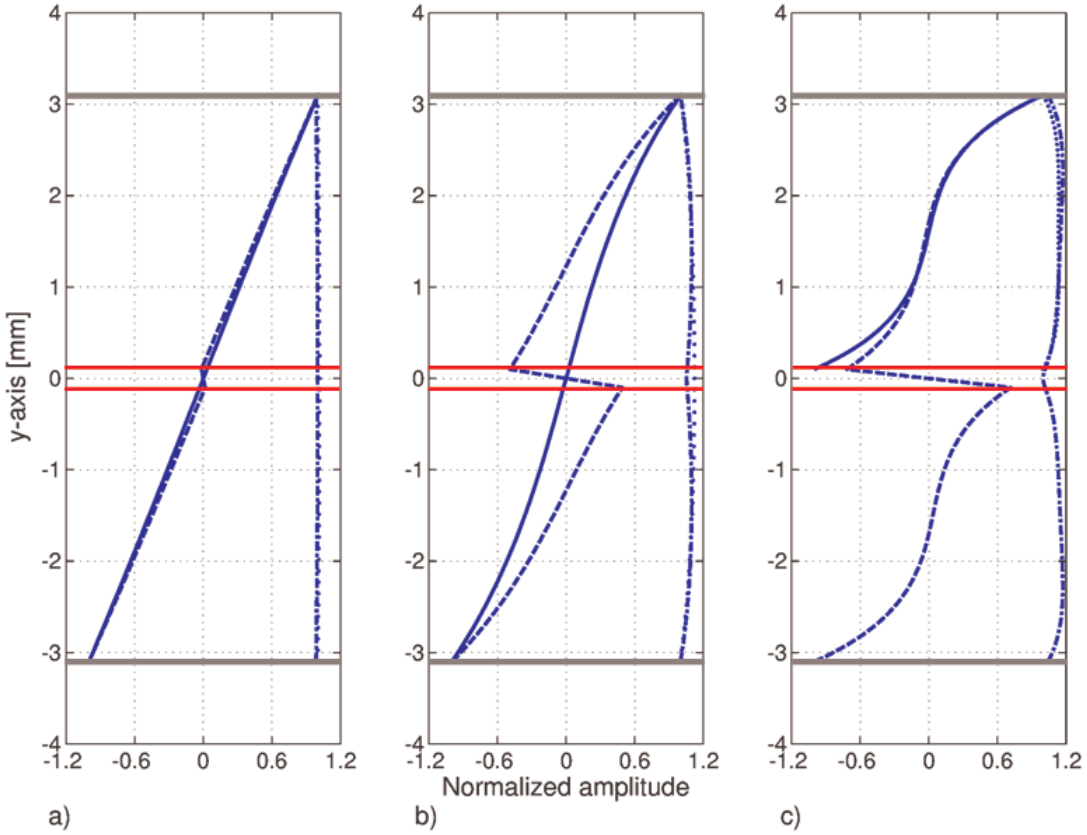

Figure 4.3: Mode shapes for the lowest flexural mode (A_0-like mode) in a multi-layered plate (6.2 mm thick) compared to the A_0 mode in single layer plates; A_0-like mode (dashed, in plane displ.; dashed-dotted, out-of-plane displ.), A_0 (solid, in plane displ.; dotted, out-of-plane displ.); (a) $f = 20$ kHz, 6.2 mm thick aluminium plate; (b) $f = 115$ kHz, 6.2 mm thick aluminium plate; (c) $f = 500$ kHz, 3 mm thick aluminium plate.

The previous sections presented results from the wave propagation in single and multi-layered plates with finite thickness, but of infinite extent. It was shown that for low frequencies a multi-layered plate is bending similar to a single layer plate with the same total thickness. For higher frequencies the wave propagation in a multi-layered structure is similar to the guided wave propagating in a single layer plate with the same thickness as one of the layers. In the next sections the wave propagation in the single and multi-layered tensile specimens (section 2.2.1) is analysed.

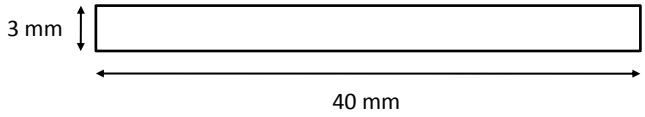

Figure 4.4: Single layer bar of rectangular cross section.

4.2 Plates of finite width

Most of the early theory for guided waves was developed mainly for single layer isotropic plates of infinite extent [46]. This theory fails though to predict the guided wave propagation in plates of finite width with an arbitrary cross section [38]. In this section some of the physics of the wave propagation in single and multi-layered bars with a rectangular cross section are presented and discussed.

4.2.1 Single layer rectangular bar

The dispersion diagram and mode shapes for a single layer tensile specimen (figure 4.4) were calculated numerically using the SAFE code [33] presented in the previous chapter. The dispersion curves obtained from calculations (figure 4.5) for the single layer tensile specimen (3 mm thick) show multiple modes (across the width) in the

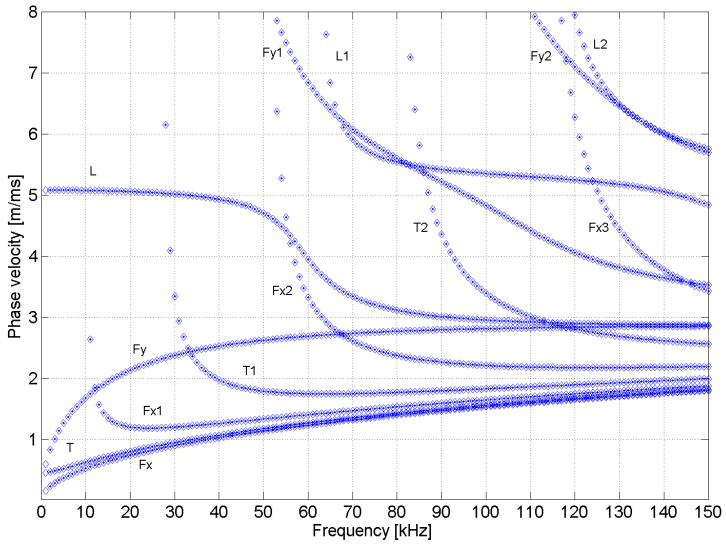

Figure 4.5: Dispersion curves for single layer aluminium tensile specimen shown in figure 4.4 (cross section: 40 mm x 3 mm).

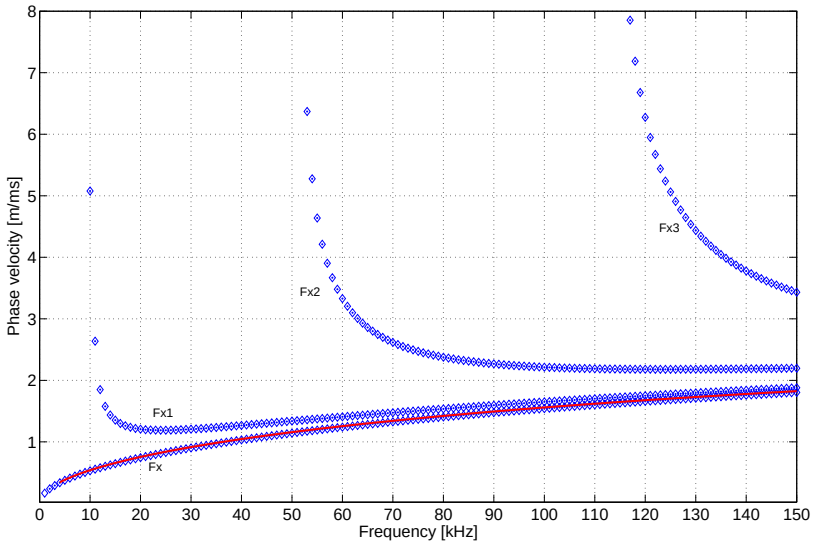

Figure 4.6: Comparison of the A_0 mode in an infinite plate (red solid) with the flexural waves (Fx, $Fx1$, $Fx2$ and $Fx3$) for the single layer bar (blue diamonds) shown in figure 4.4 (cross section: 40 mm x 3 mm).

frequency range of interest (35 - 150 kHz), which was below the cut-off frequency of higher order thickness modes for an infinite single layer plate with the same thickness. The wave modes were classed according to the dominant displacement, namely torsional (T), longitudinal (L), and flexural modes (F). There are two types of flexural modes, Fx denoting the largest displacement in the thickness direction and Fy in the width direction. Higher order modes are denoted with a number, e.g., $Fx1$ is the first higher order flexural mode in the thickness direction.

The wave propagation in similar single and multi-layered plates with a rectangular cross section was studied by Mukdadi et al. [44]. In his work the effect of varying the width on the dispersion of the guided waves in plates of finite width was studied and compared to the dispersion to a plate of infinite width. He showed that the A_0 mode and the lowest flexural mode (Fx) in a bar of rectangular cross section are similar. In figure 4.6 one can see the comparison between the A_0 mode in an infinite plate which was studied earlier in this chapter and the flexural waves (Fx, $Fx1$, $Fx2$, $Fx3$) which were shown in figure 4.5. Similar to the results found by Mukdadi et al., figure 4.6 shows that the A_0 mode and the Fx mode agree well with each other for

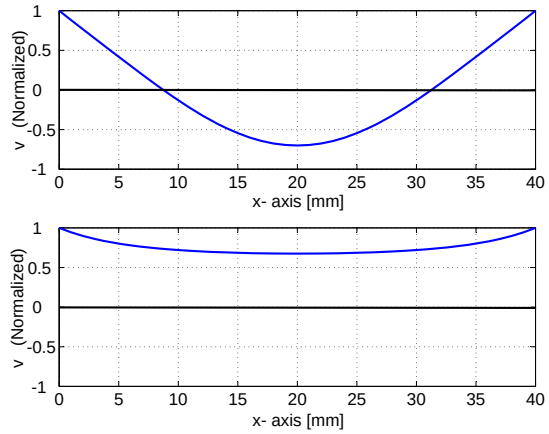

Figure 4.7: Amplitude (out-of-plane) variation across the width evaluated at the top surface of the bar at 35 kHz, for Fx (bottom) and $Fx1$ (top); cross section: 40 mm x 3 mm.

the frequency range of interest. From the same figure it is possible to estimate the cut-off frequency for the higher order modes $Fx1$ and $Fx2$. The cut-off frequency for $Fx1$, $Fx2$ and $Fx3$ is about 10 kHz, 50 kHz and 110 kHz respectively. A very interesting observation is that both higher order modes shown in figure 4.6 show a standing wave like amplitude variation across the width. At a frequency (35 kHz) below the cut-off of the $Fx2$ mode, there are only two modes propagating, making it more easy to analyse the wave propagation in the experiments. The amplitude across the width of the Fx and $Fx1$ modes at 35 kHz can be seen in figure 4.7. The lowest flexural mode (Fx) has an almost constant amplitude across the width, with an exception at the edges of the specimen, where a higher amplitude is observed. This is in good agreement with the findings of Fong [55]. On the other hand the first higher mode $Fx1$ has a standing wave amplitude variation across the width. Multi-layered bars show similar characteristics as the single layer tensile specimen presented in this section.

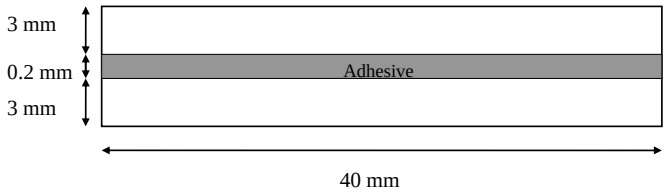

Figure 4.8: Multi-layered bar with a rectangular cross section.

4.2.2 Multi-layered rectangular bar

In this section the wave propagation in a multi-layered tensile specimen with a rectangular cross section (figure 4.8) is presented. The SAFE code presented in the previous chapter was used for studying the wave propagation in multi-layered bars. The dispersion curves for the multi-layered bar obtained with the SAFE code can be seen in figure 4.9. As for the single layer bar, torsional, flexural and longitudinal

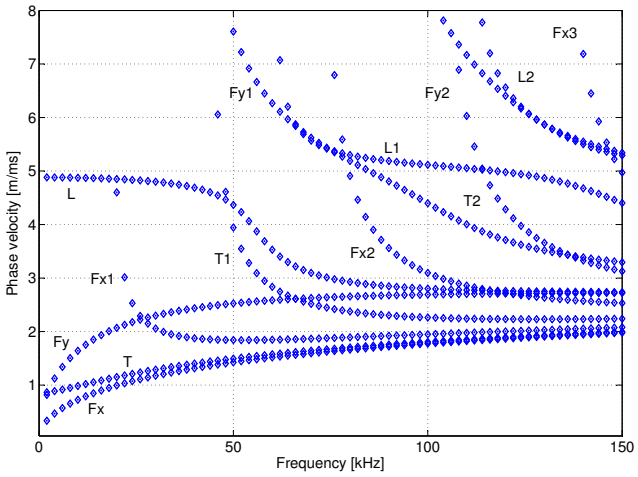

Figure 4.9: Dispersion curves for a multi-layered bar shown in figure 4.8 (cross section 40 mm x 6.2 mm).

modes are the propagating modes in this structure (figure 4.9). The same notation for the different modes is used here as for the single layer bar. These dispersion curves look qualitatively similar to the single layer bar presented in the previous section. One of the main similarities is that there are four flexural modes ($Fx, Fx1, Fx2, Fx3$) in a frequency interval between 0 - 150 kHz in these two structures. Despite this similarity between the single and the multi-layered bar, there are also some differences

between the dispersion curves, as for instance the cut-off frequencies for the higher order flexural width modes. The cut-off frequency for the $Fx1$ mode is 20 kHz, for the $Fx2$ mode about 70 kHz and for the $Fx3$ mode the cut-off frequency is about 135 kHz. The corresponding cut-off frequencies for the single layer specimen was 10 kHz for the $Fx1$ mode, 50 kHz for the $Fx2$ mode and 115 kHz for the $Fx3$ mode. The used frequency (115 kHz) for the multi-layered tensile specimen was chosen

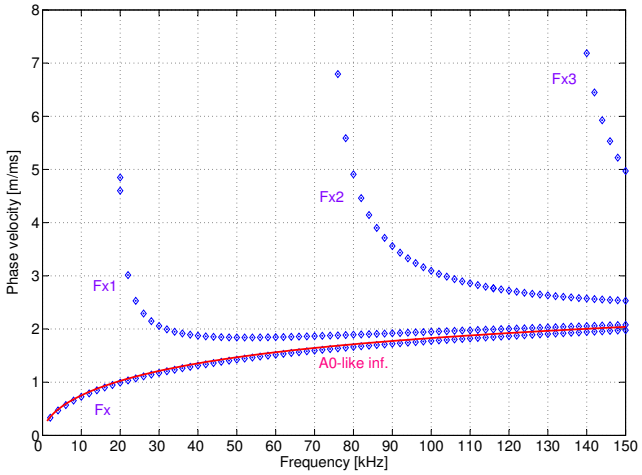

Figure 4.10: Comparison of the A_0-like mode in an multi-layered infinite plate with the flexural waves (Fx, $Fx1$, $Fx2$, $Fx3$) for the multi-layered bar shown in figure 4.8

below the cut-off frequency for $Fx3$. Similar to the single layer plate and bar the dispersion curve of Fx agrees very well with the A_0-like mode in the multi-layered plate. Mode shapes across the width were evaluated at the used frequency (115 kHz). The amplitude variations for the different flexural modes are presented in figure 4.11a. Similar to the Fx mode in a single layer bar, the amplitude across the width is almost constant (figure 4.11a, bottom). The first higher mode $Fx1$ in a multi-layered bar has standing wave amplitude variation with almost a wavelength across the width (figure 4.11a, centre), while the second higher order mode ($Fx2$) has almost two wavelengths across the width (figure 4.11a, top). The mode shapes through the thickness (115 kHz) for three flexural modes (Fx, $Fx1$, $Fx2$) are compared to the thickness mode shape of the A_0-like mode (figure 4.11b). The thickness mode shapes for the Fx mode (figure 4.11b, left) and the $Fx1$ mode (figure 4.11b, centre) agree

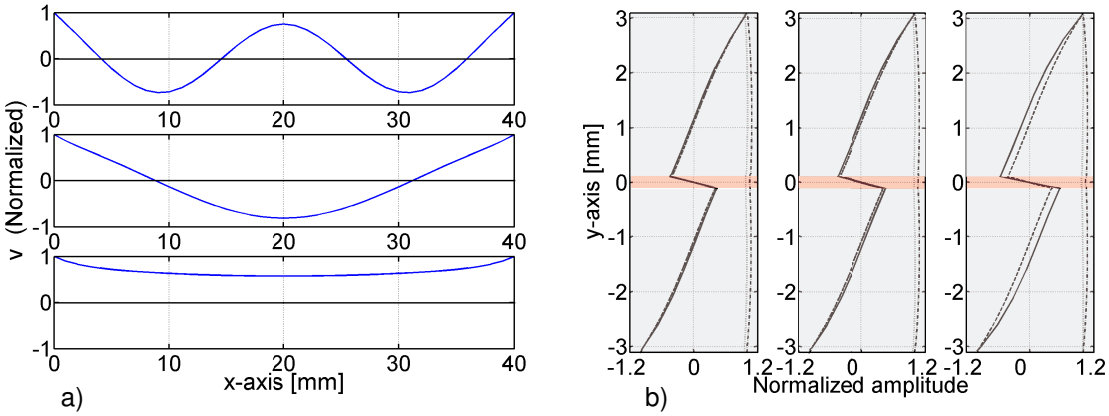

Figure 4.11: Gray colour: adherents; red colour: adhesive layer; (a) mode shapes (out-of-plane amplitude) across the width (115 kHz): $Fx2$ (top), $Fx1$ (centre), Fx (bottom); (b) mode shapes through the thickness (115 kHz): Fx (left), $Fx1$ (centre), $Fx2$ (right): out-of-plane displacement (dash, dotted) and in-plane displacement (solid) for Fx, $Fx1$, and $Fx2$, out-of-plane displacement (dotted) and in-plane displacement (dashed) for the A_0-like bending mode.

very well with the mode shape of the A_0-like bending mode. A small difference in the thickness mode shapes can be seen for the in-plane displacement of the $Fx2$ mode (solid line) and the A_0-like mode (dashed line). These results suggest that similar sensitivity to defects for the flexural width modes and the A_0-like mode (inspection of large multi-layered structures) can be expected.

4.2.3 Influence of specimen width

In order to determine an appropriate width for the multi-layered tensile specimen used for the fatigue experiments and for defect detection with guided waves, dispersion curves were obtained for wider bars. The case of study is a multi-layered bar with the same thickness as in the specimen studied previously (6.2 mm), but instead of 40 mm its width was increased to 70 mm.

The dispersion curves for the flexural modes (thickness direction) are shown in figure 4.12. As expected it is seen that the cut-off frequencies for the higher modes are lower in a 70 mm wide bar than in the 40 mm wide. This agrees with the work presented by Mukdadi et al. [44] where it was shown that the number of modes propagating within a frequency interval increase with increasing width. This could

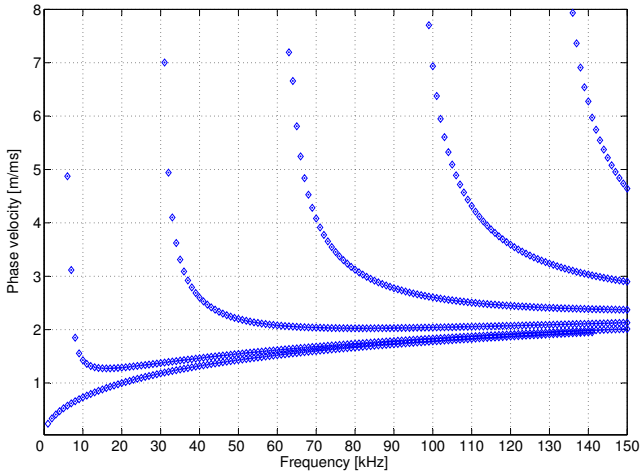

Figure 4.12: Dispersion curves for a 6.2 mm thick and 70 mm wide multi-layered bar.

make the understanding of the wave propagation and the scattering of these waves at fastener holes more difficult to understand. The width for the tensile specimen used in the fatigue experiments was therefore chosen as 40 mm.

4.3 Summary

In this chapter the propagation of guided waves in a single and a multi-layered plate was studied. The main purpose of the studies presented here was to understand the wave propagation in multi-layered plates and tensile specimen. This will help to understand the excited wave field (chapter 5) and the scattering (chapter 6) in these structures. Comparing the obtained results, it was shown that for low frequencies the dispersion curve and out-of-plane mode shape of the A_0-like mode in a multi-layered plate is similar to the A_0 mode in a single layer plate with the same thickness. For higher frequencies the dispersion curve and mode shape (in the adherents) of the A_0-like mode is similar to a single layer plate with the same thickness as one of the adherents.

Another very important part of this thesis is the wave propagation in bars of rectangular cross section. Dispersion curves in a single layer tensile specimen were presented and compared to the dispersion curves of the single layer plate. It was seen

that higher order width modes can propagate in the tensile specimens. The higher order width modes that can propagate in these bar structures show an amplitude variation across the width in the used frequency range (35 - 115 kHz). It was shown that for the working frequency (35 kHz) these amplitude variations exhibit standing wave characteristics with almost integer of wavelengths across the width. Similar to the results obtained by Mukdadi et al. [44], the dispersion curve of the A_0 mode in a single layer plate is very similar to the lowest flexural mode in a single layer bar (Fx). This lowest flexural wave mode has slightly higher amplitude on the edges of the specimen than in the centre where the amplitude does not vary significantly.

The same similarities between the A_0 mode and the flexural mode (Fx) in the single layer structure were observed for the multi-layered plate and bar. Similar to the single layer specimen the flexural modes in these bar structures show an amplitude variation with almost integer of wavelengths across the width. A comparison of the thickness mode shapes of the A_0-like mode in a multi-layered plate, with the flexural modes (Fx, $Fx1$, $Fx2$) in the multi-layered bar showed good agreement. This indicates that the flexural modes in a multi-layered bar have similar sensitivity to defects as the A_0-like mode in a multi-layered plate.

In the last part of this chapter the influence on the dispersion curves when the width of the rectangular bars is changed was studied. The most important result from this investigation is that, the cut-off frequencies for the flexural width modes in a bar of rectangular cross section are lowered as the width increases, thus there will be more modes propagating within a frequency interval as the width increases.

Chapter 5

Excitation of guided ultrasonic waves in tensile specimen

The thickness mode shape of the A_0-like mode in a large multi-layered plate was seen to be very similar to the thickness mode shapes of the flexural modes (Fx, $Fx1$ and $Fx2$). This suggests that similar sensitivity for defects can be expected in these two different structures. Initial experiments studied the possibility of exciting the Fx mode which has a constant amplitude across the width of the specimen. Results presented in this chapter investigated also the possibility of exciting other flexural modes at low frequencies (35 - 115 kHz), using transducers permanently attached to the tensile specimens.

The type of transducers which were used in these experiments were PZT discs and plates. The reason for this choice of transducers is because it is easy to attach them to the structure and that they are relatively inexpensive. These transducers have a proven track record for Lamb wave generation in plate structures [1, 56]. Even though this type of transducers has been used in large plate structures, there is not much work which has been published for tensile specimen. Even less work has been done investigating the selective excitation of guided waves in tensile specimens by using permanently attached PZT transducers. Fong [55] used PZT plates to excite guided ultrasonic waves for studying the wave propagation in a curved plate strip.

These investigations were performed at much higher excitation frequencies (0.45 - 1.3 MHz) compared to the studies presented here. Fromme [1] used the same type of PZT plates aiming to excite the lowest flexural mode (Fx) in a single layer tensile specimen, but no detailed study was made quantifying the excited wave field. In the first part of this chapter, results are presented from studies which investigated the wave field excited by a PZT plate, placed across the entire width of the specimen. Results are thereafter presented from the studies investigating the excitation of flexural waves by placing multiple PZT discs across the width of the tensile specimen. The main idea behind these two methods was to get a fairly constant pressure across the width similar to the uniform amplitude of the Fx mode. FE simulations were performed and compared to the experiments. The experimental results showed that neither the PZT plate nor the multiple discs excited the desired mode to a sufficient degree. For this reason another method was investigated in order to isolate this mode. Instead of approximating the mode shape of the Fx mode across the width, it was attempted to suppress any unwanted modes, using as few PZT discs as possible. To do this PZT discs were placed at the nodes of the mode to be suppressed (referred to as the mode suppression method). The results showed an improvement compared to the multiple discs placed across the width, but did not manage to isolate the Fx mode. Not being able to isolate the lowest Fx mode, the studies on the multi-layered tensile specimens presented at the end of this chapter focused on the excitation of the first higher order flexural mode ($Fx1$), which as the Fx mode has a very similar mode shape through the thickness to the A_0-like mode. The main aim of these studies was to obtain a repeatable amplitude pattern, which is important for the repeatability of the fatigue crack growth monitoring measurements (chapter 7).

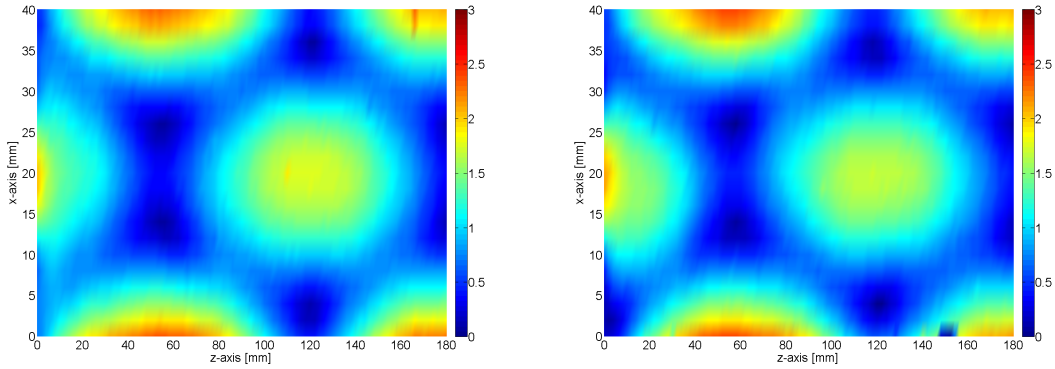

(a) (b)

Figure 5.1: Comparison between wave field amplitude (normalized) of (a) plate 1 and (b) plate 2. Amplitude measured on the surface (40 mm x 180 mm) and excited (f = 35 kHz) by a PZT plate. The waves are propagating along the positive z-direction (length direction).

5.1 PZT plate

5.1.1 Preliminary measurements

At the excitation frequency there are six possible modes that can propagate (chapter 4). In the studies performed here the out-of-plane component of the wave field was measured. This and the fact that the transducers excite waves with predominant displacements in the thickness direction [1, 55], only the torsional ($T, T1$) and flexural modes ($Fx, Fx1$) were monitored. In order to avoid to excite the second higher flexural mode ($Fx2$) which has a cut-off frequency at about 50 kHz figure 4.6, the frequency was chosen as 35 kHz.

The main aim of these investigations was to understand the guided wave field excited by a PZT plate. The PZT plate (40 mm wide, 1 mm thick and 5 mm long) described in chapter 2, was glued using an epoxy based glue to the surface of the specimen. As mentioned above the centre frequency of the excitation signal was 35 kHz. In order to investigate how repeatable the measurements are, two measurements were performed on the same specimen but with different PZT plates.

Shown in figure 5.1a and 5.1b are the normalized amplitudes obtained from the two measurements, evaluated at the centre frequency. The normalization is

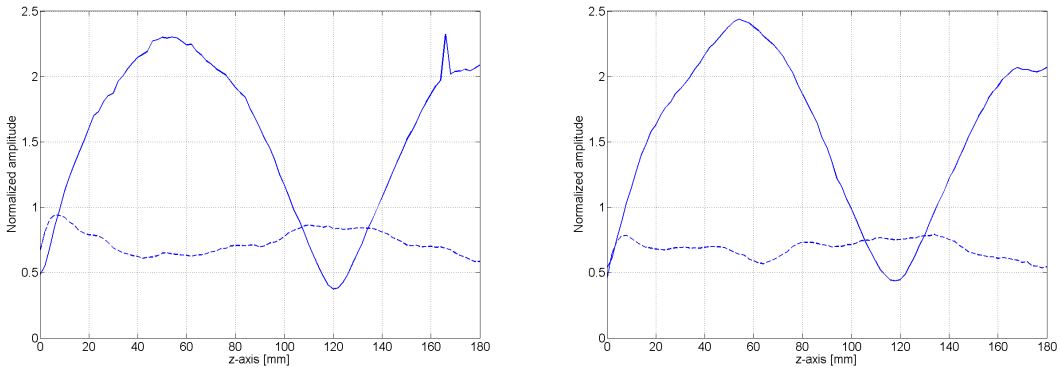

(a) (b)

Figure 5.2: Wave field amplitude (f = 35 kHz) taken along two lines from (a) figure 5.1a and (b) figure 5.1b; solid curve: x = 0 mm figure 5.1; dashed curve: x = 9 mm figure 5.1.

performed by taking the average of the wave field and dividing it by that number. In all of the figures presented in this chapter the waves are propagating along the z-axis (length direction). Figures 5.1a and 5.1b show a similar, symmetric amplitude pattern with respect to the centre of the plate. These amplitude patterns are an indication that the predominant modes are symmetrical with respect to the centre line. Seen also is a periodical amplitude variation along the length (wave propagation in z-direction) which is caused by the interference between the two flexural modes (Fx and $Fx1$) that are propagating at that frequency. The wave field amplitude taken along two lines from figure 5.1a and 5.1b (x = 0 mm and x = 9 mm) are presented in figure 5.2a and 5.2b respectively. From these two figures the almost periodical amplitude variation (solid curves, figure 5.2) along the length of the specimens is more evident. The beatlength can be estimated from the above figure by taking the distance between the points with the largest amplitude. In figure 5.2a the points with largest amplitude were manually picked from this figure and are located at 56 mm and 180 mm. This gives a beatlength of 124 mm. The beatlength (Λ) was calculated theoretically using the following equation [57]:

$$\Lambda = \frac{2\pi}{|k_1 - k_2|}, \tag{5.1}$$

where k_1 is the wavenumber for the first and k_2 is the wavenumber for the second mode. At 35 kHz the wavenumbers for the two flexural modes Fx and $Fx1$ are 0.226 $\frac{1}{mm}$ and 0.178 $\frac{1}{mm}$ respectively. The beatlength obtained by inserting these wavenumbers in equation 5.1 is 131 mm. The most probable reason for the deviation is due to the fact that the amplitude plot (figure 5.2a), from which the beatlength was estimated, did not cover a long enough distance. From these preliminary experiments it can be concluded that the excited modes are most probably the two flexural modes (Fx and $Fx1$).

5.1.2 Evaluation procedure for amplitude ratio

Another important parameter for the wave propagation in these structures is the amplitude ratio between the two different flexural modes. From figures 5.2a and 5.2b, one can obtain the amplitudes for the two flexural modes. To obtain the value of Fx one can take the average of the almost constant curve at the node of $Fx1$ (dashed curve, figure 5.2a). The average amplitude of Fx at that width location is about 0.75. In order to get the amplitude of Fx at the edge of the specimen, this amplitude value (0.75) needs to be multiplied by the relative width mode shape amplitude ratio (1/0.74) at the two width locations (x = 0 mm and 9 mm from the side, figure 4.7). The amplitude of Fx is calculated to about 1.05 at the edge. To obtain the value of $Fx1$ one can look on the interference curve at the edge of the specimen (solid curve, figure 5.2a). The two modes are in phase at the largest value (2.3 at 56 mm, solid curve figure 5.2a) on that curve. This gives a value of 1.3 for $Fx1$ and an amplitude ratio between the modes ($Fx/Fx1$) of about 0.77. This value is similar for the other measurement (0.7). To get more accurate results for the amplitude ratio and to verify that the two modes are the flexural modes, experiments were conducted on longer specimens. In this way the wave field could be measured further away from the PZT plate and over a longer distance to get a better measure of the beatlength.

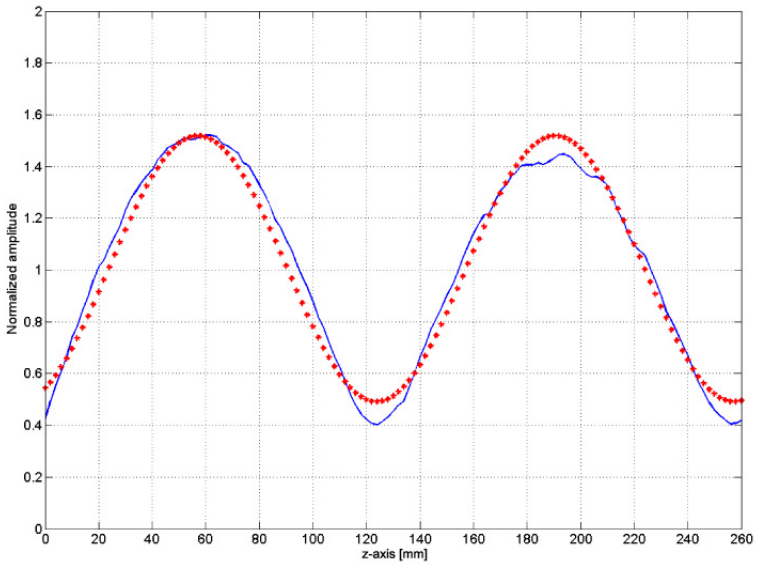

Figure 5.3: Amplitude measured (f = 35 kHz) along a line (centre of specimen) on the surface of a finite width aluminium plate (cross section: 40 mm x 3 mm); blue-solid curve: measurements; red-stars: fitted curve.

Another possible source of error is the manual estimation of the beatlength from the measurements.To get more accurate values for the beatlength, Matlab was used to fit a function to the measured interference pattern.

5.1.3 Longer specimens

The specimens used for this part of the investigations had the same width and thickness as for the initial measurements, but were longer (1 m instead of 0.6 m). In the preliminary set of experiments, guided ultrasonic waves were excited (35 kHz) using a PZT plate. The PZT plate was bonded 190 mm away from one end of the specimen, while the excited wave field was monitored on a line in the centre of the specimen. The monitoring started 40 mm away from the transducer and covered a length of 260 mm, with measurements taken every 2 mm.

The results obtained from these measurements (figure 5.3) show a similar amplitude variation as the previous experiments conducted on the shorter specimens. The wave field amplitude is normalized with the average value calculated from all

of the measurement points along the length. The measured amplitude (blue-solid) and the corresponding fitted curve are shown in the figure above (red-stars). For this particular case a sinusoidal function was used for the best fit of the measured amplitude. The beatlength obtained from the Matlab based program, which was used to fit the function, is 133.4 mm. This value is in good agreement with the theoretical value (131 mm), showing that the predominant propagating modes are the two lowest flexural modes (Fx and $Fx1$). Comparing this experiment to the previous experiments performed on the shorter specimen, one can conclude that the near field of the transducer and the length of the measured interference pattern influenced the obtained value for the beatlength.

Similar to the previous section, the amplitudes for the two flexural modes were obtained by investigating their interference patterns. The main difference between the method used here to obtain the amplitude ratio and the previous method used on the shorter specimens is that here they are taken from the same line measurement on the centre of the specimen. This was done in order to avoid the noise due to the bad reflection of the laser beam at the edge of the specimen. The ratios were obtained by setting up the following equation system:

$$0.74Fx1 + 0.69Fx = 1.52, \tag{5.2}$$

$$0.74Fx1 - 0.69Fx = 0.40. \tag{5.3}$$

In the first equation (5.2) the two flexural modes, which are multiplied by their relative mode shape amplitude at the centre, are assumed to be in phase with each other leading to the highest amplitude. This value was obtained by the program at 60 mm in figure 5.3 with a magnitude of 1.52. In the second equation (5.3) the modes are out-of phase resulting in the lowest value (0.4) at 124 mm in figure 5.3. These equations assume that the $Fx1$ mode is stronger excited than Fx, which was seen from the previous experiments. The amplitude ratio obtained by solving this equation system is about 0.62, which is close to the value obtained for the

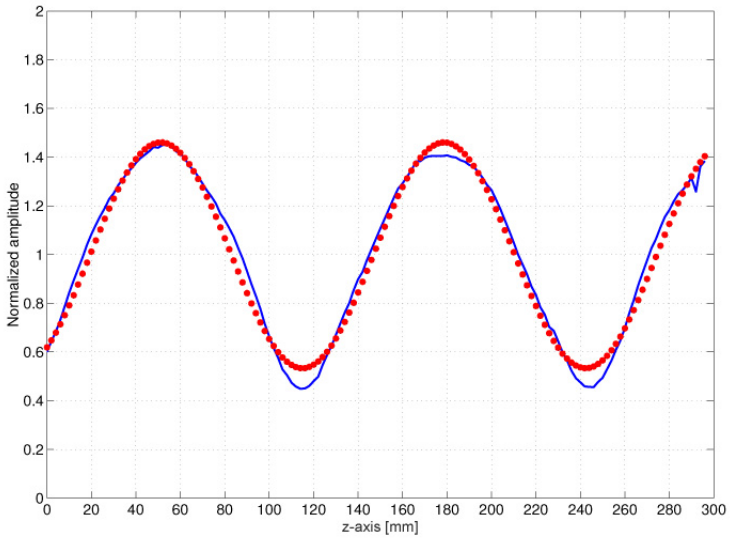

Figure 5.4: Amplitude measured (f = 35 kHz) along a line (centre of specimen) on the surface of a finite width aluminium plate (cross section: 40 mm x 3 mm); blue-solid curve: measurements; red-stars: fitted curve.

shorter tensile specimens. In order to investigate the repeatability of these results a similar investigation was carried out on another specimen of the same material and dimensions as this specimen. The excitation consisted of a PZT plate, but in order to exclude end reflections, the distance from one end of the specimen to the PZT plate was increased from 190 mm to 250 mm. The PZT plate was excited at the same frequency, while the measurements were carried out over a longer distance (300 mm). The results obtained from these measurements (figure 5.4) show a similar amplitude variation as in the previous experiments (figure 5.3). The measured amplitude (blue-solid) and the corresponding fitted curve is shown in the above figure (red-stars). The beatlength between the two modes obtained from the Matlab based program is 128 mm. This value is in good agreement with the theoretical value (131 mm) and the beatlength obtained from the experiments performed on the previous specimen (133 mm). This verifies that the predominant propagating modes with this type of excitation are the two lowest flexural modes (Fx and $Fx1$). The amplitude ratio obtained similarly as for the other specimens is about 0.6. The obtained amplitude ratios for the single layer tensile specimen indicate that the PZT plates are not able

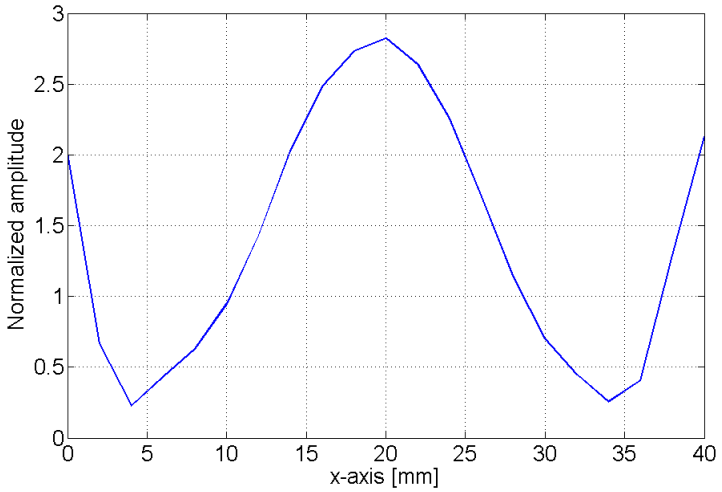

Figure 5.5: Measured amplitude (f = 35 kHz) across the width of the specimen under the PZT plate (opposite side from the transducer).

to excite the desired mode (Fx) to a large extent, but instead they excite higher modes (for this particular case the $Fx1$ mode), leading to an amplitude variation along and across the specimen. The reason for this was investigated by studying the amplitude distribution under the transducer. The amplitude was measured across the width of the specimen (on a line) on the opposite surface from where the transducer was bonded. The measured out-of-plane displacement evaluated at 35 kHz is shown in figure 5.5. It can be seen that the amplitude is not uniform across the width under the transducer, thus exciting the $Fx1$ mode more. In the next section a different approach is taken for isolating the Fx mode.

5.2 Multiple PZT discs

Similar to the previous section the main idea behind placing multiple PZT discs across the width of the specimen is to excite the Fx mode by approximating its almost constant width mode shape. The aim of the investigations presented here is to find out how many PZT discs are needed to excite the Fx mode. Both FE simulations and experiments were performed to investigate this. The results from the FE studies will be presented next.

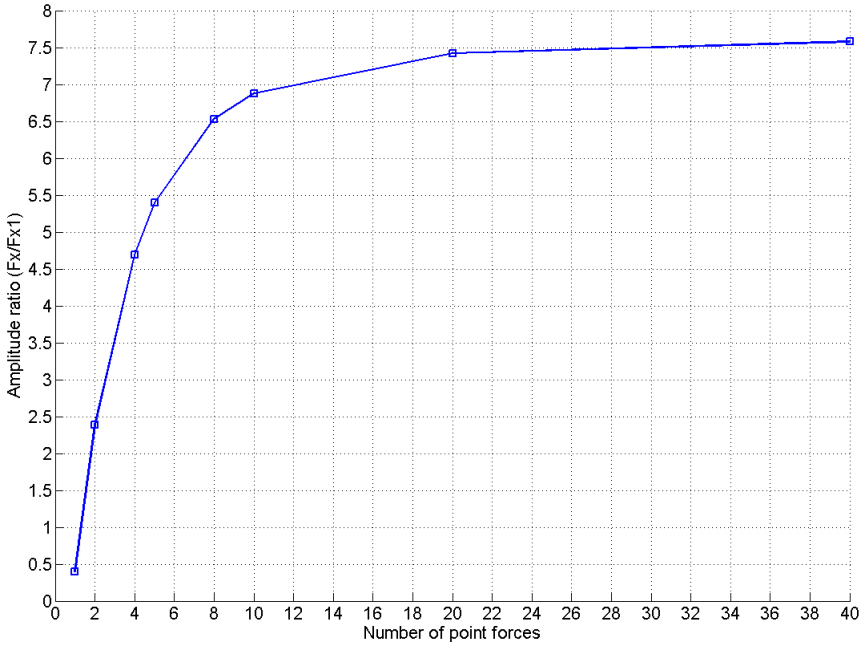

Figure 5.6: Graph showing number of point forces used in the FE simulations against the calculated amplitude ratio between Fx and $Fx1$ modes.

5.2.1 FE simulations

For the excitation of the A_0 mode in large plates the PZT discs are usually modelled as out-of-plane point forces (chapter 3). For this to be a valid approximation the diameter of the PZT discs should ideally be smaller than a quarter of the wavelength. This requirement is valid in this cases where the wavelength of the A_0 mode at 35 kHz is about 28 mm and the PZT diameter is 5 mm. The number of point forces considered across the width of the specimens were 1, 2, 4, 5, 8 10, 20 and 40. In the first part of these simulations, a single point force was placed in the centre of the specimen and 0.5 m away from one end. For more than one point force, the point forces were placed equidistant to each other. E.g., two point forces were placed with a 20 mm distance between each other, 10 mm and 30 mm away from one side respectively. The rest of the point forces were placed in a similar way, with the first point force being placed at $\frac{40}{2N}$ [mm] (N being the number of point forces) from one side and the rest were placed in multiples of $\frac{40}{N}$ from the first point force. Thus for four point forces it would mean that the first point is placed 5 mm away from one side, and the rest of the point forces every 10 mm away. The results (figure 5.6) show

that this type of excitation (35 kHz) will mainly result in flexural modes ($Fx, Fx1$). It can also be seen that the larger the number of point forces used the more Fx will be excited. This can be explained by the fact that the almost constant width mode shape of the Fx mode is approximated better for more point forces. Forty point forces across the width the amplitude ratio is about 7.5. On the other hand, one point force excites the $Fx1$ mode more than Fx. This happens because the point force pushes only the centre of the specimen in one direction, thus resembling the mode shape of $Fx1$ (bottom figure 4.7). It can be seen that for five PZT discs the FE simulations predict an amplitude ratio of about five. This would result in almost a constant incident wave field (about 20% amplitude variation along the specimen) which would make the interpretetion of the results from the fatigue crack monitoring experiments and scattering measutrements easier. Next results from the studies investigating the possibility of experimentally exciting the Fx mode by using multiple discs are presented. The experiments performed during these studies did not use exactly the same pattern for increasing point forces as in the FE simulations (one, three and five PZT discs were used).

5.2.2 Experiments

Initially experiments were performed using a single PZT disc glued in the middle of the specimen (right, figure 2.6) and 190 mm away from one end. The measured area was 40 mm wide (across the width) starting about 5 mm in front of the disc and going 180 mm along the length on the same surface where the PZT disc was located. The length of the area was selected in this way in order to avoid overlap between the incident wave and the reflected wave from the end of the specimen. In order to see how repeatable the measurements are, four set of measurements were carried out with this excitation configuration, but with different PZT discs every time.

In figure 5.7a the amplitudes at the centre frequency (35 kHz) are shown for the first specimen. The amplitude pattern is symmetric with respect to the middle of

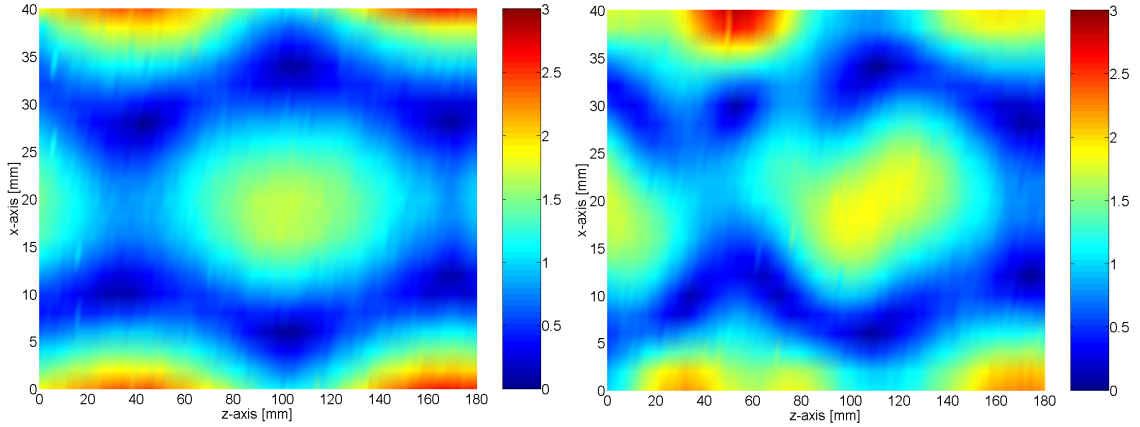

(a) (b)

Figure 5.7: Measured wave field amplitude (f = 35 kHz) on the surface (40 mm x 180 mm) of a finite width plate (40 mm wide); excitation with one PZT disc at the centre of the specimen (x = 20 mm); (a) symmetric and (b) asymmetric amplitude pattern.

the specimen, indicating that the anti-symmetrical torsional modes (T, $T1$) are not strongly excited with this excitation. The wave field exhibits a repeated amplitude variation along the length of the specimen, similar to the PZT plates. This variation is caused by the interference between the two flexural modes (Fx and $Fx1$) that are mostly excited at that frequency. Similar to figure 5.7a, figure 5.7b shows the amplitude from measurements which were done on the same specimen as above, but with a new PZT disc glued on the same place as the disc used for the measurements presented above. Comparing figure 5.7a and figure 5.7b it is possible to see that in the later figure the wave field is not as symmetric as in figure 5.7a. To understand the asymmetric amplitude pattern seen in figure 5.7b, FE simulations were carried out using a single out-of-plane force at the location of the PZT disc. In figure 5.8a the amplitudes at the centre frequency (35 kHz) are shown. The symmetric amplitude pattern seen in figure 5.8a indicates that the torsional modes are not excited to a large extent with a point force in the middle of the specimen. The amplitude variation seen in this figure is very similar to figure 5.7a. FE simulations were conducted using a point force, placed 1 mm away from the centre of the specimen. Figure 5.8b shows the amplitude for the time measurements evaluated at the centre frequency

(35 kHz). Comparing figure 5.7b and figure 5.8b it is possible to see the amplitude patterns are similar. This indicates that the PZT disc used in the measurement was probably slightly off centre, exciting torsional modes. To verify that a torsional mode was excited, a 2D FFT [58] of the measured signal at the edge of the specimen was taken. The amplitude of the obtained transform, shown in figure 5.9, reveals the existence of the second torsional mode ($T1$). This mode is causing the shift in the amplitude pattern seen in figures 5.8b and 5.7b. Looking at the dispersion curves it is possible to estimate the cut-off frequency of the torsional mode ($T1$). The excitation frequency (35 kHz), is close to the cut-off frequency of this torsional mode ($\sim$ 28 kHz) resulting in a width vibration close to the excitation. From the 2D FFT and from the interference between the torsional mode with the flexural modes it is difficult to determine the amplitude of this mode. It can though be seen that the torsional mode is not excited as strongly as the two flexural modes.

Two more measurements were taken with new PZT discs to further investigate the repeatability. Similar to what is shown in figure 5.7b one of the experiments showed an asymmetric amplitude pattern. To summarize, from the four measurements two showed an asymmetric pattern. The amplitude ratio ($Fx/Fx1$), which was obtained in the same way as for the longer specimens (PZT plate) presented earlier, ranged

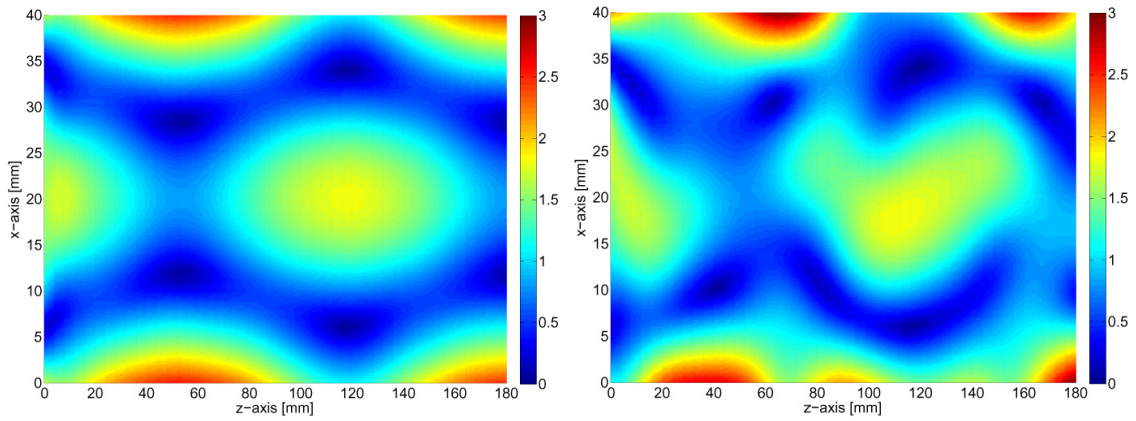

(a) (b)

Figure 5.8: Calculated (FE) wave field amplitude (f = 35 kHz) on the surface (40 mm x 180 mm) of a finite width plate (40 mm wide); excitation with one point force; (a) at the centre of the specimen (x = 20 mm) and (b) 1 mm off centre (x = 21 mm).

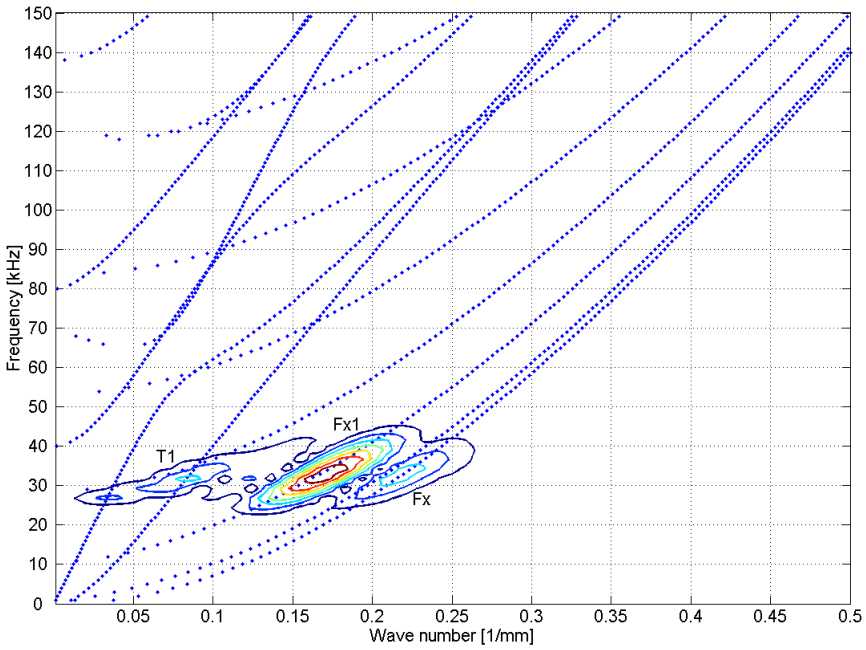

Figure 5.9: Dispersion curves for the single layer tensile specimen. Contour curves overlaid on the dispersion curves is the 2D FFT, taken on the edge of the specimen.

for the four measurements between 0.36 and 0.41 (lower than PZT plates). Good agreement was found between measurements and FE simulations, predicting an amplitude ratio of about 0.4. It can be concluded that this type of excitation did not isolate the Fx mode. Similar to what was said for the FE simulations, this can be explained by the fact that a point force placed in the centre is forcing that location in one direction while the free edges do not move much, exciting $Fx1$ more strongly than the Fx mode which has a constant amplitude across the width.

In the investigations presented next, three PZT discs were used in an attempt to excite the Fx mode. The PZT discs were placed 190 mm away from one end of the specimen and symmetrically about its centre (4, 20 and 36 mm away from one side). The amplitudes of the measurements evaluated at the centre frequency (35 kHz) are shown in figure 5.10a. As for the excitation with one PZT disc, two different measurements were carried out using the same specimen. In the later measurement the discs were replaced. Comparing figure 5.10a and 5.10b it is possible to see that the wave field in figure 5.10b is not as symmetric as in figure 5.10a. The asymmetric pattern looks similar to the experiments performed with one PZT disc,

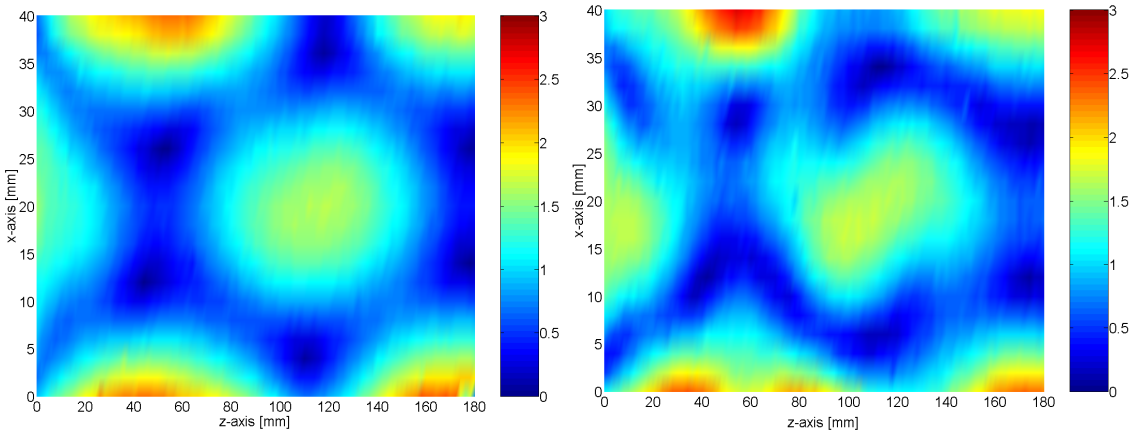

(a) (b)

Figure 5.10: Measured wave field amplitude (f = 35 kHz) on the surface (40 mm x 180 mm) of a finite width plate; excitation with three PZT discs; (a) symmetric and (b) asymmetric amplitude pattern.

where a torsional wave was excited. As for the case with a single PZT disc the excitation of the torsional mode seen here was probably caused by the position of the PZT discs. Another experiment was carried out with this type of excitation. In that experiment the torsional mode was also visible. From the three specimens investigated the torsional mode was excited significantly in two of them. The amplitude ratios ($Fx/Fx1$) obtained from the three measurements ranged between 0.45 and 0.62 (FE prediction: ~ 3). Comparing this to a single disc a very small improvement was made with this type of excitation.

Finally experiments were carried out using five PZT discs trying to excite the Fx mode. In an attempt to obtain the amplitude distribution of this mode across the width, discs were placed symmetrically about the centre of the specimen and across the width, 4, 12, 20, 28 and 36 mm away from the side. Figure 5.11a shows the amplitude at the centre frequency (35 kHz). The wave field shows a similar wave pattern to figures 5.7a and 5.10a. In this case the amplitude is symmetric and the dominant modes are the flexural modes. On the other hand the wave field in figure 5.11b shows a similar wave pattern to the previously shown wave fields which were slightly asymmetric. Another two experiments were carried out with five PZT discs. The amplitude ratios obtained for these cases ranged between 0.43 to 0.62.

Compared to one and three PZT discs very little improvement was made. From the four specimens examined, three showed a significant asymmetry in the amplitude patterns, indicating that the torsional modes were excited to a significant degree.

Placing multiple discs on a tensile specimen did not manage to isolate the Fx mode. Increasing the number of PZT discs placed across the width showed only a small increase in the amplitude ratio between the two flexural modes. Good agreement for the wave propagation was found between experiments and FE simulations for one PZT disc. In the case of five discs FE simulations predict a much larger amplitude ratio (about 5). From these investigations it was also observed that the PZT discs could result in an asymmetric amplitude pattern. The larger the number of discs used, the more difficult it was to obtain a symmetric amplitude pattern. This suggests that as few discs as possible should be used to avoid the excitation of any unwanted torsional modes and in order to compare to FE simulations. From the experiments it was also seen that the replacement of the discs could have an effect on the overall wave field as this was not very repeatable. Two possible reasons for that can be given. The first one is the bonding layer and the second one is the location inaccuracy of the PZT discs.

The possibility of isolating the Fx mode by using only two point forces will be

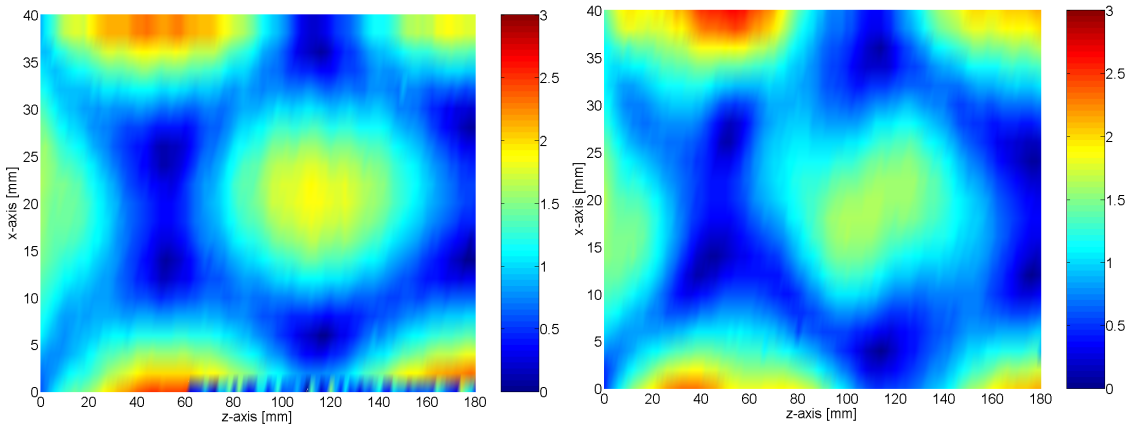

(a) (b)

Figure 5.11: Measured wave field amplitude (f = 35 kHz) on the surface (40 mm x 180 mm) of a finite width plate 40 mm wide; excitation with five PZT discs; (a) symmetric and (b) asymmetric amplitude pattern.

examined. To improve the repeatability of the measurements the discs were placed using a holder which fits on the width of the specimen. In this way the location accuracy could be improved and controlled.

5.3 Mode suppression

5.3.1 FE simulations

In this section a different approach is taken towards trying to isolate the Fx mode in a tensile specimen. The methodology used is based on the suppression of any other modes in order to isolate the desired mode. At the working frequency (35 kHz) there are 6 modes propagating. With the PZT discs vibrating mostly in the out-of-plane direction the longitudinal mode (L) and the flexural mode which has the largest displacement in the width direction (Fy) will not be excited to a significant extent. If the point forces are placed symmetrically about the centre line of the specimen (x = 20 mm) it is possible to eliminate any torsional modes. As it was seen from the previous results the flexural modes are the two main propagating modes in this frequency range. In order to try to eliminate the $Fx1$ mode one could for instance place the discs at points were the $Fx1$ mode will not be excited. This assumption was studied with FE simulations by placing two point forces symmetrically at the nodes of the $Fx1$ mode, 9 mm from each side. The monitoring area (40 mm x 400 mm) did not include the point forces which are placed at z = - 10 mm in figure 5.12. Results from the FE simulations predict an amplitude ratio between the two modes (Fx and $Fx1$) of about 24. This leads to almost constant amplitude (figure 5.12) along the length of the specimen. Across the width of the tensile specimen higher amplitude is found at the edge of the specimens, similar to the mode shape of the predominant Fx mode. As for the previous experiments, mode suppression could be sensitive to the location accuracy of the discs. This was investigated by shifting the point forces along the length and the width by small distances. The shift in the z-direction

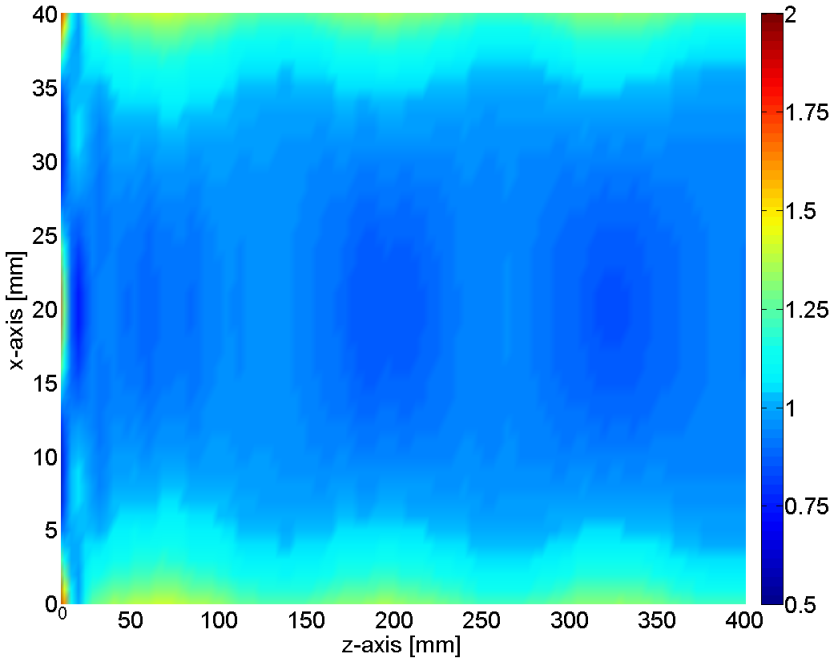

Figure 5.12: Amplitude pattern at 35 kHz obtained from FE simulations for the mode suppression method. Exciting with two point forces placed at z = -10 mm (not shown in this figure) and 9 mm away from the sides (nodes of $Fx1$).

(along length) does not influence the $Fx1$ mode since the point forces still remain on its nodes with respect to the width. On the other hand it influences the amount by which the torsional modes are excited. It was observed that the torsional modes were excited more and more as the shift increases. Figure 5.13 shows the influence of a shift in the width direction on the amplitude ratios for the flexural modes. This shift is influencing the amount by which the $Fx1$ mode is excited since the force is moving away from the node. As the distance increases the $Fx1$ mode is excited more strongly. This asymmetric excitation pattern is also resulting in an increase of the excited torsional modes. Investigations were also carried out by increasing the excitation amplitude of one point force while the position remains fix at the nodes of $Fx1$ to study how the excitation amplitude from the PZT discs is influencing the excited wave field. As expected, it was seen that the ratio between the two flexural modes is not changed with increasing amplitude difference, while as the amplitude increased it was seen that the amount of the torsional modes increased. To conclude, only the shift of the point forces across the width changed the amplitude ratio for

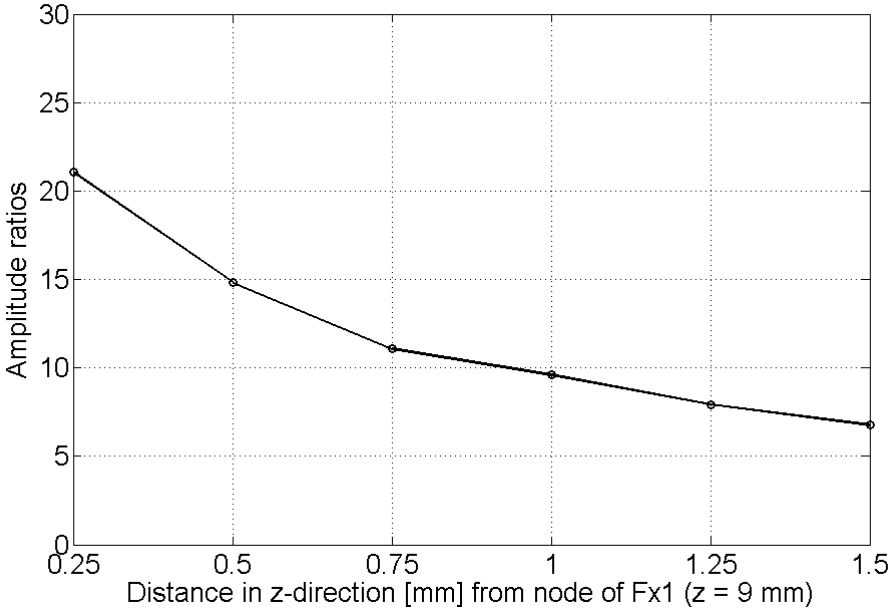

Figure 5.13: Calculated amplitude ratio between Fx and $Fx1$ for different width locations (relative to node of $Fx1$) of one point force (35 kHz).

the flexural modes ($Fx/Fx1$). For a shift of about 1 mm, which is a reasonably large placement inaccuracy using the PZT holder, the amplitude ratio between the flexural modes (about 8) would be still good enough for the fatigue crack monitoring experiments. The placement of the disc in the experiments was measured with a digital caliper resulting in an average measurement of 8.8 mm $\pm$ 0.15 mm from the sides.

5.3.2 Experiments

The FE simulations predicted that the Fx mode can be isolated to a large degree by placing point forces at the nodes of the $Fx1$ mode. Experiments were carried out to investigate this. The specimens used for these experiments had the same dimensions as the FE model presented above. Two PZT discs were placed at the nodes of the $Fx1$ mode about 9 mm away from the sides on the same surface. One main difference between these experiments and the FE simulations is that the extent of the PZT discs (5 mm in diameter) and their extra added mass were not modelled. In order to suppress the torsional modes the discs had to be placed accurately at

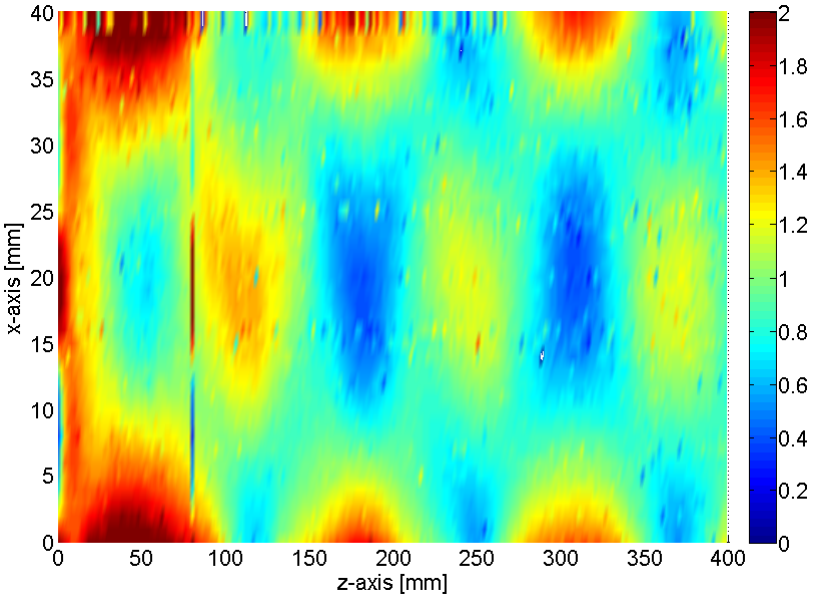

Figure 5.14: Measured amplitude of the wave field on the surface (40 x 180 mm) of a finite width plate (35 kHz, two discs at the nodes of $Fx1$).

these locations. To get an accurate location a disc holder was manufactured out of aluminium. Different to the FE simulations, the results from the measurements (figure 5.14) show a significant amplitude variation across and along the specimen caused by the interference of the two flexural modes (Fx and $Fx1$). The amplitude ratio ($Fx/Fx1$) is in this case about 2.4. The amplitude pattern is symmetric which indicates that the torsional modes are not excited to a significant extent with this excitation setup. Four more measurements were taken with new discs glued on in order to investigate the repeatability of these results. Measurements were taken on a line on the centre of the specimen and 240 mm along the length of the specimens starting 60 mm (along length) away from the centre of the PZT discs. The amplitude ratio for the four measurements is 2.1 (figure 5.15a), 1.8 (figure 5.15b), 2 (figure 5.15c) and 2.1 (figure 5.15d). The average ratio for these four measurements is about two. The average beatlength between Fx and $Fx1$ for these specimens is 128 (theoretical value of 131 mm). With this type of excitation the torsional modes are not as strongly excited as for the previous measurements (multiple discs). This would suggest that the location accuracy of the discs influenced the results, since this time it was controlled using a PZT holder. Even though the torsional modes

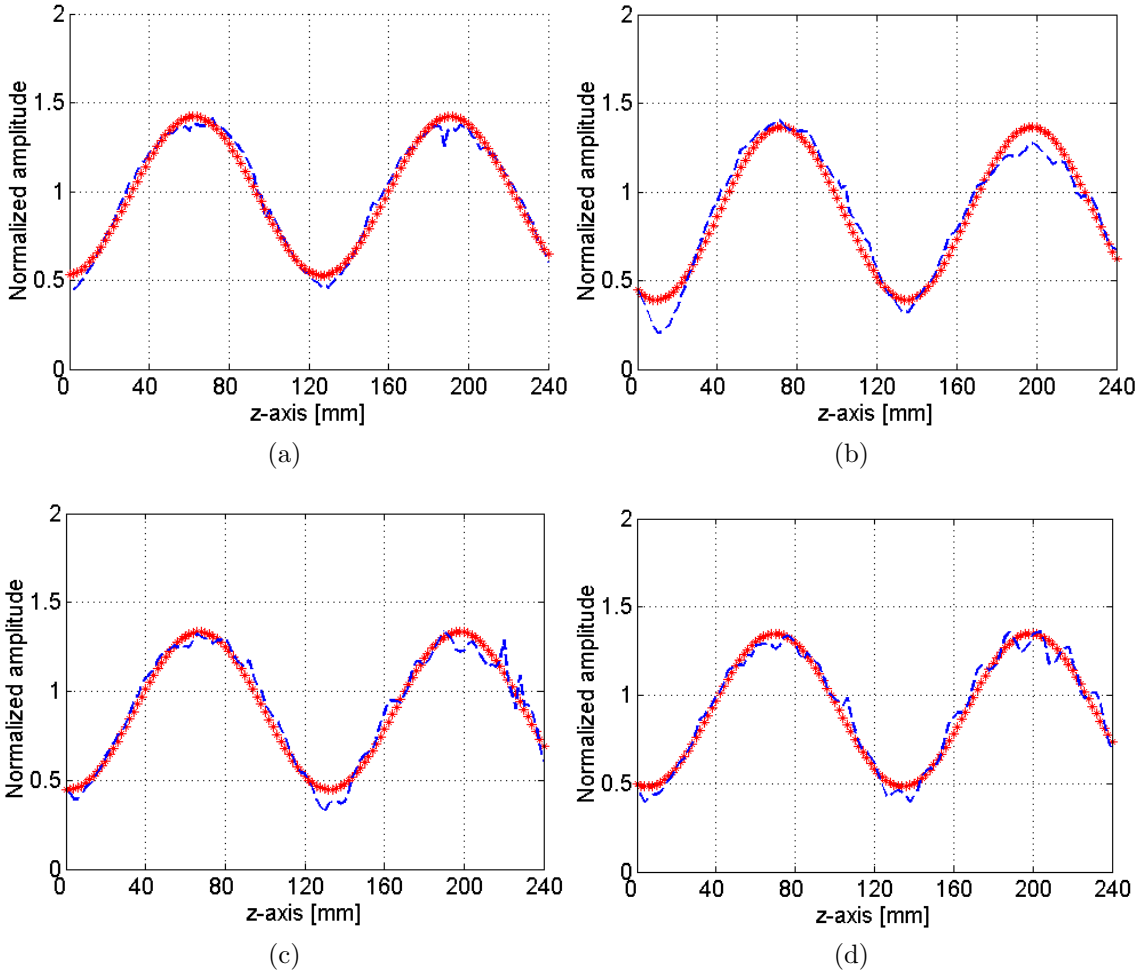

Figure 5.15: Measured wave field amplitude at 35 kHz for four specimens (a) measurement 1; (b) measurement 2; (c) measurement 3; (d) measurement 4.

are not excited to a significant extent and there is an improvement of the amplitude ratio compared to five PZT discs (about four times larger), the measured ratios are still much lower than the ratio predicted from the FE simulations. Two possible reasons for this could be the location of the discs relative to the nodes of $Fx1$ and the amplitude distribution generated by the transducers. Looking at the sensitivity study (FE, figure 5.13) it is possible to say that the location inaccuracy (8.8 mm $\pm$ 0.15 mm from the sides) of the discs cannot account for the large difference between FE simulations and experiments. In order to investigate the second cause the amplitude patterns under the transducers were measured (figure 5.16). Comparing these figures it is very clear that the excitation used in the FE simulation (figure 5.16b) is different from the excitation used in experiments (figure 5.16a), which in turn is causing the

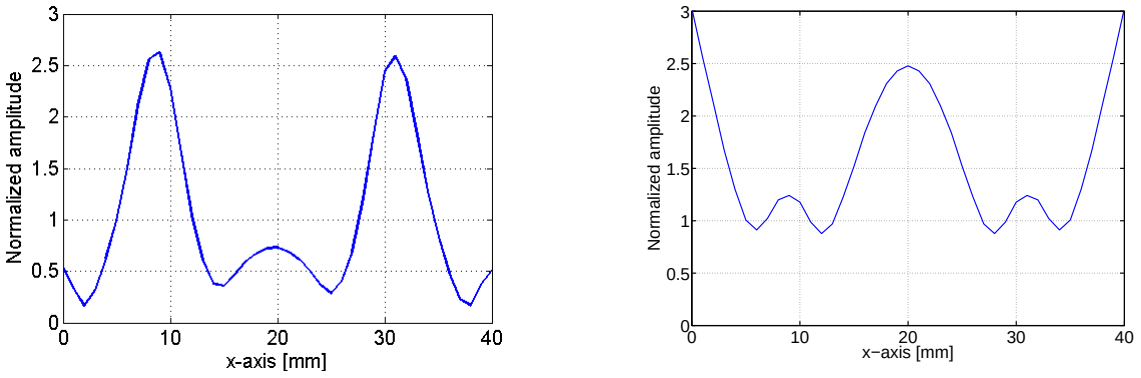

(a) (b)

Figure 5.16: Measured amplitude (f = 35 kHz) across the width of the specimen under the excitation (opposite side from the transducers); (a) experiments, two PZT discs at the nodes of $Fx1$; (b) FE calculations, two point forces at the nodes of $Fx1$.

large discrepancy between the amplitude ratios. Similar to the findings of Belanger [59] it is believed here that the difference between experiments and FE using multiple PZT discs is probably due to the fact that the excitation with point forces in the FE simulations does not take into account the interaction between the excited wave field and the discs and the added mass of the PZT discs.

5.4 Summary for excitation methods

The above sections presented results from studies examining the possibility to isolate the Fx mode. Three different methodologies were used during these investigations. In the first part of these studies a PZT plate was used as excitation. The PZT plate was placed across the width of the specimens aiming to obtain a constant amplitude across the width which would result in exciting mostly the Fx mode. By studying the interference patterns of the excited wave field it was observed that the amplitude ratio ($Fx/Fx1$) was below one, exciting mostly the $Fx1$ mode at the excitation frequency. The reason for that was that the PZT plate did not create a constant amplitude across the width of the specimen. Instead an amplitude variation was the result of this excitation.

The second technique investigated the possibility of exciting Fx by placing

multiple PZT discs across the width. FE simulations predicted an increase in amplitude ratio by increasing the number of point forces. The predicted amplitude ratio for five point forces across the width was about five, resulting in a 20 % amplitude variation along the specimen, acceptable for the fatigue experiments. Experiments did not achieve the same amplitude ratio for five PZT discs. The measured amplitude ratio (below one) was in the same range as for one and three discs. No improvement was achieved compared to the PZT plate. It was also seen that when more discs were used the more likely it was to excite a torsional mode. For this reason the next methodology used as few discs as possible.

The idea behind the mode suppression technique was instead of approximating the mode shape of Fx across the width, to try and suppress the unwanted $Fx1$ mode. For this reason only two discs were used, placed at the nodes of the $Fx1$ mode. FE simulations predicted that it was possible to isolate the Fx mode using this approach. Even though experiments showed a significant improvement in terms of amplitude ratio compared to the previous two methods, the measured amplitude ratio was significantly smaller than the prediction from the FE simulation. An important result is that the torsional modes were not significantly excited, which was one of the problems of the previous method. This was achieved by using a disc holder when gluing the discs, which gave better control of the location accuracy.

To conclude, from the different techniques which were investigated here, mode suppression was the method which gave the highest amplitude ratio and no significant excitation of any torsional modes. Another important observation was that for more than one disc the FE results, which used point forces, and the experiments predict a different type of excited wave field. In order to get better agreement between the experiments and the FE simulations one could try to model the discs. Due to time constraints and the fact that the FE simulations using point forces for the multi-layered tensile specimens (presented next) showed good agreement with measurements, no further investigations were performed trying to model the PZT discs.

5.5 Waves in multi-layered tensile specimen

5.5.1 Introduction

The specimens investigated here are the multi-layered tensile specimens described in section 2.2.1. During the fatigue experiments of these specimens (chapter 7) the excitation frequency which was used previously in this section (35 kHz) proved to be too low to detect reasonable sized defects. For this reason the frequency had to be increased to 115 kHz. At this frequency there is an additional flexural mode ($Fx2$) propagating compared to the single layer tensile specimens at 35 kHz. Regarding this and the fact that it was not possible to isolate the Fx mode to a great extent even in simple single layer specimen, it was decided to try and excite the $Fx1$ mode instead. This mode has like the Fx mode very similar thickness mode shapes to the A_0-like mode. The mode suppression technique proved to give the best results from the previous methods investigated. Because of that, it was used here for exciting the $Fx1$ mode, by suppressing the Fx and $Fx2$ mode. The purpose of these studies was to obtain a repeatable and relative constant amplitude pattern at the location of the fastener hole. Both FE simulations and experiments were compared in order to understand the wave propagation in the multi-layered tensile specimen.

The excitation setup used consists of three PZT discs permanently bonded 190 mm from the end of the specimen using a two-component epoxy glue. For suppressing the $Fx2$ mode two of the discs (black dots in centre figure 2.6) were placed symmetrically using a disc holder at its nodes (4 mm from the side edges on the top layer (left figure 2.6)). The third disc was placed in the centre and on the opposite layer (right figure 2.6). The idea behind this was that this disc would be forcing the centre of the specimen in the opposite direction from the location of the nodes of $Fx2$ where the two discs were placed, resembling in this way the width mode shape of $Fx1$ and thus suppressing the excitation of the Fx mode. The frequency of 115 kHz was chosen below the cut-off frequency for the $Fx3$ mode (135 kHz). The wave field was measured 10 mm away from the excitation, 200 mm along the length of the

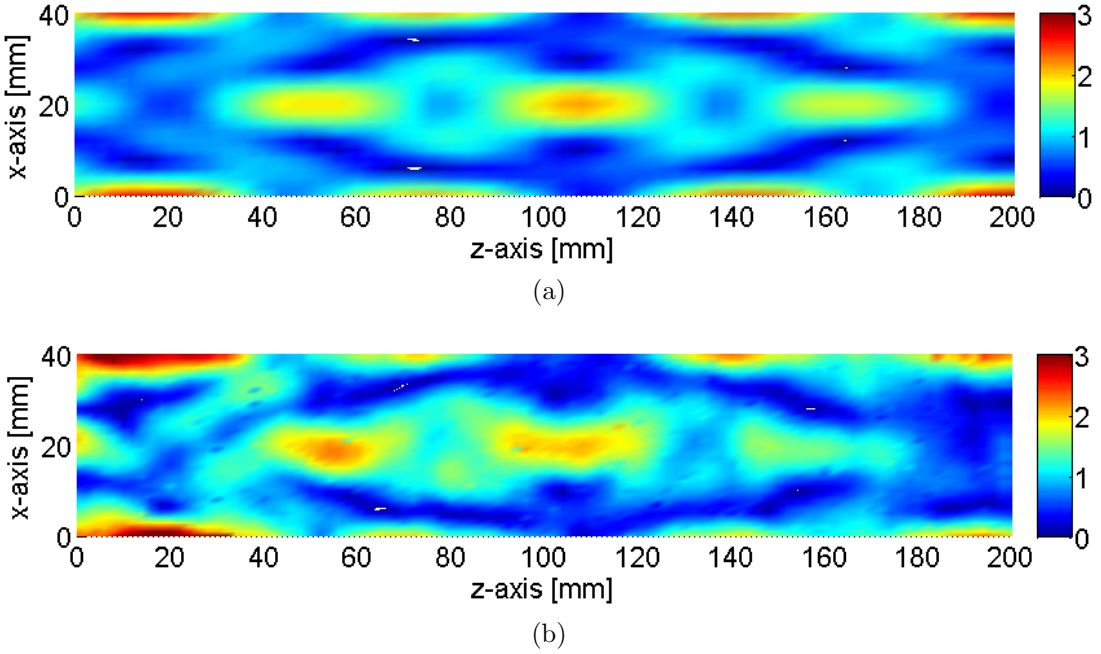

Figure 5.17: Amplitude variation along multi-layered specimen at excitation frequency (115 kHz); (a) FE simulations; (b) measurements on specimen 6.

specimen and across the width ($\Delta x = 1$ mm, $\Delta z = 2$ mm) according to the procedure described in chapter 2 (centre figure 2.6).

5.5.2 Preliminary results

In the FE simulations the geometry was approximated with the Cartesian mesh described in chapter 3 (plates: 0.5 mm x 0.5 mm x 0.75 mm; sealant: 0.5 mm x 0.5 mm x 0.1 mm). The PZT discs used in the experiments were modelled as out-of-plane point forces at the excitation locations and the wave field was monitored on the same Cartesian grid (chapter 3) as in the experiments. The measurement area and grid was the same as for the experiments.

From the FE results (figure 5.17a) an amplitude variation can be seen along the width (x-axis) and length (z-axis, wave propagation direction) of the specimen, caused by the interference between the flexural modes that can propagate at this frequency. The measured wave field (specimen 6) looks very similar to the FE simulations, but is not as smooth and as symmetric as in the FE simulations. The wave propagation was quantified further by calculating the amplitude ratios (FE).

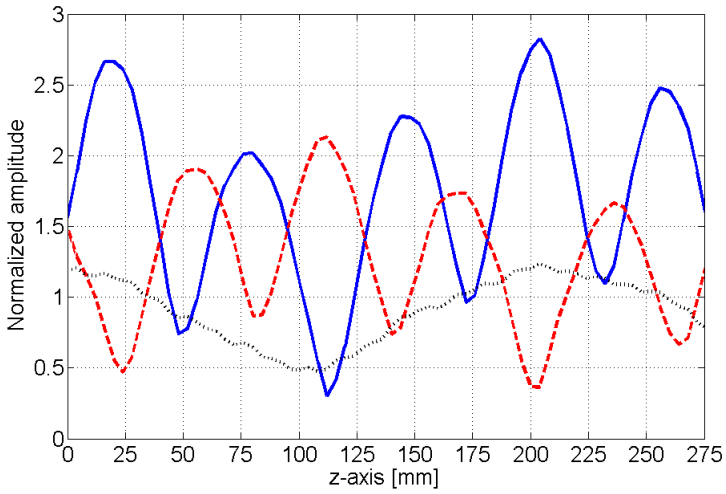

Figure 5.18: Amplitude variation along the length of the specimen at excitation frequency (115 kHz) from FE simulations at three different width locations; at the centre of the specimen (red-dashed); at the edge (blue-solid) and at the node of $Fx2$ (z = 4 mm) (black-dotted).

As for the single layer specimens these ratios were obtained by studying the interference patterns in more detail. In the case of the multi-layered specimens the beatlength at 115 kHz between the Fx and the $Fx1$ mode is 217 mm. The specimens used in the experiments here were too short to evaluate this and to obtain the amplitude ratios. Another problem was the attenuation and the uneven amplitude variation along and across the specimens which can be seen in the experiments. For this reason the amplitude ratios were evaluated from the FE simulations. Since the amplitude patterns look qualitatively similar the amplitude ratios in the experiments could be taken to be of a similar order of magnitude to the FE simulations. This study should though be seen as an approximate way of obtaining an understanding of the modes that have been excited in the multi-layered specimens. For studying the interference in more detail the wave field was monitored along the length of the specimen at three different width locations from the simulation results. The first measurement was taken along the length on the edge of the specimen (blue-solid curve in figure 5.18). The second and third measurements were taken along the node of $Fx2$ (black-dotted curve in figure 5.18) and along the centre of the specimen (red-dashed curve in figure 5.18) respectively. From the black-dotted curve in figure

5.18 the beatlength between Fx and $Fx1$ can be predicted. The Matlab based program which was used to predict the amplitude ratios gave a beatlength of 212 mm. The theoretical calculated beatlength between the two modes of 217 mm agrees well with the FE simulation. The shorter interference length seen from this figure is 46 mm. This agrees well with the beatlength between Fx and $Fx2$ which has a theoretical value of 48 mm. From this it can be concluded that the predominant modes are the three flexural modes. The amplitude ratios for these were obtained in a similar fashion as for the single layer specimens. The following equations were set up for obtaining the amplitude ratios between the modes:

$$Fx + Fx1 + Fx2 = 2.83, \tag{5.4}$$

$$0.75Fx + 0.54Fx1 = 1.23, \tag{5.5}$$

$$0.58Fx + 0.81Fx1 + 0.75Fx2 = 2.13. \tag{5.6}$$

Assuming that all of the modes are in phase resulting in the maximum total amplitude (z = 205, blue-solid curve in figure 5.18) of 2.83 at the edge, one obtains the first equation. The second equation is taken at a point of the line measurement at the node of $Fx2$. At this location the Fx and $Fx1$ mode are in phase resulting in the largest total amplitude of 1.23 (at z = 205, black-dotted curve in figure 5.18). The last equation assumes that all of the modes are in phase, but this time at the centre of the specimen. This results in their maximum total amplitude which is 2.13 (at z = 112, red-dashed curve in figure 5.18). Solving this equation system one obtains the following amplitude ratios:

$$Fx/Fx1 = 0.35, \tag{5.7}$$

$$Fx/Fx2 = 0.73, \tag{5.8}$$

$$Fx1/Fx2 = 2.1. \tag{5.9}$$

From this it is possible to see that $Fx1$ is the predominant mode. It is about three times larger than Fx and about two times larger than the $Fx2$ mode. For investigating the validity of these results another set of equations was solved obtaining the amplitude ratios of the flexural modes. In these calculations equations 5.4 and 5.5 were used. The third equation was obtained by studying the interference between Fx and $Fx2$ along the length of the specimen, on the node of $Fx1$ (x = 9 mm). This method gave amplitude ratios with an error of less than 10 % compared to the method presented here. This indicates that the calculated amplitude ratios give an acceptable indication of the amplitude ratios for these modes. To conclude this excitation manages to excite mostly the $Fx1$ mode, but did not manage to suppress the other modes. An important result from the simulations presented here is the high and relative constant amplitude at an area at the centre of the specimen (z = 100 - 120 mm x = 15 - 25 mm, figure 5.17a). This area could be used as the location for the fastener hole in the fatigue experiments. Similar amplitude distribution at this location can be seen in figure 5.17b. The repeatability of these amplitude patterns was further studied experimentally.

5.5.3 Wave propagation in tensile specimens

The wave propagation in the specimens used for the fatigue crack monitoring was studied experimentally. In the experiments transducers were placed as in the previous measurement (figure 5.17b). The amplitude pattern shown in figure 5.19a is for specimen 8, which was the first specimen to be fatigued successfully. The pattern shown is quite symmetrical with respect to the centre of the specimen. It is possible to see that the maximum amplitude is at around 108 mm. In this specimen the fastener hole was placed though at 90 mm away (figure 5.19a). The amplitude pattern looks also quite similar to the FE simulations (figure 5.17a) and the previous measurement (figure 5.17b). Three more specimens were used in the second set of fatigue experiments (specimen 10, 13 and 14). Specimen 10 (figure 5.19b) shows

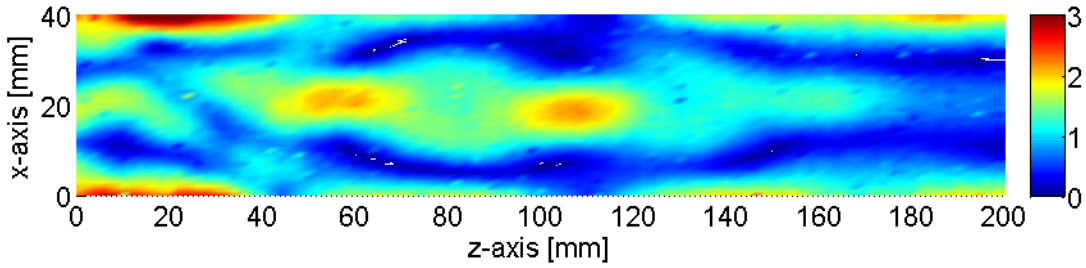

(a)

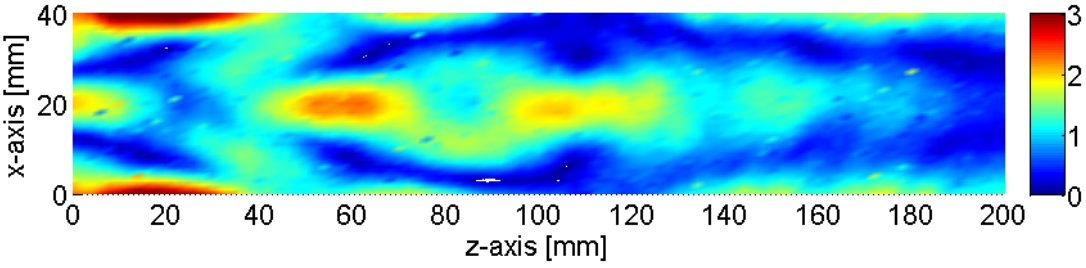

(b)

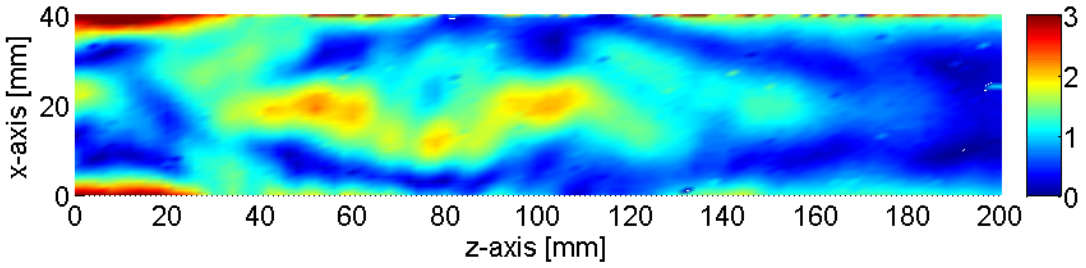

(c)

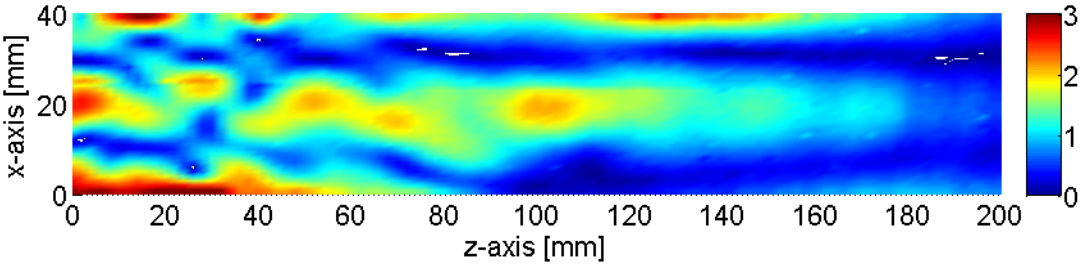

(d)

Figure 5.19: Measured amplitude (115 kHz) variation along and across four multi-layered tensile specimens; (a) specimen 8; (b) specimen 10; (c) specimen 13; (d) specimen 14.

an amplitude map very similar to the previous specimens (figure 5.17b and 5.19a) and also quite similar to the FE simulations. The amplitude is quite symmetrical indicating that the torsional modes are not strongly excited. At a distance of 100 mm along the length a relative high and constant amplitude pattern can be seen. In this specimen it was decided to place the fastener hole at this location. Since

the measurements are taken 10 mm away from the excitation this meant that it was placed 110 mm away from the excitation instead of 100 mm for specimen 8. The amplitude of the wave field for specimen 13 is shown in figure 5.19c. This field looks very similar to the previous experiments, but shows a larger amplitude variation across and along the specimen. A relative constant and high amplitude area can be found at a similar location to specimen 10 (z = 100 mm). The fastener hole was placed in this specimen 110 mm away from the excitation. For the specimen 14 the amplitude pattern looks different from the previous specimens. The reason for this is not known, but the most probable cause is that one of the discs at the nodes was not working properly, resulting in the asymmetric pattern seen in figure 5.19d. Even though some torsional modes were excited, since they have a zero displacement at the centre of the specimen, a similar amplitude area to the previous specimen can be observed at the location of high amplitude in the middle of this specimen. As for the previous specimens the fastener hole was placed 110 mm away from the excitation.

In order to investigate the detection of sub-layer defects from a single accessible side (excitation and measurement), the single PZT disc on the opposite layer where the defect grew was removed. The excitation setup used here consists thus of two PZT discs placed on the same side and on the nodes of the $Fx2$ mode (right figure 2.6). The same measurement procedure as in the previous experiments was used in these investigations. The amplitude pattern shown in figure 5.20a looks relatively symmetrical indicating that the predominant modes are the flexural modes. The figure shown here looks also quite similar to the previous four specimens. The main difference between this figure and the previous ones is the location for the highest amplitude in the centre of the specimen. In the case shown here the area of high and constant amplitude is further away (about 120 mm along the length) than in the previous experiments (about 100 mm along the length). For the study of the influence of a defect on the scattered field, the fastener hole was placed in the centre of the specimen 130 mm away from the excitation. In the last specimen the measurement was stopped because of an error during the scanning, thus covering only part of the

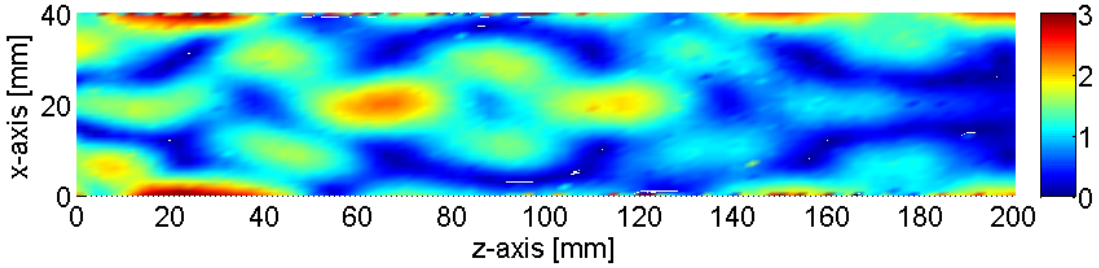

(a)

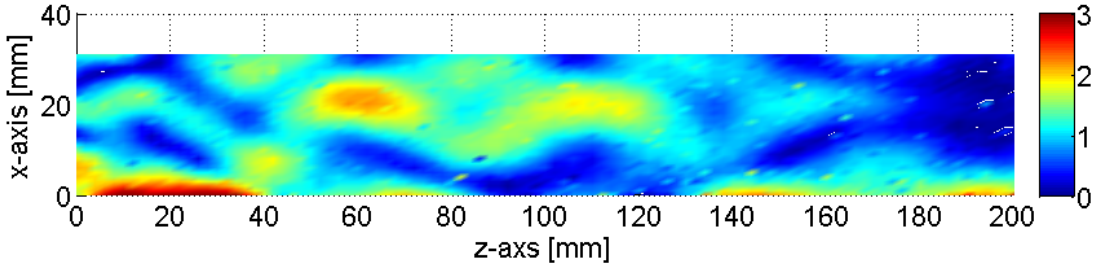

(b)

Figure 5.20: Measured amplitude (115 kHz) variation along and across two multi-layered tensile specimens; (a) specimen 17 and (b) specimen 18.

specimen. For this region, a good agreement is seen to the previous specimen (figure 5.20a). Again the largest amplitude is found about 130 mm away from the excitation. To be able to later compare the results for the scattering studies (chapter 7) in these tensile specimens, it is useful to study the amplitude patterns at the scanned regions close to the fastener hole.

5.5.4 Amplitude at fastener hole location in tensile specimens used for fatigue experiments

The amplitude patterns presented here are from the same measurements on the tensile specimens (specimen 8, 10, 13, 14, 17 and 18) presented above. These results shown here include the location of the fastener hole and the scanned area for the scattering measurements (section 2.4.2). Figure 5.21a (same coordinate system as in figure 5.19) shows the amplitude pattern for specimen 8. In figure 5.21c the amplitude pattern obtained from the FE simulations is shown for the same region. It can be seen that there is a good overall agreement between these figures. Comparing these two

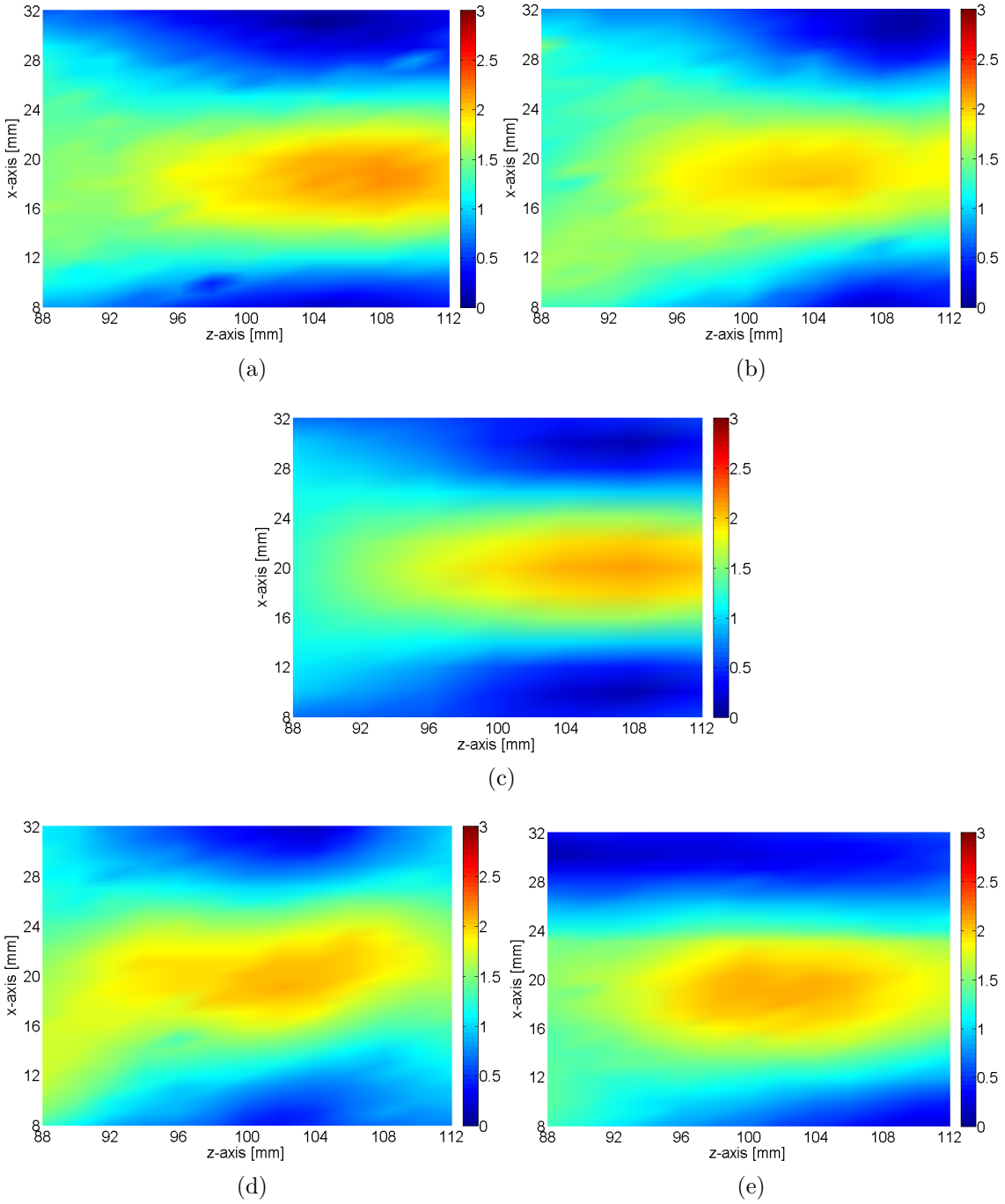

Figure 5.21: Measured amplitude (evaluated at 115 kHz) variation on the monitoring grid (section 2.4.2) used in the scattering experiments for the multi-layered tensile specimens; (a) specimen 8; (b) specimen 10; (c) FE simulation; (d) specimen 13; (e) specimen 14.

figures locally it can be seen that the amplitude pattern in the experiments is slightly asymmetric. At the location where the fastener hole was placed in this specimen (z = 90 mm, figure 5.21a) the two figures have similar amplitude distribution. For this

reason similar overall scattering behaviour can be expected for this specimen and the FE simulations, but probably with a slightly higher amplitude in front of the fastener hole in the experiments. In figure 5.21b the amplitude pattern for specimen 10 is presented. Compared to the FE simulations (figure 5.21c) the area of high amplitude at the centre of the specimen is shorter (z-direction) and not as symmetric. At the beginning of the scanned area (z = 88 mm, figure 5.21b) the region of high amplitude in the experiments is wider than in the FE simulations. At the location of the fastener hole (z = 100 mm, figure 5.21b) the experiments show a similar amplitude distribution to the FE simulations. Specimen 13 (figure 5.21d) shows a higher degree of asymmetry and variation compared to the previous specimens (8 and 10), especially at the centre of the specimen. The region of high amplitude pattern at the centre of the same figure starts also earlier (z = 92 mm, figure 5.21d) compared to the previous figures (z = 96 mm, figure 5.21a, 5.21b and 5.21c). At the location of the fastener hole (z = 100 mm, figure 5.21c) and in front of it (z = 96 mm, figure 5.21c) the amplitude is higher compared to the FE simulations. For the last specimen (figure 5.19d) the amplitude pattern at the location of the largest amplitude looks quite similar to the other specimens. Looking further away (x-direction) from this location a larger degree of asymmetry is seen compared to FE simulations and other specimens. The asymmetry in the incident field can better be seen in figure 5.19d. Because of the large degree of asymmetry, specimen 14 was not included in the investigations for the influence of a defect on the scattered field. Figure 5.22a shows part of the amplitude pattern presented in figure 5.20a. This amplitude pattern includes the location of the fastener hole (x = 20 mm, z = 120 mm in figure 5.22) and the scanned area for the experiments investigating the influence of a fatigue crack on the scattered field. The shown amplitude pattern is relative symmetric with respect to the centre of the specimen. At the location of the fastener hole, an area of high and relative constant amplitude can be seen. The amplitude pattern of specimen 18 (figure 5.22b) shows a similar, but wider area (x-direction) of high and relative constant amplitude at this location. In this case the amplitude at the location of the fastener hole is slightly

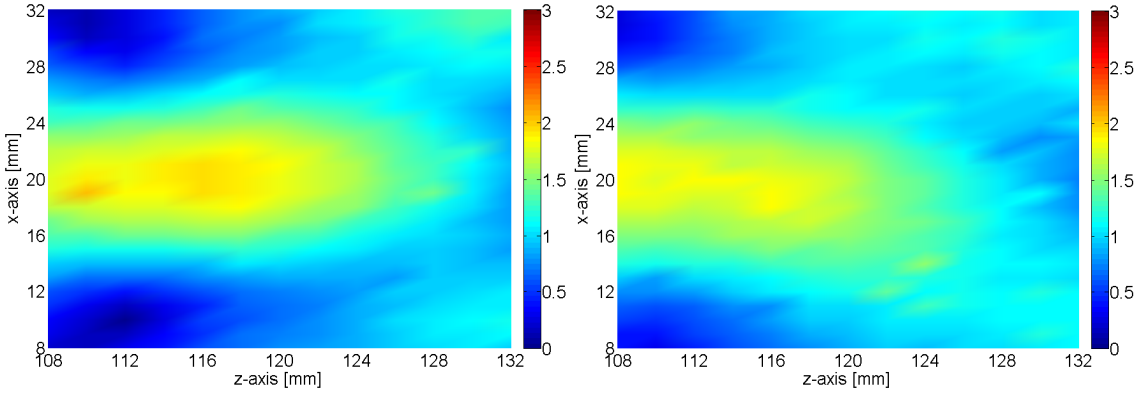

(a) (b)

Figure 5.22: Measured amplitude (evaluated at 115 kHz) variation on the monitoring grid (section 2.4.2) used in the scattering experiments for the multi-layered tensile specimens; (a) specimen 17 and (b) specimen 18.

lower compared to specimen 17. The amplitude pattern is also not as symmetric as for specimen 17. For both these specimens the location for the largest amplitude is further away (about 120 mm in figure 5.22) compared to the previous specimen (about 100 mm in figure 5.21). Overall the amplitude distribution at an area around the location of the fastener hole is quite similar though.

5.5.5 Summary

In this section the wave propagation in multi-layered tensile specimens was investigated. From the experiments on the single layer specimen it was found that the lowest flexural mode (Fx) could not be isolated to a significant degree (excitation frequency: 35 kHz). During the fatigue experiments (chapter 7) on the multi-layered specimens it was also observed that the excitation frequency of 35 kHz was too low to detect any reasonable sized defects. For this reason in the multi-layered specimen the frequency was increased to 115 kHz, below the cut-off frequency of the $Fx3$ mode. This and due to the fact that it was not possible to isolate the lowest flexural mode in the simpler single layer specimen, it was decided to investigate the possibility of exciting the second flexural mode ($Fx1$). The excitation setup (figure 2.6) consisting of three PZT discs, aims to suppress the unwanted modes (Fx and $Fx2$). Both

FE simulations and experiments were carried out during these studies. From the FE simulations it was seen that the $Fx1$ flexural mode was the strongest excited mode (2 - 3 times stronger) of the three flexural modes propagating ($Fx, Fx1$ and $Fx2$), but not with a significantly larger amplitude compared to the other modes. The experiments showed a similar amplitude pattern to the FE simulations. Since it was not possible to obtain just one mode ($Fx1$), the main objective with this type of excitation was to obtain an area of relative high and constant amplitude. Measurements on the four fatigued specimen (chapter 7) were performed. The measured amplitude patterns for three of the specimens showed quite repeatable wave propagation (figures 5.19a, 5.19b and 5.19c). For one specimen (figure 5.19d) the amplitude pattern was more irregular than the other specimens. The reason for that is believed to be that a PZT disc was not functioning properly, thus exciting torsional modes leading to the observed asymmetry. At an area in the centre of the specimen and half way along the length (about 100 mm in figures 5.21) of the measured areas a large and relative constant amplitude pattern was observed. For the fatigue experiments the fastener hole was placed at this location. Because of this fairly constant amplitude as compared to a large plate and the similar thickness mode shapes of the flexural modes ($Fx, Fx1, Fx2$) to the A_0-like mode, similar sensitivity for defects can be expected in the multi-layered plate and tensile specimen. To prove the concept of single sided access (excitation and measurement) to detect hidden fatigue cracks in the sub-layers, the excitation in two specimens (17 and 18) consist of two discs bonded on the same layer. This type of excitation produced a very similar amplitude pattern to the previous four specimens. Good repeatability was observed for the two specimens. The area of high amplitude was further away compared to the previous specimens (about 120 mm in figures 5.22; location of fastener hole).

Chapter 6

Scattering and defect detection in large plates

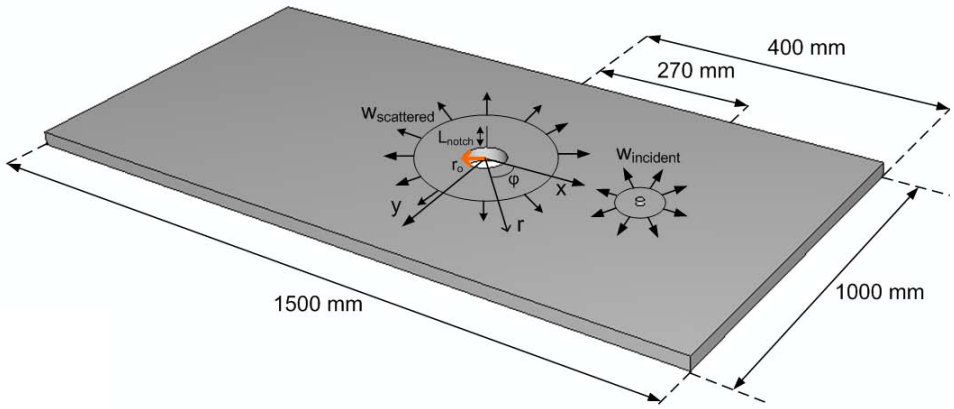

Figure 6.1: Geometry for the scattering at a fastener hole with a notch in an aluminium plate (not to scale); hole radius: $r_o = 10$ mm; thickness: $h = 5$ mm; excitation frequency: $f = 100$ kHz; wavelength: $\lambda = 18.5$ mm.

The aim of this thesis is to detect fatigue cracks at a single fastener hole in multi-layered structures using guided ultrasonic waves. These cracks are detected by studying the changes in the scattered field amplitude around a fastener hole caused by such a defect. The results presented in this chapter are from studies performed to understand the scattering of flexural waves at a fastener hole and the change in amplitude caused by a defect in single and multi-layered plates.

Since the physics of the scattering of flexural waves in a single layer plate are

well described in the literature [60, 61, 62] and more easily understood than the scattering in multi-layered plates, they will be revised in the first part of this chapter as an introduction. In that section 3D FE simulations are compared and validated for the scattering of flexural waves at a fastener hole in a single layer plate against an analytical solution and experiments. Similar studies have also been performed for the S_0 mode [63]. The scattering of Lamb waves at defects have been previously studied by Alleyne et al. (A_0 mode) [64] and by Lowe et al. (S_0 mode) [65]. Fromme et al. [66] studied the scattering of the A_0 mode at a fastener hole with the presence of a defect. A similar study had been earlier carried out by Chang [67] using the S_0 mode instead. In this chapter a study comparing and validating the FE code against experiments for the scattering of the A_0 mode at a fastener hole with a notch is presented.

In the second part of this chapter (6.2) results from the scattering of the A_0-like mode at a fastener hole with and without a defect in a multi-layered plate are presented and discussed. In section 6.2.1 the scattering in a single and a multi-layered plate are compared. The FE code for the multi-layered plate is later validated against experimental results for the scattering at a fastener hole (section 6.2.2). Sections 6.2.3 and 6.2.4 investigate the scattering of flexural waves at a fastener hole with a defect in the multi-layered plate. The main aim of these studies is to specify the detection limit for the defect size in this type of multi-layered plate.

In section 6.3 the scattering in a multi-layered tensile specimen is presented. The scattering in this structure is compared with the scattering in the large multi-layered plate studied earlier. From this comparison it is possible to explain the scattering in the tensile specimen. Finally all of the main results together with the conclusions are summarized at the end of this chapter.

6.1 Scattering at a fastener hole with and without a defect in a large single layer plate

The 5 mm thick (h) aluminium plate (figure 6.1) which was used for these experiments is described in section 2.3. The frequency (100 kHz) of the five cycle signal which was used for the excitation was well below the first cut-off frequency for any higher order modes. At that frequency there are two modes propagating, namely the A_0 and the S_0 mode. The PZT disc used for the excitation of the guided waves will mostly excite the A_0 mode. The out-of-plane component of the A_0 mode is measured with the laser interferometer. The wavelength of the A_0 flexural wave is 18.5 mm at this frequency. As described in chapter 2, the measurements were taken on a radial grid around the hole (r_o = 10 mm) every 5^o and every 0.5 mm in the radial direction (r = 10.5 mm to 32.5 mm). The excitation and measurement procedure were kept the same throughout the experiments presented in this section. At a later stage a notch was cut at the fastener hole. In the FE simulations interpolation was used in order to obtain the amplitude at the monitoring points. The A_0 mode was excited with a point force, placed at the location of the PZT disc and in the mid-plane of the plate in order to excite only the A_0 mode. As for the experiments all of this

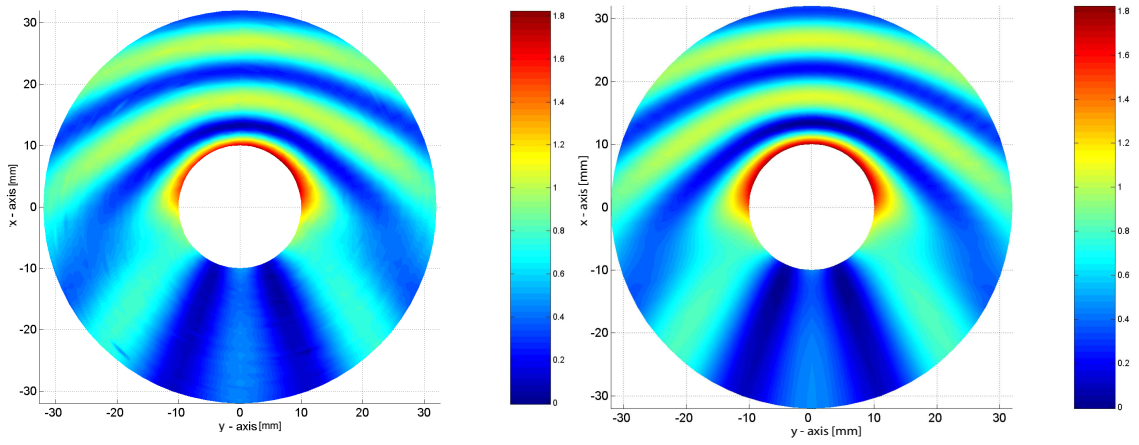

(a) (b)

Figure 6.2: Comparison between (a) measured and (b) calculated (analytical solution) scattered wave field (f = 100 kHz) amplitude (λ = 18.5 mm) around a fastener hole (r_o = 10 mm) in a single layer aluminium plate (h = 5 mm).

was kept the same during the investigations presented here. In all of the figures which are shown in this chapter the waves are propagating from top to bottom (from positive to negative x-direction, figure 6.1). The figures shown in this chapter have been normalized with the average value of the total wave field (incident + scattered). This average was calculated by adding together the amplitude values (evaluated at the centre frequency) from all of the monitored points and dividing that number with the number of monitoring points. The FE simulations were validated against an analytical solution for the scattering at a fastener hole in a single layer plate based on Mindlin theory [53]. Since the analytical solution has been previously derived by several authors no details will be given here. A detailed description of this solution can be found in the paper of Pao and Chao [60]. In this thesis an existing Matlab based code developed by Fromme [1, 66] was used for calculating the scattering around a fastener hole in a single layer plate.

6.1.1 Scattering at a fastener hole

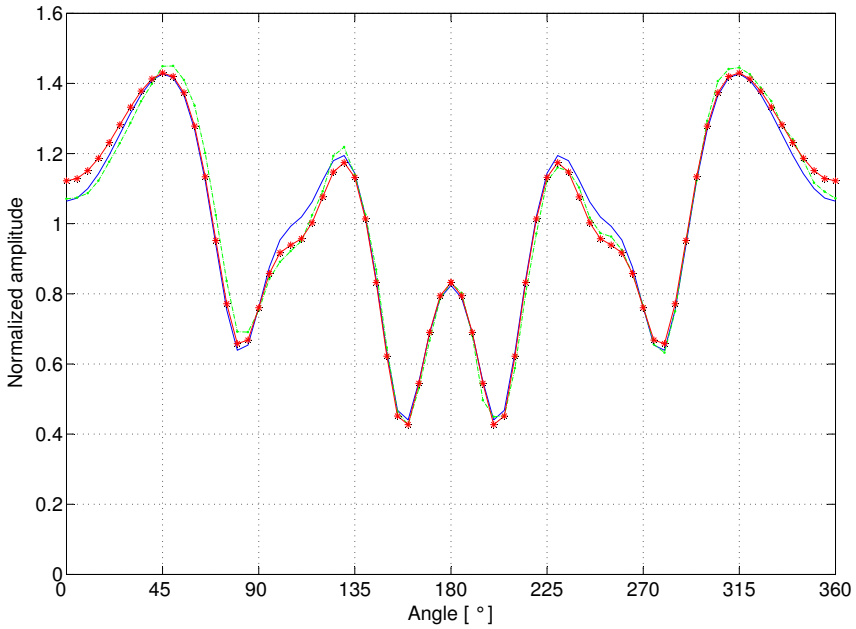

Figure 6.3: Scattered wave field (f = 100 kHz) amplitude at r = 13 mm around a fastener hole in a single layer aluminium plate (h = 5 mm); measured (green, dashed-dotted), analytical solution (blue, solid), FE simulation (red, solid-stars).

Results from the measurements performed on the large plate are shown in figure 6.2a. In figure 6.2b the scattered field shown is obtained from the analytical solution. In both figures it is possible to distinguish a typical area of low amplitude behind the hole, where destructive interference occurs between the incident and the scattered wave. Similar to the findings by Fromme [62], in front of the hole an area of varying amplitude can be seen. This is due to interference between the incident and the scattered wave. The FE code was validated against these solutions on a circle (r = 13 mm) around the hole (figure 6.3). It can be seen that the amplitude of the scattered field on this circle obtained from the FE simulation agrees well with the analytical solution and the measurements. The largest difference of the scattered field obtained from the FE simulation and the analytical solution found at 0, 100, 260 and 360 degrees is about 5 % of the incident wave amplitude. This is most probably caused by the Cartesian approximation of the hole. From the results presented above it can be concluded that the different approaches of calculating the scattered field around a fastener hole in a single layer plate show good agreement with each other. In the next section the FE code is validated against measurements for the scattering around a hole with the presence of a notch.

6.1.2 Scattering at a fastener hole with a defect

This investigation was carried out on the same plate as the one presented in the previous section. With a fine blade saw a notch was cut through the thickness of the plate. The notch had initially a length (L_{notch}) of about 2 mm and a width of about 1 mm and was placed perpendicular to the propagation direction of the incident wave field ($\phi = 270^o$, figure 6.1). The ratio of the notch length relative to the plate thickness and the hole diameter is in this case 0.4 and 0.1 respectively. Measurements were also performed for a twice as long notch ($L_{notch} = 4$ mm). The same excitation setup and monitoring grid as in the previous section was used for this investigation. In the FE simulations the notch was introduced by removing elements (chapter 3).

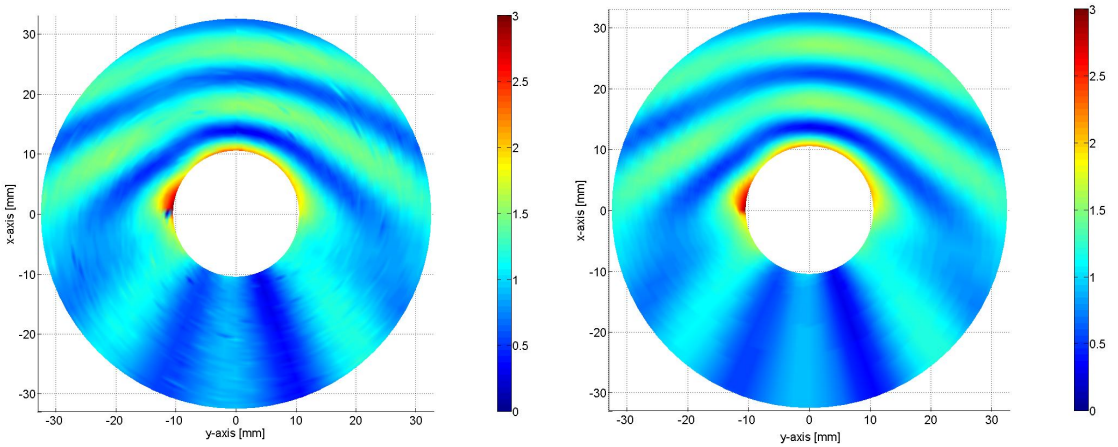

(a) (b)

Figure 6.4: Comparison between (a) measured and (b) simulated (FE) scattered wave field ($f = 100$ kHz) amplitude ($\lambda = 18.5$ mm) around a fastener hole ($r_o = 10$ mm) with a 2 mm notch placed at the left side of the hole in a single layer aluminium plate ($h = 5$ mm).

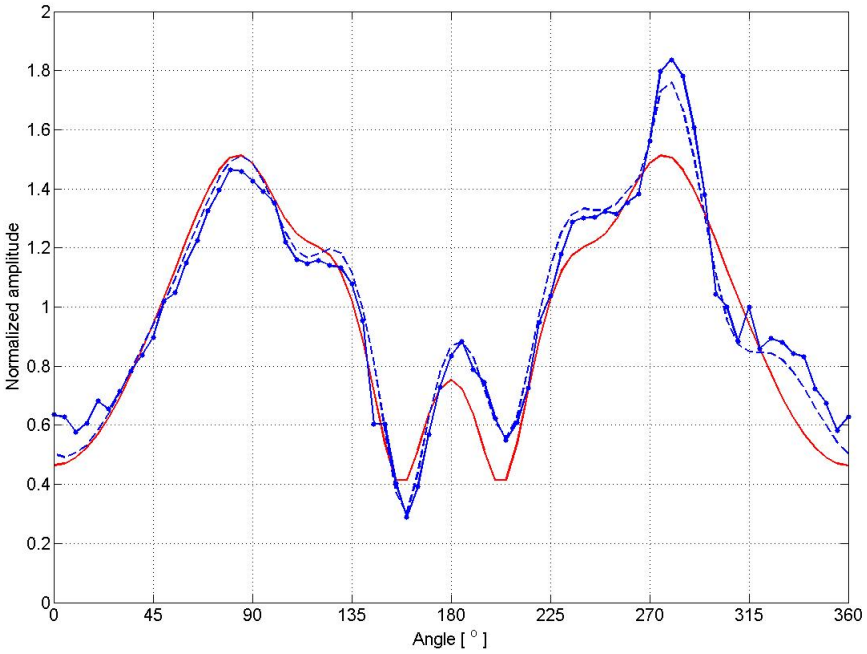

Figure 6.5: Amplitude of the scattered wave field ($f = 100$ kHz) on a circle ($r = 13$ mm) around a fastener hole with a 2 mm notch in a single layer aluminium plate ($h = 5$ mm); FE simulation (blue, dashed); analytical solution without notch (red, solid); measurements (blue, solid-dotted).

The amplitude of the scattered field around the fastener hole with a 2 mm notch obtained from experiments is shown in figure 6.4a. The additional reflection of the flexural wave caused by the presence of the notch interacts with the incident wave

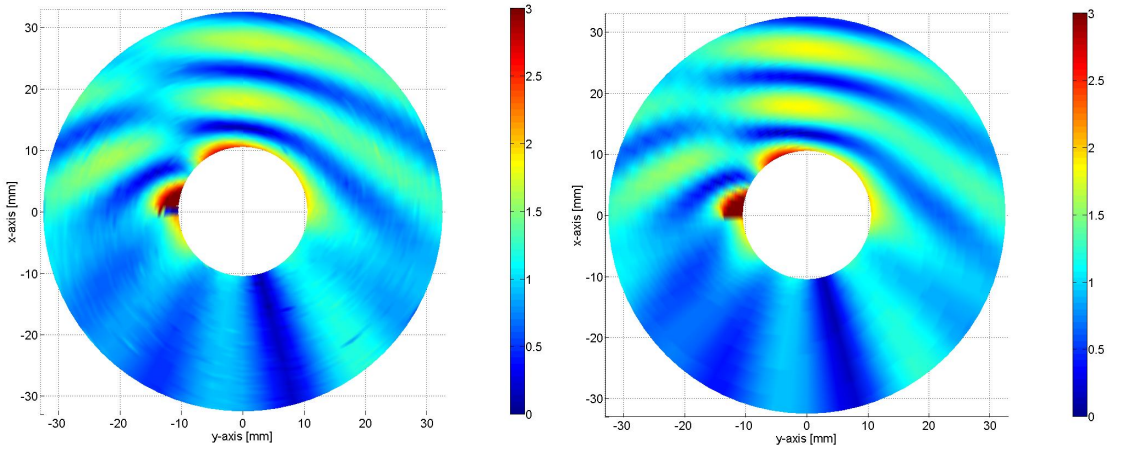

(a) (b)

Figure 6.6: Comparison between (a) measured and (b) simulated (FE) scattered wave field (f = 100 kHz) amplitude (λ = 18.5 mm) around a fastener hole (r_o = 10 mm) with a 4 mm notch placed at the left side of the hole in a single layer aluminium plate (h = 5 mm).

and the wave scattered at the hole, producing a small increase in amplitude at the left side of the hole (figure 6.4a). Figure 6.4b shows the scattered field around the hole with a 2 mm notch obtained from the FE simulation. Similar to the scattered field obtained from the measurements, this figure shows an increase in amplitude at the left side of the hole where the notch is located. In figure 6.5 the amplitude of the scattered fields on a circle (r = 13 mm) around the fastener hole obtained from FE simulation and experiment are compared against the analytical solution of the scattered field (without defect). The results from measurements and FE simulations agree very well with each other. At an angle of 270^o, where the notch is located, a peak in the amplitude can be distinguished. The increase in amplitude due to the presence of the notch is about 25 % of the incident wave amplitude for both simulation and experiment. Measurements and FE simulations were repeated for a longer notch. The amplitude of the scattered field around the hole with a 4 mm notch obtained from the measurements is shown in figure 6.6a. Similar to figure 6.4a the additional reflection of the flexural wave caused by the presence of the notch, interacts with the incident and scattered wave at the hole producing an increase in amplitude at the left side of the hole (figure 6.6a). Figure 6.6b shows the scattered

field around the hole with a notch (4 mm) obtained from the FE simulation. Similar to the scattered field obtained for a 2 mm notch this shows an increase in amplitude at the left side of the hole where the notch is located. Comparing the scattered field amplitudes obtained from measurements and FE simulation for a 4 mm notch to the scattered field for a 2 mm notch one can see that the amplitude increase in front of the hole is higher for a 4 mm notch, but also the change of the amplitude pattern is larger. This would suggests that as the length of the notch increases the change in the scattered field amplitude pattern increases as well.

To summarize, the results for the scattering at a fastener hole in a single layer plate showed good agreement between FE simulations and experiments, thus validating the FE code. The scattering of a flexural wave at the fastener hole results in an increase of amplitude in front of the fastener and an amplitude variation further away from the hole boundary. When a defect is present the amplitude pattern is slightly shifted, increasing the amplitude in front of the defect. These changes were said to be caused by the interference between the scattered wave and the incident wave. The increase in amplitude due to the defect was about 25 % of the incident wave field for a small notch (2 mm long).

Because of the similarities in the thickness mode shapes of the flexural waves in a single and in a multi-layered plate (figure 4.2.2), similar scattering behaviour can be expected in these two structures at the used frequency (115 kHz). The knowledge obtained for the scattering in a single layer structure can be used to explain and understand the scattering in a multi-layered structure. In the next section, results are presented from a study done in order to investigate the possibility of detecting fatigue cracks present only in one of the layers of a multi-layered plate/tensile specimen, by monitoring the undamaged layer.

6.2 Scattering at a fastener hole with and without a defect in a large multi-layered plate

In the first part of this section the FE code for the scattering in a large multi-layered plate is compared against the analytical solution for the scattering in a large single layer plate of the same total thickness. The analytical solution is calculated in the same way as in the previous section. The FE model for the multi-layered plate used here (600 mm x 600 mm x 6.2 mm) consisted of two 3 mm thick aluminium alloy (2014-T6) plates, connected with a 0.2 mm thick adhesive layer (HYSOL-9394 EA [32]). The element size used in the FE simulations were 0.75 mm cubic elements in the adherents and 0.1 mm x 0.75 mm x 0.75 mm elements in the adhesive layer. The excitation consisted of an out-of-plane point force, placed 110 mm away from the centre of the fastener hole. The excitation frequency was increased from the previous section to 115 kHz (as used for fatigue experiments) which is well below the first cut-off frequency for any higher order thickness modes (figure 4.2). At that frequency there are two modes propagating, namely the A_0-like mode and the S_0-like mode. The out-of-plane displacement was monitored on a radial grid around a 6 mm diameter fastener hole, every 5^o and every 1.5 mm in the radial direction (r = 3.75 mm to 15.75 mm).

In the last part of this section the wave propagation and scattering at a fastener hole with and without a defect in a large multi-layered plate was studied experimentally and compared to FE simulations. The manufactured plate used, described in chapter 2, had an adhesive layer (0.55 mm) thicker than the plate used in the first section. In the FE simulations the same mesh size was used in the adherents as in the first section, but due to the thicker adhesive layer, a different mesh was used for it (0.275 mm x 0.75 mm x 0.75 mm). For the FE simulations the same monitoring grid and excitation was used. The geometry of the plate, excitation and monitoring procedure used in the experiments are described in detail in chapter 2. To study the influence of defects on the scattered field, machined notches of various lengths and

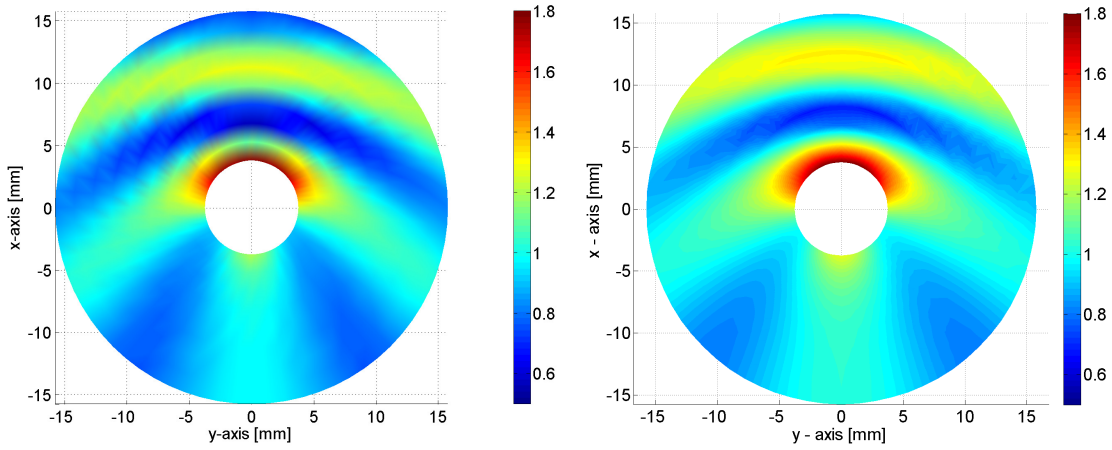

(a) (b)

Figure 6.7: Amplitude of scattered wave field (f = 115 kHz) around a fastener hole (r_o = 3 mm); (a) multi-layered plate (FE simulation, h = 6.2 mm, λ = 16.6 mm); (b) single layer plate (analytical solution, h = 6.2 mm, λ = 18.5 mm).

depths were milled in only one of the layers of the multi-layered structure. In all of the investigations the defects were oriented perpendicular to the incident wave and the scattered field was measured and calculated (FE) on the opposite layer from where the defect was placed.

6.2.1 Comparison to a single layer plate

In chapter 4 it was shown that the mode shapes of the A_0-like and the A_0 mode are very similar for low frequencies. This suggests that similar scattering at a fastener hole can be expected for a single and a multi-layered plate. Figure 6.7a shows the scattered field obtained from the FE simulation for the large multi-layered plate. Figure 6.7b shows the results obtained from theory for the scattered field in the single layer plate (λ = 18.5 mm) of the same total thickness as the multi-layered plate (λ = 16.6 mm). A good general agreement is found between the amplitude patterns for these two structures. Similar to the scattered field patterns seen at the beginning of this chapter (figure 6.2), these figures have a region of high amplitude in front of the fastener hole. This is caused by the interference between the incident and the scattered wave at the fastener hole. The interaction between the two waves also

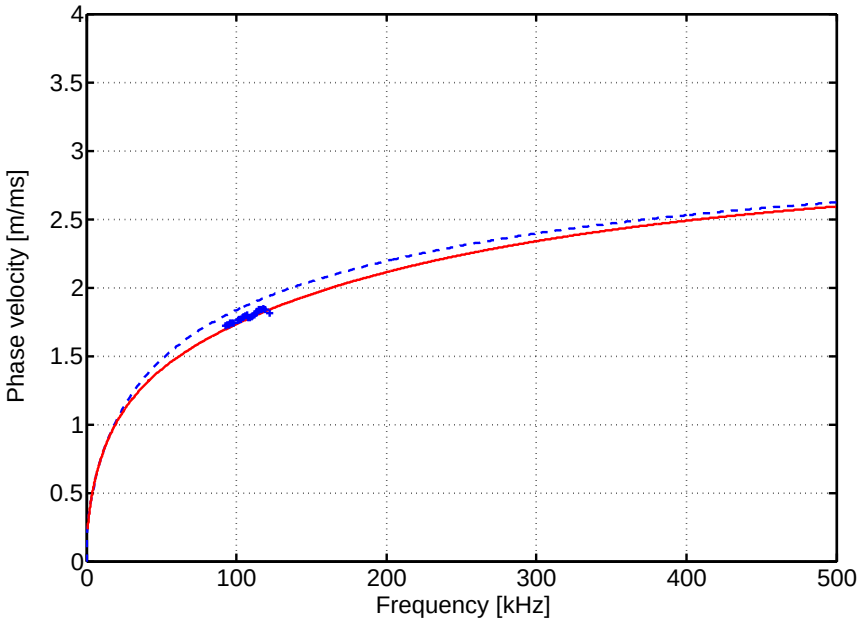

Figure 6.8: Calculated and measured dispersion curves for multi-layered plate; 0.2 mm thick adhesive layer (blue, dashed), 0.55 mm thick adhesive layer (red, solid) and measured phase velocity (blue, crosses) on a large multi-layered plate.

results in the amplitude variation seen further away from the fastener hole. The main difference seen between these two figures are caused by the different wavelengths for the two cases. This can be seen by studying the distances between the regions of low amplitude in front of the fastener hole for the two figures.

6.2.2 Wave propagation and scattering at a fastener hole in a large multi-layered plate

This section presents results from the comparison between FE simulations and measurements for the wave propagation and scattering at a fastener hole in the large multi-layered plate described in chapter 2. Initially the wave propagation in the manufactured multi-layered plate was studied. The phase velocity was measured (as described in chapter 2) in a frequency range between 100 and 115 kHz. The results from the measurements were compared to the dispersion curves obtained from Disperse [52] for two different thicknesses of the adhesive layer (0.2 mm and 0.55 mm).

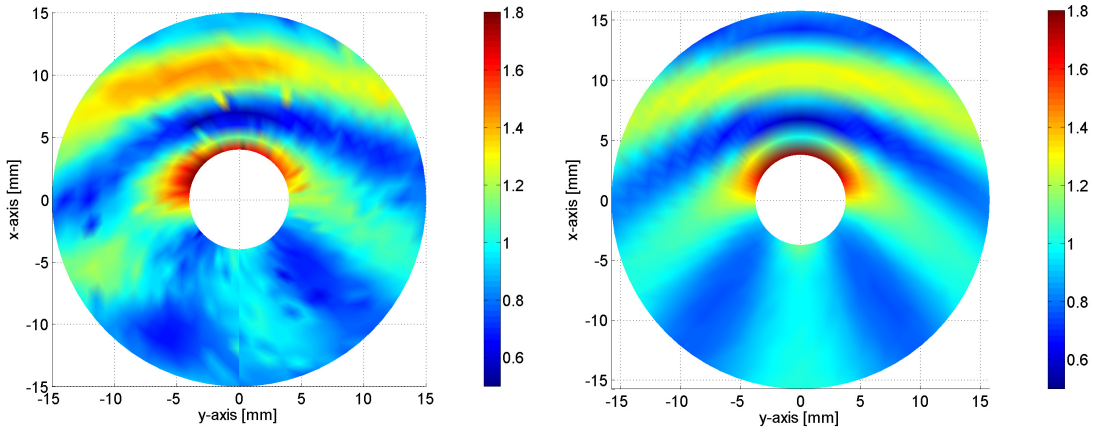

(a) (b)

Figure 6.9: Comparison between (a) measured and (b) calculated (FE) scattered wave field ($\lambda = 15.8$ mm) amplitude ($f = 115$ kHz) around a fastener hole ($r_o = 3$ mm) in a multi-layered plate ($h = 6.55$ mm).

This was done in order to see if it is necessary to change the adhesive layer thickness from 0.2 mm to 0.55 mm which is the thickness of the large manufactured plate in the FE model. The measured phase velocities (blue, crosses) are shown in figure 6.8 together with the calculated curves for 0.2 mm adhesive (blue, dashed) and 0.55 mm adhesive layer (red, solid). From this figure it is possible to see that the calculated dispersion curves are similar for low frequencies, but deviate for higher frequencies. It is also seen that the measured phase velocities are closer to the calculated dispersion curve for a 0.55 mm thick adhesive layer. At the chosen working frequency (115 kHz) the phase velocity obtained from the measurements is 1.824 m/ms, while the calculated phase velocities for a 0.2 mm and 0.55 mm thick adhesive is 1.908 m/ms and 1.809 m/ms, respectively. The percentage difference between 0.2 mm and 0.55 mm is quite significant (5.5 %) therefore it was decided to use a 0.55 mm thick adhesive layer in the FE simulations.

For the scattering around a fastener hole in the large multi-layered plate a comparison between experiment and FE simulation was done. The results from the experiment (figure 6.9a) and FE simulation (figure 6.9b) show qualitatively a good agreement. Similar to a single layer plate (figure 6.7b) both figures show an increased amplitude in front of the fastener hole and an amplitude variation further away. In

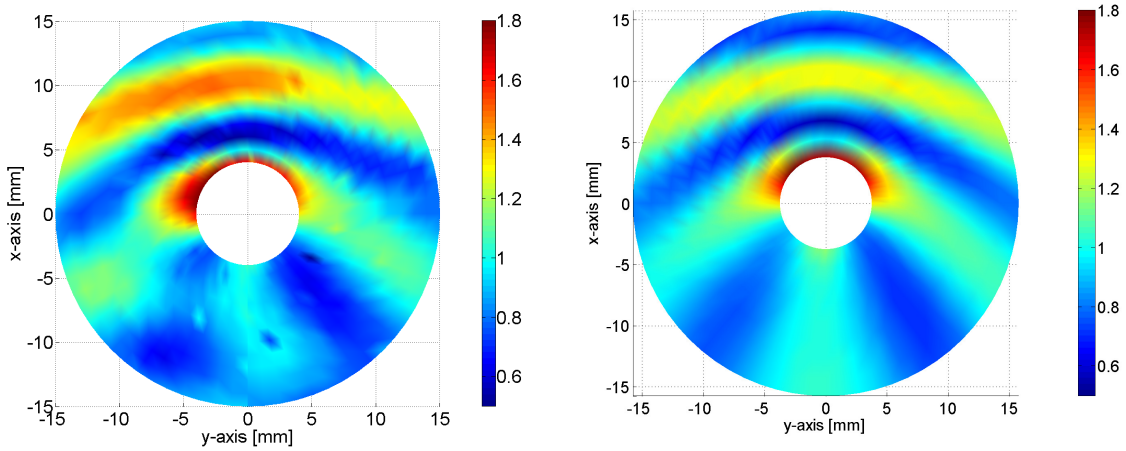

(a) (b)

Figure 6.10: Comparison between (a) measured and (b) calculated (FE) scattered wave field (λ = 15.8 mm) amplitude (f = 115 kHz) around a fastener hole (r_o = 3 mm) with a 2.25 mm long notch, partly through one of the layers (h = 3 mm) of a multi-layered plate (h = 6.55 mm).

the experiments it can be seen that this increase is not symmetrical as in the FE simulations, with a higher amplitude found at the left hole boundary (x = 0 mm, y = -5 mm figure 6.9a). The difficulties in manufacturing the plate resulted in a non-uniform adhesive layer and/or bonding state at the location of the fastener hole in the multi-layered plate, resulting most probably in the asymmetry seen. Also in the experiment the pattern is not smooth as in the FE simulation, with very high or low amplitude found in certain locations. This was caused by the bad reflection of the laser beam at these points. Overall, it is possible to say that the scattered fields obtained from the experiment and FE simulation agree qualitatively quite well with each other, thus verifying the FE code for the multi-layered plate.

6.2.3 Scattering at a fastener hole with a 2.25 mm long defect part through one of the layers

One of the main objectives of these studies was to investigate the possibility of using guided waves for detecting a hidden defect in just one layer at a fastener hole, by accessing only the opposite (undamaged) layer. This is investigated here for a notch

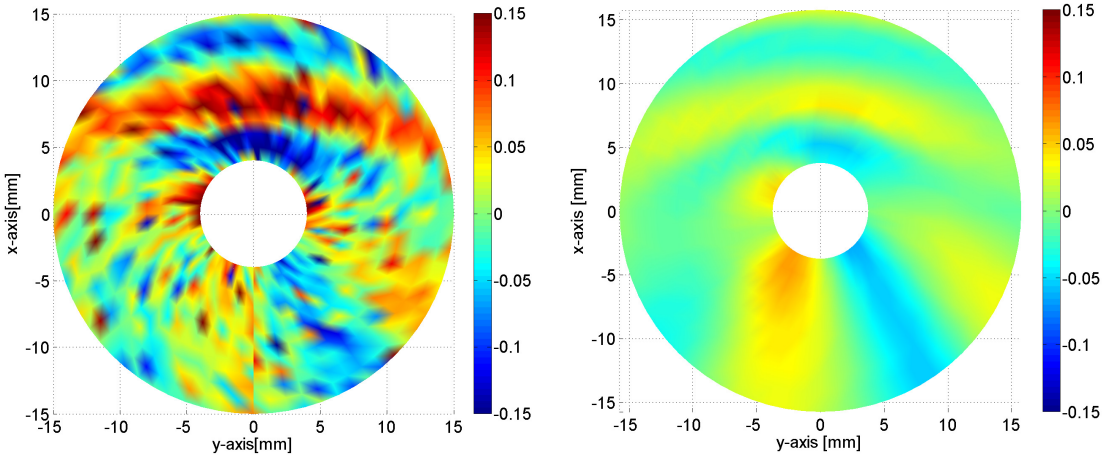

(a) (b)

Figure 6.11: Change in amplitude (f = 115 kHz) of scattered wave field (λ = 15.8 mm) around a fastener hole (r_o = 3 mm) due to a 2.25 mm notch part through one of the layers and located at the left side of the hole and on the opposite layer from the measurements; (a) experiments; (b) FE simulation.

partly and later completely through one of the layers, while exciting and monitoring the guided waves only in the opposite layer. The machined notches were milled at the hole boundary and in only one of the aluminium layers. In the first experiment the defect was machined part through one of the layers. The defect was about 1 mm wide and had a length and depth of 2.25 mm ($\sim$ 1/3 of total plate thickness). The orientation of the notch was perpendicular to the wave propagation direction (270 degrees, coordinate system in figure 6.1). The same excitation and measuring procedure as in the previous section was used during this investigation. Figure 6.10a shows the measured scattered field amplitude (115 kHz) for the 2.25 mm notch. As for the undamaged case, a slightly higher amplitude can be seen on the left side of the hole (x = 0 mm, y = -5 mm figure 6.10a) in the measurements. The similarities between these two cases, but also the bad quality of the scattered field amplitude patterns obtained from the measurements makes it very difficult to draw any conclusions about any changes caused by the defect. The FE simulation (figure 6.10b) shows a similar amplitude pattern. From the FE simulation it is possible to investigate in more detail eventual changes which are caused by the defect. One way of investigating this is by taking the difference between the damaged and undamaged

cases. This difference is shown for the experiments in figure 6.11a and for the FE simulations in figure 6.11b. In both figures it can be seen that there is not much change in the scattered field due to the presence of the part thickness notch. In the FE simulations the average overall change in front of the notch is about 5 %. An overall similar shift of the amplitude pattern is seen in the experiments (figure 6.11a), but the amplitude variation is in this case about 10 %. This value is representing the noise levels during these experiments. The effect of the defect on the scattered field has to be larger than this value in order to detect such a defect. The large variation was caused by the poor quality of the measured signal at this point (figure 6.11a). Another reason for the bad quality of figure 6.11a could be that the measurement grid (with notch) was shifted relative to the undamaged case when the plate was moved during the machining of the notch. Improvements in the measurement procedure and in the way the notch is cut, e.g. by using a hand held cutting tool and without moving the plate, could potentially improve the quality of the measurements. To conclude, comparing the large variation from the measurements to the predicted change from the FE simulations it is possible to say that a defect part through one of the layers and 2.25 mm long would most probably not be detected using this experimental setup.

6.2.4 Scattering at a fastener hole with a 5.25 mm long defect through one of the layers

In order to investigate the sensitivity of the guided waves to defects which are through one of the layers, a notch almost one third of the wavelength (5.25 mm long $\sim$ total plate thickness) was machined through the thickness of one aluminium layer ($\sim 1/2$ through overall plate). During the machining of the notch the transducer disc was damaged and replaced by another disc. The same type of transducer was placed at the location of the previous transducer, 110 mm away from the centre of the fastener hole. The monitoring grid was the same as in the previous sections.

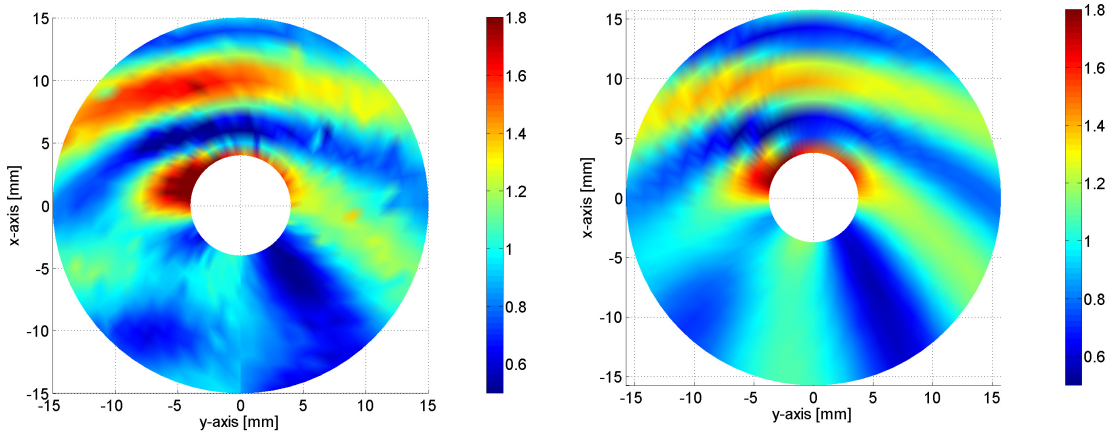

(a) (b)

Figure 6.12: Comparison between (a) measured and (b) calculated (FE) scattered wave field (λ = 15.8 mm) amplitude (f = 115 kHz) around a fastener hole (r_o = 3 mm) with a 5.25 mm long notch through one of the layers (h = 3 mm) of a multi-layered plate (h = 6.55 mm).

Figures 6.12a and 6.12b show the results from these measurements. Results from the FE simulation and experiment look qualitatively similar, both showing a significant amplitude increase at the location of the notch (x = 0 mm, y = -5 mm figure 6.12). The predicted increase in amplitude is much larger compared to the 2.25 mm long notch part through on of the layers. Similar to a single layer plate the presence of the notch shifts the amplitude patterns clockwise. The shift of the amplitude pattern is better seen from the difference between the damaged and undamaged case. Figures 6.13a and 6.13b show the measured and simulated change in amplitude due to the presence of the 5.25 mm long notch.

Despite the poor quality of the measurements (figure 6.13a), the results shown in these figures agree well with each other. In both figures it can clearly be seen that the notch shifts the amplitude patterns, increasing the amplitude in front of the notch. The average amplitude change close to the fastener hole and in front of the notch is about 30 % for the experiments and 25 % for the FE simulations. This change is three times larger than the noise levels ($\sim$ 10 %) and would therefore be detected.

To isolate and study the additional wave which is scattered at the notch, the

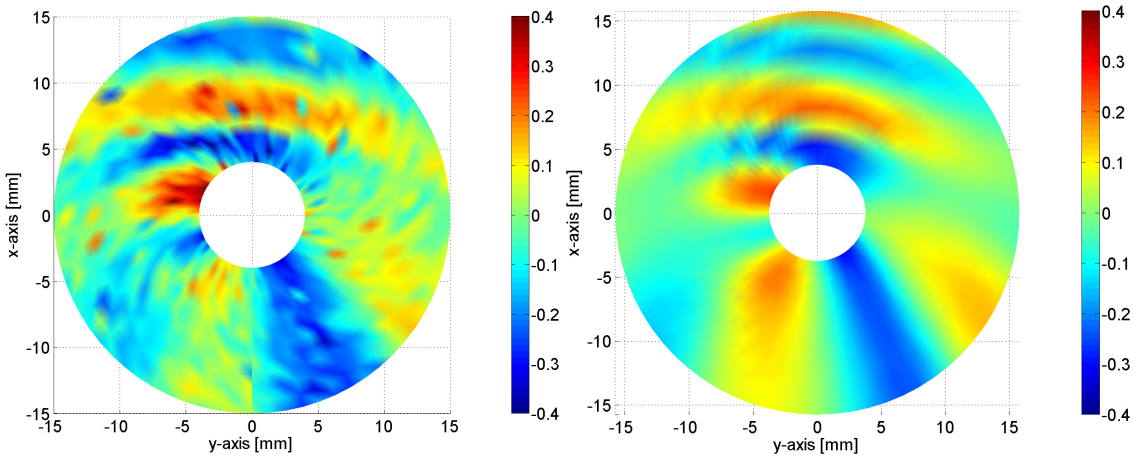

(a) (b)

Figure 6.13: Change in amplitude (f = 115 kHz) of scattered wave field (λ = 15.8 mm) around a fastener hole (r_o = 3 mm) due to a 5.25 mm notch part through one of the layers and located at the left side of the hole and on the opposite layer from the measurements; (a) experiments; (b) FE simulation.

magnitude of the complex difference can be taken [1]. The magnitude of the complex difference between the scattered fields when a notch is present and without a notch was evaluated at the centre frequency (figure 6.14). This takes into account both the magnitude and the phase of the scattered wave at the notch.

The new disc resulted in a different phase and amplitude of the incident wave as compared to the measurements performed on the plate without a notch. Because of this reason and the bad quality in the measurements discussed earlier, only FE results will be shown here. It has been shown [1] that the presence of an additional scattered wave due to the notch, would result in an increase in the complex magnitude in front of the defect. The magnitude of the complex difference for a 5.25 mm long through notch was compared to a 2.25 mm long notch part through one of the layers (figure 6.14). By comparing these two figures it can be seen that the notch part through one of the layers (figure 6.14a) produces almost no additional ($\sim$ 10 %) scattering compared to the notch through one of the layers, where a much larger back scattered amplitude ($\sim$ 45 %) can be seen (figure 6.14b). The interference of the back scattered wave with the incident and scattered wave at the fastener hole results in an amplitude increase in front of the notch at the left

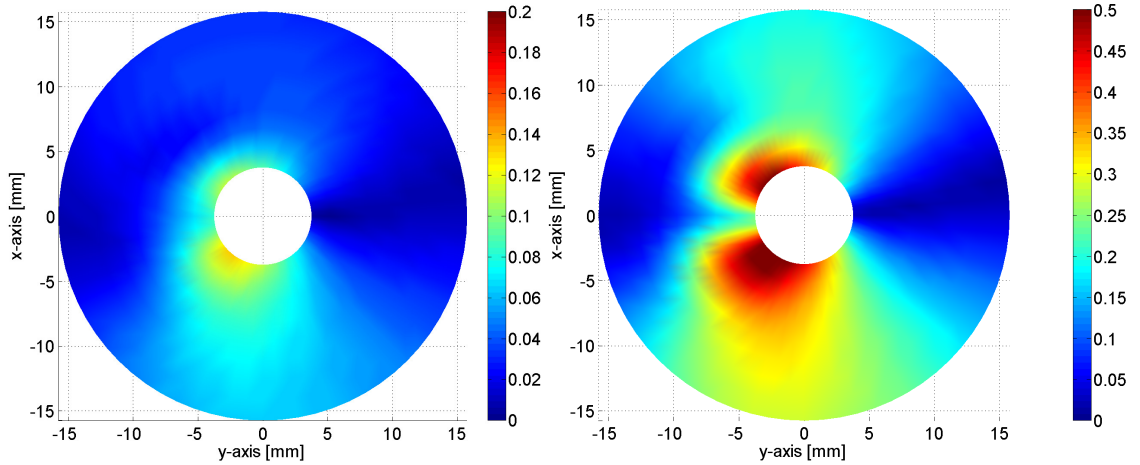

(a) (b)

Figure 6.14: Magnitude of complex difference (with and without a defect; FE) of scattered wave field (f = 115 kHz) around a fastener hole (r_o = 3 mm); (a) 2.25 long notch part through one of the layers;
(b) 5.25 mm long notch through one layer.

boundary of the fastener hole (figure 6.13b). Also seen from figure 6.14b is that behind the notch a significant forward scattering occurs ($\sim$ 50 %). The forward scattered wave will cause an amplitude decrease behind the notch (figure 6.13b) where it interferes destructively with the other waves. The additional scattering ($\sim$ 10 %) for the 2.25 mm notch part through one of the layers is of the same order as the noise levels observed during the measurements. A crack of this size would not be detected. On the other hand the 5.25 mm long crack through one of the layers would be detected. This suggests that defects part through one of the layers would not be detected with the experimental setup used here.

In the next section results from the scattering in a multi-layered plate will be compared against the scattering around a fastener hole with the presence of real fatigue damage through one of the layers in a multi-layered tensile specimen.

6.3 Scattering in a multi-layered tensile specimen

One of the multi-layered tensile specimen (spec.13) used here was fatigued until a 6.0 mm long fatigue crack had grown through one of the layers. The orientation of

the crack in one of the layers was perpendicular to the incident wave. The scattered field was monitored on a radial grid around a 6 mm diameter fastener hole, every 5^o and every 1 mm in the radial direction (r = 4 mm to 10 mm). Measurements were taken under tensile loading before and after the crack had grown through one of the layers and on the opposite layer (undamaged) from where the crack was located.

FE simulations were performed for this specimen using the model described in chapter 3. In the FE simulations the fatigue crack was modelled as a zero width crack (6 mm long) through one of the layers. The scattered field in the FE simulations was monitored on the same radial grid as in the experiments on the opposite layer from where the crack was located. In the end of this chapter results from the scattering in the multi-layered tensile specimen obtained from FE simulations were compared to a large multi-layered plate. The FE model used for the plate had the same mesh and dimension as in section 5.2.1 where it was compared to a single layer plate. The monitoring area was slightly smaller (r = 3.75 mm to 9.75 mm) than for the tensile specimen, while the defect was modelled as for the tensile specimen.

6.3.1 Measurements and FE simulations of the scattering in a multi-layered tensile specimen

The measurement of the scattering around the fastener hole without a defect (figure 6.15c) shows a similar but more noisy amplitude pattern to the FE simulation (figure 6.15a). The measured amplitude pattern is not perfectly symmetrical as the incident wave field is not symmetrical (figure 5.21d). The incident field for the tensile specimen is also different from the incident field in the large multi-layered plate as there is an amplitude variation along the length and width of the specimen. This and the finite width of the tensile specimen which reflects the waves scattered at the fastener hole results in a slightly different amplitude pattern compared to a large multi-layered plate. However, it would be expected to see a similar local change due to a defect in these two structures. In both cases a similar amplitude increase in front of the

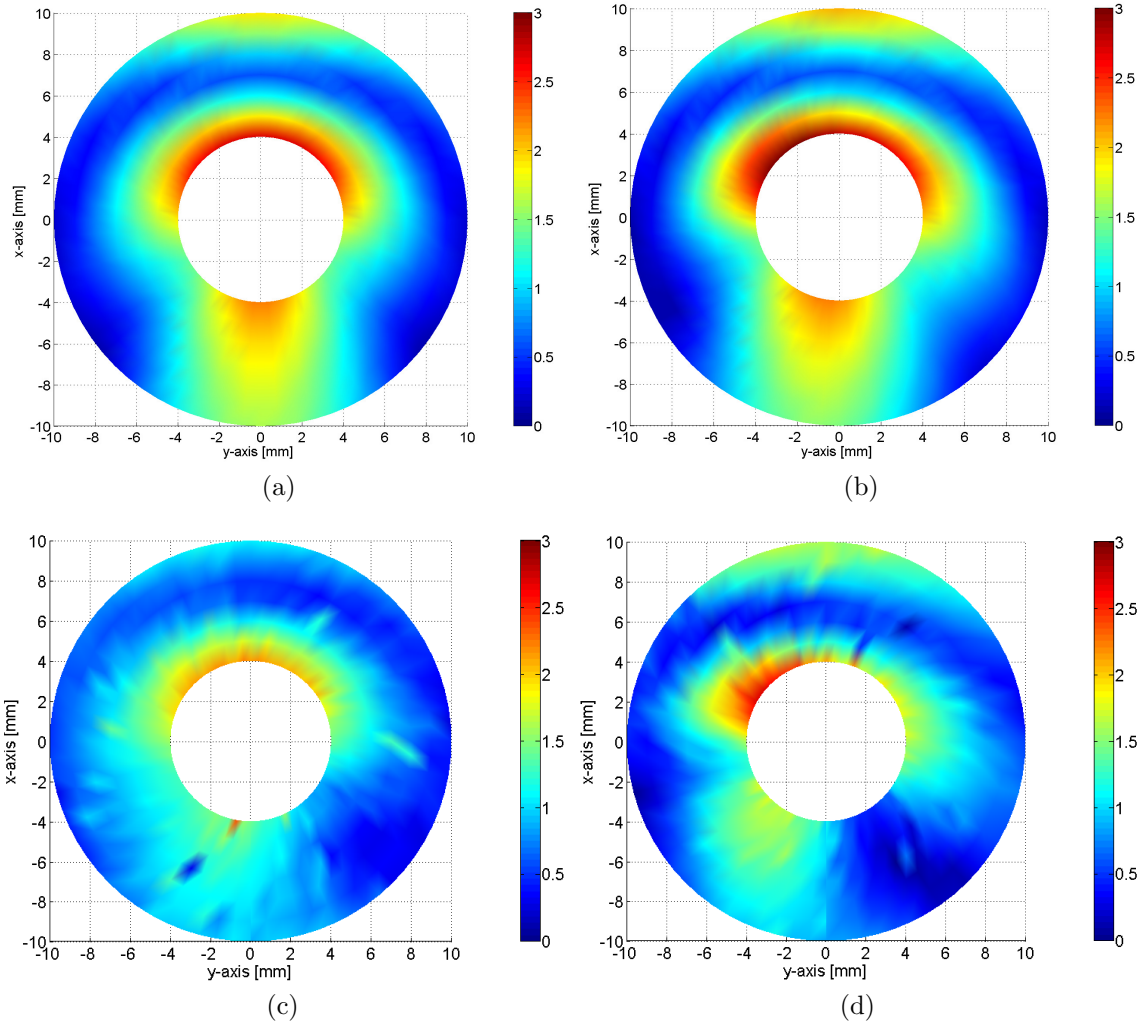

Figure 6.15: Amplitude (f = 115 kHz) of scattered field around fastener hole (r_o = 3 mm) with a 6 mm crack and without a crack in one of the layers of the tensile specimen (h = 6.2 mm); (a) FE, without crack; (b) FE, with a 6 mm crack; (c) experiment, without crack; (d) experiment, with a 6 mm crack.

fastener hole can be seen. In the same figures an amplitude variation can be seen further away from the fastener hole (positive x-dir figure 6.15c and 6.15a). This is due to the interference between the incident wave and the wave scattered at the fastener hole. A small amplitude increase can be seen behind the fastener hole.

The scattered fields obtained from the measurements with the presence of the crack in one of the layers show quite good overall agreement with the FE simulation. Again the difference seen between experiment (figure 6.15d) and FE simulation (figure 6.15b) is most probably caused by the different incident fields and the noise in the measurements. Both FE simulation and experiment show a significant change

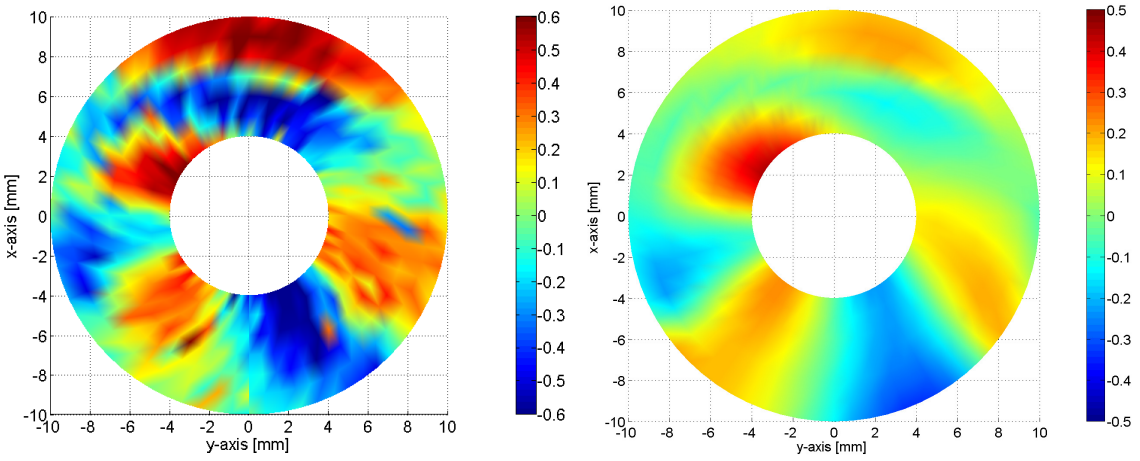

(a) (b)

Figure 6.16: Amplitude (f = 115 kHz) difference of scattered wave fields (FE) due to a 6 mm long crack around a fastener hole (r_o = 3 mm) in a tensile specimen (h = 6.2 mm); (a) experiments; (b) FE simulations.

due to the crack. In figure 6.15d it is possible to see that the amplitude pattern is shifted due to the presence of the crack. The shift in the amplitude pattern seen in the FE simulation (figure 6.15b) looks overall the same as in the experiments. In both cases the additional reflection of the ultrasonic wave at the fatigue crack results in an amplitude increase in front of the defect. The change of the scattered field can be better observed from the difference of the amplitude patterns with and without a crack. The difference in amplitude obtained experimentally for a tensile specimen is shown in figure 6.16a. From this figure a clear shift of the amplitude pattern and an increase in front of the crack can be seen. Behind the location of the crack a region of smaller amplitude can be found. The measurements seen in figure 6.16a are quite noisy. For this reason an average change of the amplitude increase (at the crack) due to the presence of the crack was calculated. The average change is in this case about 55 % in the tensile specimen. A similar shift in amplitude due to the presence of a crack can be seen from the FE simulations. The magnitude of the change ($\sim$ 40 %) is in this case slightly smaller than in the experiments. The most probable reason for that is the difference in the incident wave field between FE and experiments. To summarize, from the results obtained from the experiments and FE simulations it was seen that a defect causes an overall similar change of the amplitude pattern.

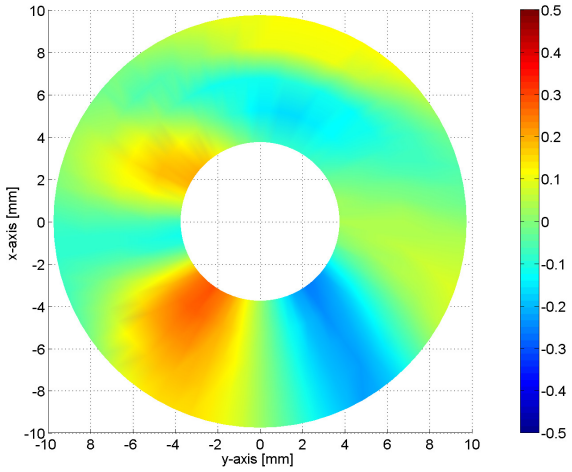

Figure 6.17: Amplitude (f = 115 kHz) difference of scattered wave fields (FE) due to a 6 mm long crack around a fastener hole (r_o = 3 mm) in a large multi-layered plate (h = 6.2 mm).

6.3.2 Comparison to a large multi-layered plate

In this section the scattering in the tensile specimen is compared to the scattering in the large multi-layered plate. The same size fastener hole (r_o = 3 mm) and crack (through one layer, 6 mm long) was used in the large plate as in the tensile specimen. The monitoring was carried out on the undamaged layer on a slightly smaller radial grid than for the tensile specimen. In figure 6.17 the difference (FE) in amplitude between a damaged plate and an undamaged plate is shown. The overall change in the amplitude pattern due to the presence of a crack is very similar to the tensile specimen (figure 6.16b). It can be seen that the crack is shifting the amplitude pattern, increasing the amplitude in front and decreasing it slightly behind the crack. The magnitude of the change in front of the crack ($\sim$ 25 %) is in this case sligthly lower than in the tensile specimen. In figure 6.18a the complex difference (115 kHz) is shown for the tensile specimen. It is possible to see that the presence of the crack results in a significant back scattered wave (x = 2 mm, y = -4 mm figure 6.18a). Also seen is that behind the crack a significant forward scattering occurs. The same study was also performed for the large multi-layered plate. The results from the FE simulations (figure 6.18b) show a similar scattering to figure 6.18a. For the large plate the back and forward scattered waves are of similar amplitude as in the tensile

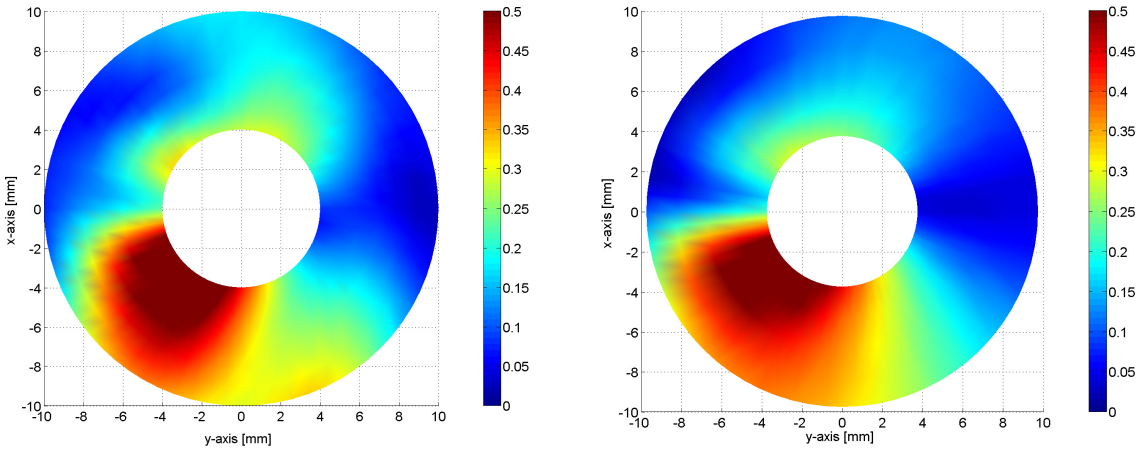

(a) (b)

Figure 6.18: Complex difference of scattered wave (f = 115 kHz) fields (FE) with a 6 mm long crack and without a crack around a fastener hole (r_o = 3 mm); (a) multi-layered tensile specimen; (b) large multi-layered plate.

specimen. A small difference between the two figures (probably caused by the finite width of the tensile specimen) can be seen at the top part of the scattered field (x = 8 mm, y = 2 mm figure 6.18a). In general these two figures show a good agreement, thus it is possible to transfer results from the tensile specimen studied in the next chapter, to the large plates studied in this chapter.

6.4 Summary

This chapter presented results from studies performed on the scattering of flexural waves at a single fastener hole with and without a defect in single and multi-layered plates. Since the physics for the scattering of the A_0 mode at a fastener hole in a single layer plate is fairly well described in the literature [1] the first part of this chapter presented results from this investigation. Similar to what has been observed by other authors [66] the interference between the incident and the scattered wave at the fastener hole results in an amplitude variation in front of the fastener hole and a decrease in amplitude behind it. The presence of a defect at the fastener hole, perpendicular to the incident wave, results in an amplitude increase at the location of the defect. It was also seen that the amplitude pattern was shifted more

for larger defects. With the setup used here, small defects (2 mm long) and through the thickness of the plate could easily be detected.

From chapter 4 it was seen that for low frequencies the mode shapes for the lowest anti-symmetric modes through the thickness for a single layer plate and a multi-layered plate are similar. This leads to the hypothesis that also similar scattering can be expected in these structures. The scattering of low frequency guided ultrasonic waves at a fastener hole in the multi-layered plate used here has not been studied before and at this moment there is no general analytical solution. In this chapter the analytical solution for the scattering at a fastener hole in a single layer plate was compared against the FE results for the scattering in a multi-layered plate. From this comparison a good general agreement was found between the two cases. This verifies the initial hypothesis for the similarities in the scattering between these two structures. Experiments for the scattering of the A_0 like-mode at a fastener hole were performed. These results were compared against the FE code used for these investigations. Results from this showed a good agreement with each other, verifying the FE model.

Experiments and simulations were performed for investigating the scattering in the multi-layered plates with the presence of a defect. The main aim of these investigations was to obtain an estimate of the smallest defect size that can be detected using this type of waves. Results from the investigations performed here show that defects part through one of the layers cannot be detected experimentally by monitoring the scattered field on the opposite layer (undamaged layer), with the noise levels present in the experiments. On the other hand it was found that defects through one of the layers and with a length of almost one third of the wavelength (~ 5.25 mm) can be detected.

The obtained results from FE simulations for a large multi-layered plate were compared to the scattering in a multi-layered tensile specimen. The scattering has been studied in single layer tensile specimen [1], but not much work has been done for multi-layered tensile specimen. From the FE calculations presented here, it was seen

that a good general agreement is found between the scattering in these two types of structure, but with the tensile specimen predicting a slightly larger influence of the defect on the scattered wave field amplitude. The presence of a defect resulted in a similar overall change of the amplitude patterns in these two structures. This means that the results from the fatigue experiments on the tensile specimen presented in the next chapter can be transfered to the large plates.

Chapter 7

On-line fatigue crack growth monitoring

This chapter presents the application of low frequency guided ultrasonic waves for the on-line monitoring of fatigue crack growth in multi-layered tensile specimens. Similar studies have been carried out using low frequency (40 and 160 kHz) guided ultrasonic waves for the monitoring of fatigue cracks in single layer tensile specimen [68, 69]. Fatigue crack growth in single layer tensile specimen has also been carried out using high frequency guided ultrasonic waves [70] and bulk waves [71, 72, 73]. Monitoring fatigue cracks using ultrasonic waves in multi-layered tensile specimen has not been studied to the same extent as for single layer specimen.

Three sets of experiments investigating the sensitivity of these waves to real fatigue cracks which grew in only one layer (referred to as the bottom layer) of the multi-layered specimens were performed.

In order to understand the methodology used in the fatigue experiments, preliminary on-line fatigue crack growth monitoring was performed for two specimens. The influence of a defect on the scattered field was studied for one specimen by comparing the scattered field amplitudes on the top layer around a fastener hole between experiments and FE simulations before and after fatigue crack growth.

The second set of experiments includes the on-line fatigue crack growth monitoring

for three specimens. The results from this set of experiments were compared to 3D FE simulations. As in the first set of experiments the influence of a defect on the scattered field was studied experimentally and compared to FE simulations before and after fatigue crack growth.

In the last set of experiments fatigue crack growth monitoring was conducted on one specimen using a different excitation (single sided) compared to the previous fatigue experiments. The influence of a defect on the scattered field was studied experimentally. Finally the results from these experiments will be discussed and compared against the results from the previous chapter for the defect detection in a large multi-layered plate.

7.1 First set of fatigue experiments (preliminary set)

7.1.1 Description

Three multi-layered tensile specimens (specimen 6 - 8) were manufactured for the first set of experiments (chapter 2). During the fatigue experiments the specimens were subjected to cyclic tensile loading in a servo-hydraulic testing machine (figure 2.8). For monitoring the fatigue crack growth the cyclic loading was stopped initially every 10 000 cycles and after a crack was visible every 1 000 cycles. To monitor the crack growth the maximum tensile load was applied (30 kN) and a measurement of the ultrasonic wave field was taken at a single point on the top layer with the laser interferometer. In the initial phase of the fatigue experiments, which included two specimens (6 and 7) the measured single point was located close to the hole and in front of the crack relative to the wave propagation direction. For specimen 8 the measured single point was behind the crack on the top layer (red dot in figure 2.9).

Measurements were performed on one specimen to study the influence of a crack on the scattered field around the fastener hole. Under loading, the measurements

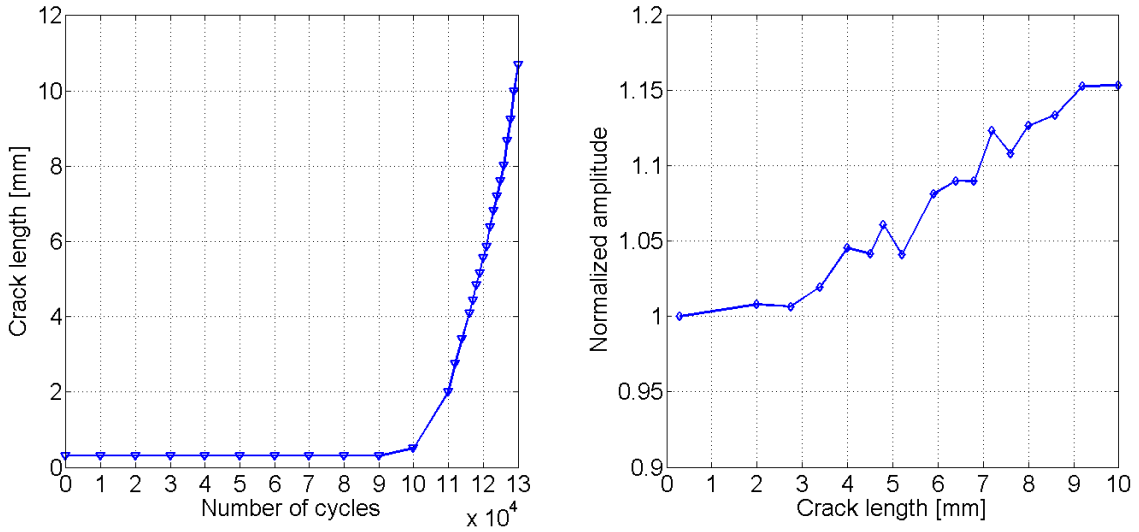

(a) (b)

Figure 7.1: Results from first set of fatigue experiments on specimen 7; (a) optically measured crack length on bottom surface of the specimen against number of cycles; (b) measured ultrasonic amplitude ($f = 40$ kHz) at single monitoring point against optically measured surface crack length (normalized with initial amplitude).

were taken as described in chapter 2 on a radial grid (figure 2.9) on the surface of the top layer (undamaged). In all of the figures presented in this chapter the waves are propagating from bottom to top.

During the first fatigue experiment on specimen 6, the fatigue crack started growing on the opposite side to the starter notch and results will therefore not be shown here. This was most probably caused by a small defect which was introduced there during the drilling of the hole. For the other two specimens the surface area around the hole was polished with fine sandpaper. Two different type of excitation setups and frequencies were used for specimen 7 and 8. A PZT plate (chapter 2) excited at 40 kHz was used to generate the guided ultrasonic waves in specimen 7. The excitation setup (115 kHz) consisting of three PZT discs (figure 2.6) was used for specimen 8.

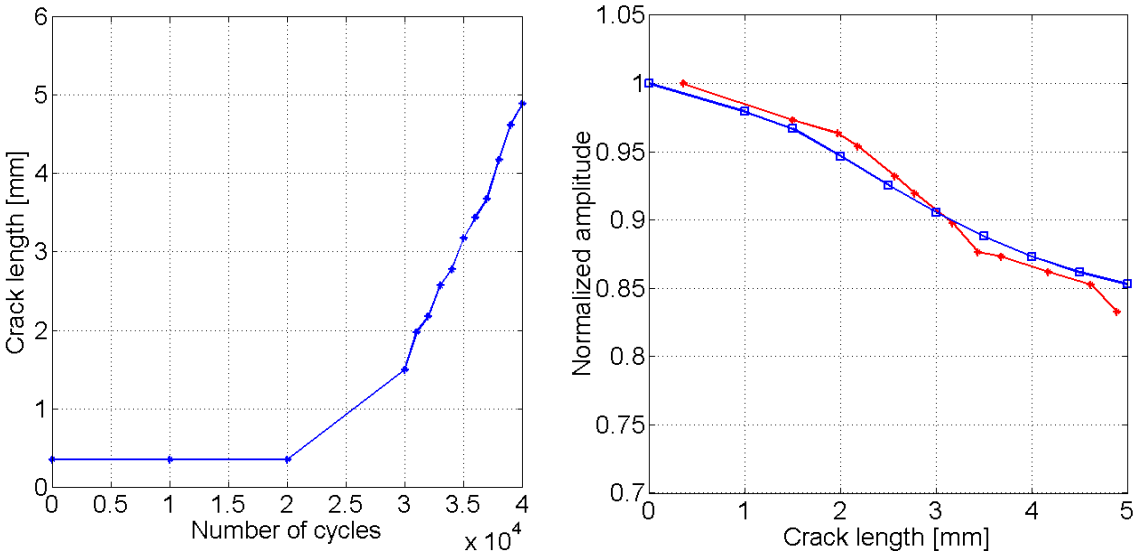

(a) (b)

Figure 7.2: Results from first set of fatigue experiments on specimen 8; (a) optically measured crack length on bottom surface of the specimen against number of cycles; (b) measured ultrasonic amplitude (f = 115 kHz) at single monitoring point against optically measured surface crack length, normalized with initial amplitude (FE: blue, solid-squares; measured: red, solid-stars;).

7.1.2 On-line fatigue crack growth monitoring

Figure 7.1a shows the optically measured surface crack length against the number of cycles for specimen 7 (40 kHz). From this figure it can be seen that crack initiation occurred between 85 000 and 100 000 cycles.

From the results obtained in the second set of experiments it was seen that the crack grew quarter elliptically until it reached the thickness of the bottom layer. After 130 000 cycles the fatigue crack had grown to a surface length of about 11 mm. Figure (figure 7.1b) shows the amplitude (normalized with respect to undamaged case) of the guided ultrasonic wave at the single measurement point against the variation in crack length. It can be seen that the amplitude increases for larger fatigue cracks.

For a 10 mm long crack through the bottom layer a significant amplitude increase (evaluated at 40 kHz) at the single point compared to without a crack (15 %) was observed. From the previous chapter it was seen that with the experimental setup

used here the noise levels could be up to 10 %. In this section this will serve as an estimate of the present noise level. It will be later shown that the actual noise levels in the experiments presented here were slightly lower ($\sim$ 4 %, section 7.3.2), thus the noise level used here can be seen as an upper estimate. This means that a 10 mm long crack could be detected with this setup. For cracks with a typical surface length of 5 mm and through the bottom layer the increase in scattered field amplitude at the single point was about 4 %. This crack would most probably not be detected with the setup used here.

For this reason in the next fatigue experiment (specimen 8) the excitation setup was changed and the excitation frequency was increased from 40 kHz to 115 kHz.

For specimen 8, crack initiation occurred between 20 000 and 30 000 cycles (figure 7.2a). The fatigue crack was first measured optically with a surface length of 1.5 mm after 30 000 cycles. The fatigue crack grew to a surface length of 4.8 mm at 40 000 cycles. At this stage there was no observed cracking of the top layer of the specimen. Figure 7.2b (red, solid-stars) shows the measured amplitude (evaluated at 115 kHz) at the single measurement point against the optically measured crack length. It can be seen that the amplitude decreases with increasing crack length. FE simulations were performed in order to validate these results. At the time of these investigations the FE code was not able to model cracks, so the fatigue crack was modelled as a notch (0.5 mm wide; through the bottom layer; 1 - 5 mm long in steps of 0.5 mm).

The predictions from the FE simulations (blue, solid-squares figure 7.2b) show a very similar decrease in amplitude with increasing crack length. The drop in amplitude for a 4.8 mm long fatigue crack is about 17 % (about twice the noise level) for the experiments and 15 % for the FE simulations (5 mm long notch). A defect of this size would be detected using this measurement setup. In the next section results from the influence of a fatigue crack on the scattered field amplitude pattern at a fastener hole are presented.

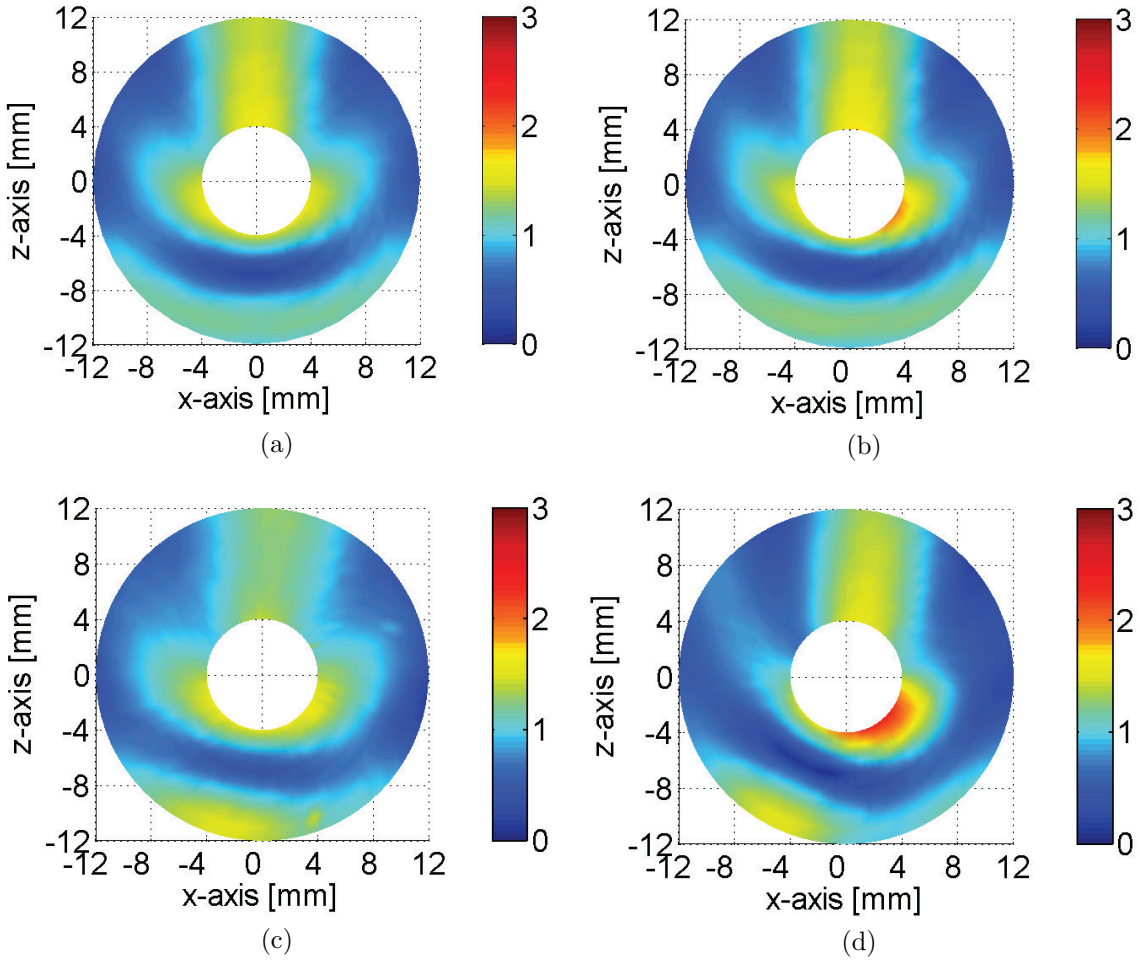

Figure 7.3: Amplitude of scattered field around hole (r_o = 3 mm) at centre frequency (115 kHz); (a) FE simulation, no defect; (b) FE simulation, 5 mm notch in bottom layer at right side of hole (z = 0 mm, x = 3 mm); (c) experiment, no defect; (d) experiment, 4.8 mm long fatigue crack in bottom layer at right side of hole.

7.1.3 Influence of a defect on the scattered field around a hole

Measurements were conducted and compared to FE simulations in order to study the influence of the defect on the scattered field. As in chapter 6 the amplitude patterns shown here are normalized with the average of the total wave field. The defect investigated was the fatigue crack which had grown after 40 000 cycles to a length of 4.8 mm, through the bottom layer of specimen 8. The results obtained from FE simulations (figure 7.3a) for the scattered field around the fastener hole without a defect are symmetrical. From chapter 5 it was seen that the incident wave

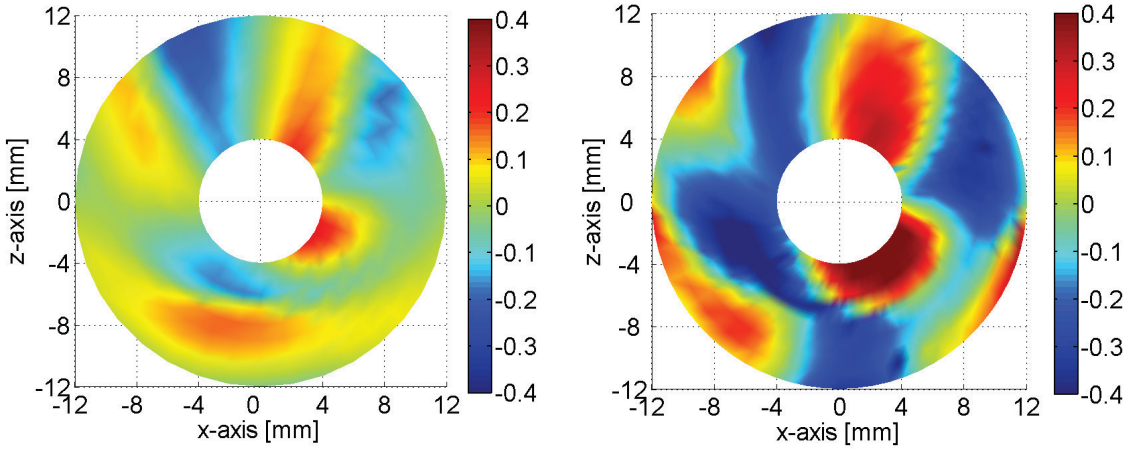

Figure 7.4: Difference in amplitude (f = 115 kHz) between the scattered field around a fastener hole (r_o = 3 mm) and the scattered field at a fastener hole with a fatigue crack; incident wave propagating from bottom to top; (a) FE simulation, 5 mm notch in bottom layer at right side of hole (z = 0 mm, x = 3 mm); (b) experiment, 4.8 mm long fatigue crack in bottom layer at right side of hole.

field between the FE simulations (figure 5.21c) and the measurements on specimen 8 (figure 5.21a) showed a good overall agreement. Good agreement between the measured scattered field around the fastener hole (without a defect, figure 7.3c) and the FE simulation (figure 7.3a) is observed here. However, in the experiments the scattered field distribution is not perfectly symmetrical as the incident wave field is not symmetrical (figure 5.21a). In the FE simulations the fatigue crack was modelled as a notch (0.5 mm wide and 5 mm long) through the bottom layer. In figure 7.3b it can be seen from the FE simulations that the presence of the notch results in a small change of the scattered field. The amplitude is increased slightly before the defect on the right side of the fastener hole, while the overall amplitude pattern is also shifted by a small amount. The experimental results in figure 7.3d show a more significant influence of the fatigue crack on the scattered field as compared to the FE simulations. This can be seen more clearly in figure 7.4, where the difference between the scattered fields (with and without defect) is taken. An amplitude decrease of about 30 % was observed behind the crack in the experiment, while from the FE simulations behind the defect a smaller decrease (15 %) was predicted. The most

possible reason for this disagreement could be the difference in the incident fields between the FE simulations and the experiments. Another possible reason is the fact that the specimen was moved during the two scans thus shifting the measurement grids. The qualitative change of the amplitude patterns is though quite similar in the two cases. The measured amplitude increase of about 40 % in front of the crack (figure 7.4b) is about the same as the change ($\sim$ 30 %) predicted from the FE simulations (figure 7.4a). These measured changes agree also quite well with the measurements on a similar tensile specimen shown in chapter 6.

This section investigated preliminarily the possibility of using low frequency guided ultrasonic waves for the monitoring of fatigue crack growth at a fastener hole in multi-layered tensile specimens. Two frequencies were used during these experiments. In the experiment which used a 40 kHz excitation (specimen 7), cracks through the bottom layer and with a typical surface length of 10 mm could be detected. For detecting smaller cracks guided ultrasonic waves of higher frequency (115 kHz) were used (specimen 8). With this type of excitation fatigue defects with a surface length of 5 mm resulted in a significant amplitude change. From the study of the influence of a defect on the scattered field amplitude patterns were quite similar between experiments and FE simulations. The largest measured (at the defect) change due to the crack was similar to the change predicted from the FE simulations. In both experiments and FE simulations the magnitude and area of the amplitude change was larger in front of the crack than behind it. For this reason the location chosen to monitor changes in the scattered amplitude in the second set experiments was changed. Some additional changes were implemented in order to improve the experimental setup for the second set of fatigue experiments. Some of these changes had to do with the fatigue setup used, the measurement of the crack dimensions and the monitoring setup used for studying the scattered field around the fastener hole. These changes are presented in more detail in the next section for the second set of fatigue experiments.

7.2 Second set of fatigue experiments

7.2.1 Description

Similar to specimens 7 and 8, the specimens investigated here were subjected to cyclic tensile loading in a servo-hydraulic testing machine. Because the initial measurement of the crack length on specimen 8 was done after the crack had grown significantly, in this set of fatigue experiments crack initiation was monitored initially after 10 000 cycles and there after every 5 000 cycles. After a crack had become visible the cyclic loading was stopped every 1 000 cycles and a measurement of the ultrasonic wave field was taken on the top layer at a single point in front of the crack (black dot at z = -3 mm and x = 3 mm in figure 2.9b). In the previous set of experiments the crack length was only measured optically on the surface of the specimen. For the second set of experiments the crack depth was measured on the inner surface of the fastener hole by placing a mirror-film at an angle inside the fastener hole. The last modification was done on the monitoring setup used for studying the influence of a defect on the scattered field around the fastener hole. A scanning rig for the laser was set up close to the fatigue machine, allowing for the scanning of the specimens while clamped. Before any measurements were performed, the maximum tensile load was applied to the specimens (30 kN). Measurements were then taken on a radial grid (dark area in figure 2.9) on the surface of the top layer (layer opposite to crack location). The scanning rig improved also the repeatability of the measurements because the location of the monitoring point could be found much more accurately compared to the previous set of experiments which used a tripod.

For the second set of fatigue experiments, 6 multi-layered tensile specimens (specimen 9 - 14) were manufactured. In specimen 9 the wave propagation was found to be not symmetrical as for the rest of the specimens, so no fatigue experiments were carried out on this specimen. In the rest of the specimens a 6 mm diameter hole was drilled 110 mm away from the excitation transducers. The reason for increasing

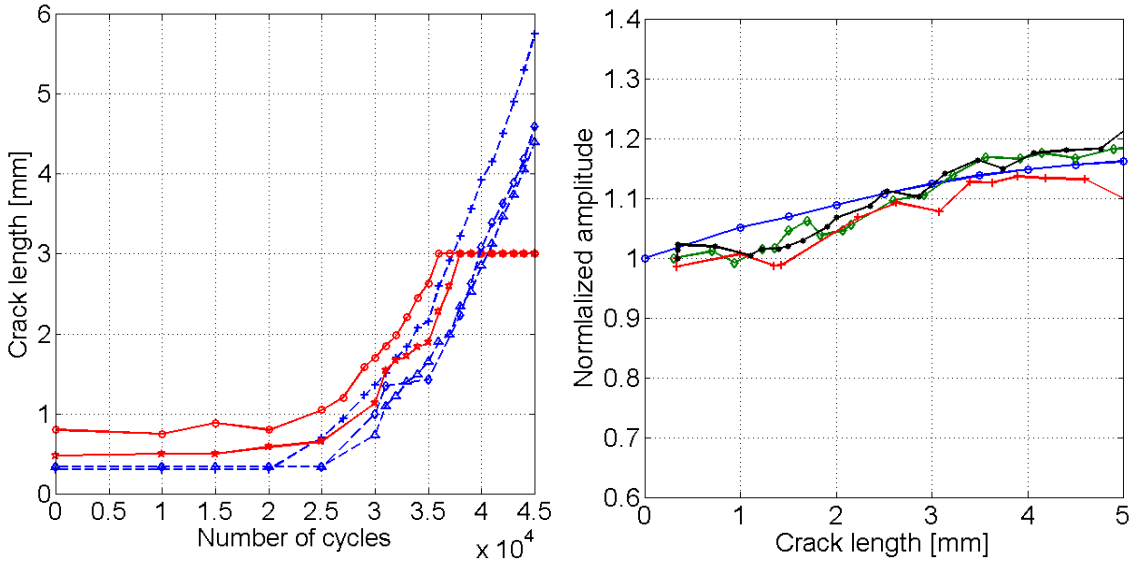

(a) (b)

Figure 7.5: Results from second set of fatigue experiments; (a) optically measured crack length on top surface (spec.10: blue, dashed-diamonds, spec.13: blue, dashed-triangles; spec.14: blue, dashed-crosses) and crack depth inside hole (spec.13: red, solid-stars; spec.14: red, solid-circles) against number of cycles; (b) measured ultrasonic amplitude ($f = 115$ kHz) at single monitoring point against optically measured surface crack length, normalized with initial amplitude (FE: blue, solid-circles; spec.10: red, solid-crosses; spec.13: black, solid-dots; spec.14: green, solid-diamonds).

(from 100 to 110 mm) the distance from the previous experiments (specimen 8), was that a higher amplitude can be found at this location (figure 5.21b). The same excitation setup (115 kHz) as for specimen 8 was used in these experiments.

7.2.2 On-line fatigue crack growth monitoring

During the monitoring of fatigue crack growth on specimen 11, the signal changed. This was most probably caused by a disconnection between the wire and the PZT disc, so the results from these measurements will not be presented here. Results are not shown as well for specimen 12, where the fatigue crack grew on the opposite layer to the starter notch. Because of these events a couple of adjustments were carried out for the next experiments. Once again the drilling and the surface polishing at the hole were performed more cautiously, as well as the wire connection to the PZT discs. Specimen 10 was the first specimen which was successfully fatigued for the

second set of experiments. In figure 7.5a the measured surface crack length against the number of cycles is shown for specimens 10, 13 and 14. In the same figure the optically measured crack depth (inside surface of fastener hole) against the number of cycles is shown for specimens 13 and 14. From this figure it is possible to see that crack initiation occurred for all three specimens between 20 000 and 30 000 cycles. In the first stage of crack growth the crack grew quarter-elliptically in the bottom layer (figure 7.5a). After reaching the thickness of the bottom layer (3 mm), the crack continued to grow as a through crack in this layer reaching a length of about 4.6 mm in specimen 10, 4.4 mm in specimen 13 and 5.8 mm in specimen 14 after 45 000 cycles. At this point there was no observed cracking of the top layer.

Figure 7.5b compares the amplitude at the single measurement point for three specimens (10, 13 and 14) against FE simulations for different crack lengths. The amplitude is normalized with respect to the amplitude of the scattered field at the measurement location without the presence of a crack. In the FE simulations the crack was this time modelled as a crack with zero width (chapter 3). From figure 7.5b it can be seen that the measured and (FE) predicted amplitude increase for different crack lengths agrees very well with each other. The measured and predicted amplitude increases for larger crack lengths, reaching an average change of 18 % for the three specimens and 16 % for the FE simulations, for a 5 mm long crack through one layer. For crack lengths typically smaller than 3 mm the results for the FE simulations ($\sim$ 12 %) are larger than the experiments ($\sim$ 9 %). The larger predicted amplitude for the FE simulations is explained by the fact that in the FE simulations the crack was simulated through the bottom layer from the beginning, while in the experiments the fatigue crack was growing quarter-elliptically. Seen from these measurements is that defects with lengths typically about 2 mm (quarter-elliptical) and below do not give any significant change in the scattered field amplitude. A crack of this size would not be detected using this experimental setup. On the other hand a 5 mm crack produced a similar change for all three specimens. This change is almost twice as large as the previously estimated noise level ($\sim$ 10 %) and

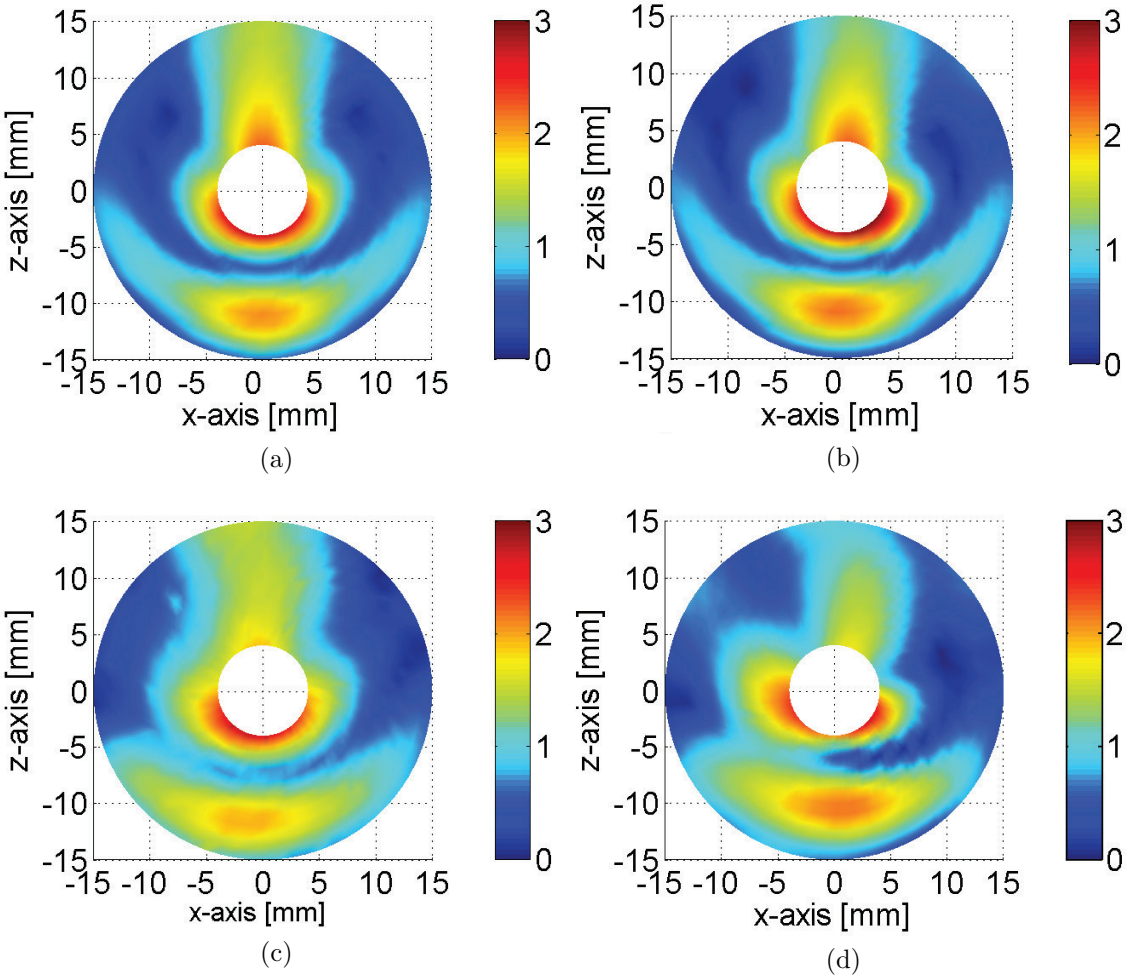

Figure 7.6: Amplitude of scattered field around hole (r_o = 3 mm) at centre frequency of 115 kHz, incident wave propagating from bottom to top; (a) FE simulation, no defect; (b) FE simulation, 6 mm notch in bottom layer at right side of hole (z = 0 mm, x = 3 mm); (c) experiment, no defect; (d) experiment, 5.9 mm long fatigue crack in bottom layer at left side of hole (z = 0 mm, x = 3 mm).

almost five times larger than the noise observed in the next set of fatigue experiments ($\sim$ 4 %) and would therefore be detected.

7.2.3 Influence of a defect on the scattered field around a hole

The influence of a fatigue crack in one of the layers on the scattered field around the fastener hole was investigated. The scattered field around the hole was measured before the start of the fatigue experiments and after a 5.9 mm long fatigue crack

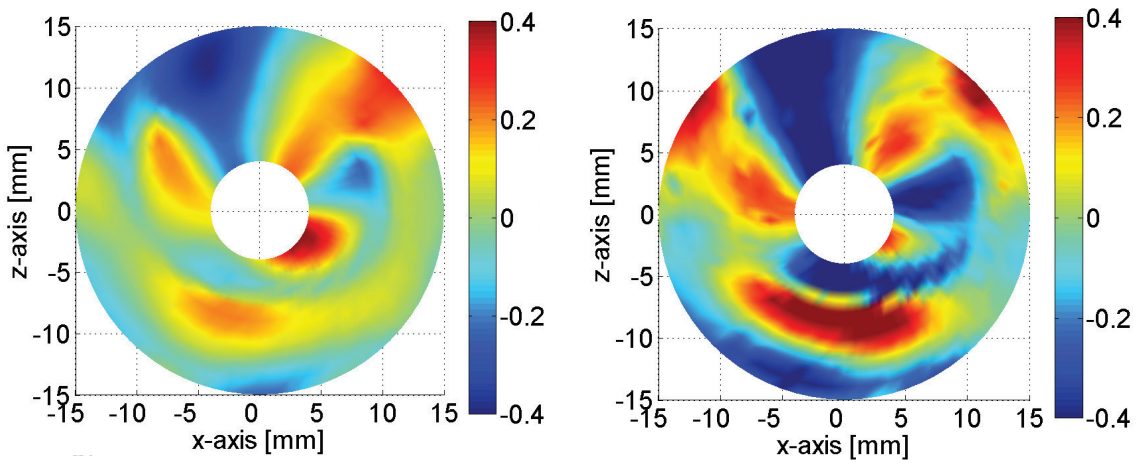

Figure 7.7: Difference in amplitude (f = 115 kHz) between the scattered field around a fastener hole (r_o = 3 mm) and at a fastener hole with a fatigue crack; incident wave propagating from bottom to top; (a) FE simulation, 6 mm crack in bottom layer at right side of hole (z = 0 mm, x = 3 mm); (b) experiment, 5.9 mm long fatigue crack in bottom layer at right side of hole (z = 0 mm, x = 3 mm).

had grown through the bottom layer (specimen 10, after 48 000 cycles). For the 3D FE simulations the defect was modelled as a zero width crack (6 mm long) through the bottom layer.

The results obtained from FE simulations (figure 7.6a) for the scattered field around the fastener hole without a defect are symmetrical. The measurement of the scattering around the hole without a defect (figure 7.6c) shows a similar amplitude pattern to the FE simulations, but is not symmetrical as the incident wave field is not symmetrical (figure 5.21b). The amplitude increase in front of the fastener hole in the experiments (at z = -5 mm and x = 0 mm in figure 7.6c) is slightly different from the FE simulations. This is most probably caused by the different incident fields. From the FE simulations (figure 7.6b) it can be seen that the presence of the crack results in an increase of the amplitude before the defect on the right side of the fastener hole. Similar to the first set of fatigue experiments the measurements (figure 7.6d) show a slightly more significant influence of the crack on the scattered field pattern as compared to the FE simulations, but overall the amplitude patterns look quite similar. Like for the FE simulations an amplitude increase can be seen

in front of the crack. The shift of the amplitude patterns can be seen in both FE simulation and experiment. The shape of the amplitude patterns around the fastener hole is slightly different between FE simulations and experiments. As in the initial experiments for specimen 8 the differences between FE simulations and experiments is most probably caused by the differences in the incident field and an eventual disbond in the experiments which is not modelled. Signs of some sort of adhesive damage were observed on this specimen (black ellipse figure 2.10), suggesting that the largest cause for this difference could be an eventual damage/disbond of the adhesive layer.

The changes caused by the defect (difference between amplitudes, notch and without notch) on the amplitude patterns are more evident for both FE simulations and experiments in figure 7.7. In these figures the increase in amplitude in front of the defect and the decrease in amplitude behind the defect can be seen. The amplitude decrease found in the FE simulations behind the crack (15 %) is smaller than the amplitude decrease observed in the experiments (30 %). The largest measured amplitude increase of about 30 % in front of the crack (figure 7.7b), is though of the same order as for the FE simulations (35 %). In general the observed change in the overall amplitude pattern due to a fatigue crack between FE simulations and experiments is quite similar. The measured overall amplitude change shown here agrees reasonably well with the measurements shown in chapter 6 for specimen 13 (figure 6.16a) and to the measured change in the large multi-layered plate studied in chapter 6 (figure 6.13a) for a similar defect. In front of the defect the average change (30 %) in specimen 10 is also in good agreement with the measured average change due to a defect in the large multi-layered plate ($\sim$ 30 %).

7.3 Third set of fatigue experiments: single sided access

7.3.1 Description

In the previous sections the excitation of the guided ultrasonic waves was carried out by placing PZT discs on both layers. This section investigates the concept for the inspection from a single accessible side for hidden fatigue damage in the bottom layer, exciting and monitoring from the top layer only. The excitation setup (115 kHz) consists of two PZT discs bonded on the top layer as in the previous experiments. The two discs were placed on the nodes of $Fx2$ at 4 mm from each side of the specimen (left in figure 2.6). This type of excitation resulted in a very similar wave field as compared to the excitation used in the previous experiments.

Another four multi-layered tensile specimens (specimen 15 - 18) were manufactured for the third set of fatigue experiments. A 6 mm diameter hole was drilled 130 mm from the excitation on the multi-layered tensile specimens. The reason for increasing the distance from the second set of fatigue experiments (from 110 to 130 mm) was that a higher amplitude can be found at this location. In these experiments a 45^o angle mirror was used instead of a mirror-film which was used in the previous experiments for measuring the crack depth. In order to get more measurements prior to crack initiation a measurement of the ultrasonic wave field was taken this time every 1 000 cycles. The first two specimens (15, 16) were fatigued up to 100 000 and 150 000 cycles where no crack initiation occurred. One of the reason for this could be that for these specimens the holes were reamed. This could possibly have created a plastic zone at the hole boundary which slows down crack initiation. Specimens 17 and 18 were fatigued successfully. To investigate the influence of a fatigue crack on the scattered field the same measurement procedure was used here as in the previous experiments. Measurements were for these two specimens taken prior to crack initiation and after a 6.2 mm crack had grown through the bottom layer.

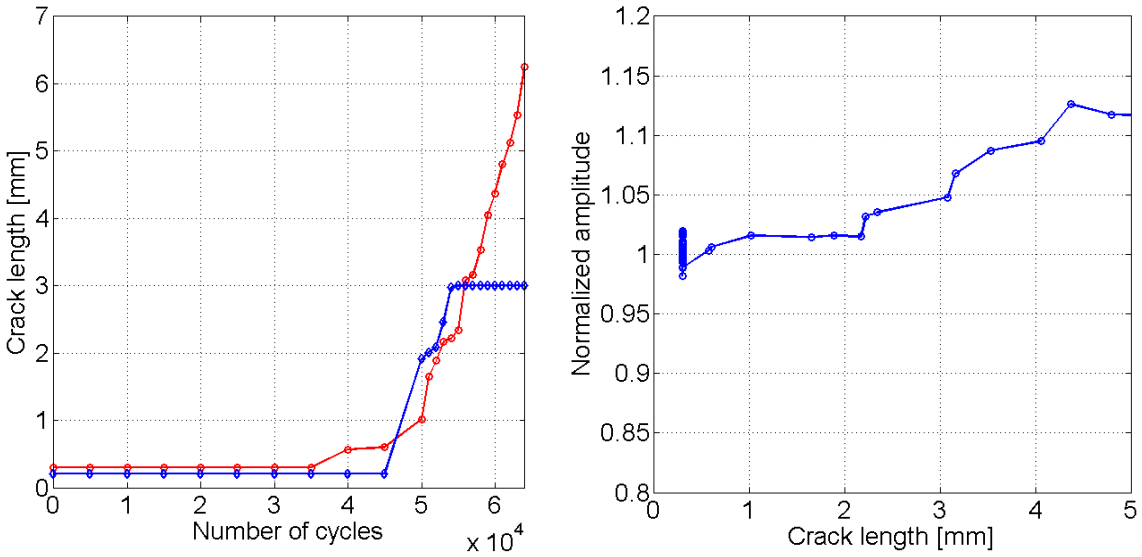

(a) (b)

Figure 7.8: Results from third set of fatigue experiments on specimen 18; (a) optically measured crack length on top surface (red, solid-circles) and crack depth inside hole (blue, solid-diamonds) against number of cycles; (b) measured ultrasonic amplitude at single monitoring point against optically measured surface crack length, normalized with initial amplitude (blue, solid-circles).

Because the previous specimens did not develop any cracks, for specimen 17 crack initiation was monitored initially every 1 000 cycle up to 50 000 cycles. At that point there were no visible cracks so the specimen was fatigued directly up to 80 000. At 80 000 cycles a visible crack had developed in the specimen. A measurement of the ultrasonic wave field was taken (as for the second set of experiments) every 1 000 cycles. The crack continued to grow in this layer reaching a length of about 6 mm after 90 000 cycles. The measured amplitude at the single point did not show a significant increase with increased amplitude during the fatigue experiments. The most probable reason for this, which was observed after the experiments was that the PZT disc had detached from the surface of the specimen.

7.3.2 On-line fatigue crack growth monitoring

In figure 7.8a the measured surface crack length (red, solid-circles) and depth (blue, solid-diamonds) is shown against the number of cycles for specimen 18. The surface

crack length and the crack depth were measured every 5 000 cycles up to 50 000 cycles and then every 1 000 cycles. A measurement of the ultrasonic wave field was taken from the start of the fatigue experiments every 1 000 cycles at the same point as in the second set of fatigue experiments. It is possible to see that crack initiation occurred between 35 000 and 40 000 cycles. In the first stage of crack growth the crack grew quarter elliptically in the bottom layer (figure 7.8a). After 64 000 cycle it had grown to a surface length of 6.2 mm. At this point there were no cracks observed on the top layer.

Figure 7.8b shows the amplitude at the single measurement point for specimen 18 against the surface crack length. The amplitude is normalized with respect to the average amplitude of the scattered field for the first 20 measurements (without crack) taken every 1 000 cycles from the start up to 20 000 cycles. The variation of the measured amplitude (normalized) from these 20 measurements was further investigated. From these measurements the mean value is 1, while the standard deviation is about 1 % of that value. The range of these measurements (maximum value - minimum value) is four times larger than the standard deviation. This number (4 %) is an estimate of the noise level in these experiments and will be the criterion for the smallest measured amplitude change needed to detect a crack. From figure 7.8b it can be seen that the amplitude increases with increasing crack length. For a 5 mm long crack through one of the layers the amplitude change is about 12 %. This change is in the same range as the average observed amplitude increase (18 %) for a 5 mm long crack for the specimens shown in the previous section (figure 7.5b). The measured increase for a 5 mm long crack (12 %) is about three times larger than the noise level. A crack of this size would therefore be detected with the single sided excitation and measurement setup used here. With the present noise level it is reasonable to say that quarter-elliptical cracks with a typical length below 2 mm do not produce a significant change ($\sim$ 3 %) in the measured wave amplitude and would most probably not be detected using this setup. This is similar to the findings from the second set of fatigue experiments and the measurements on the

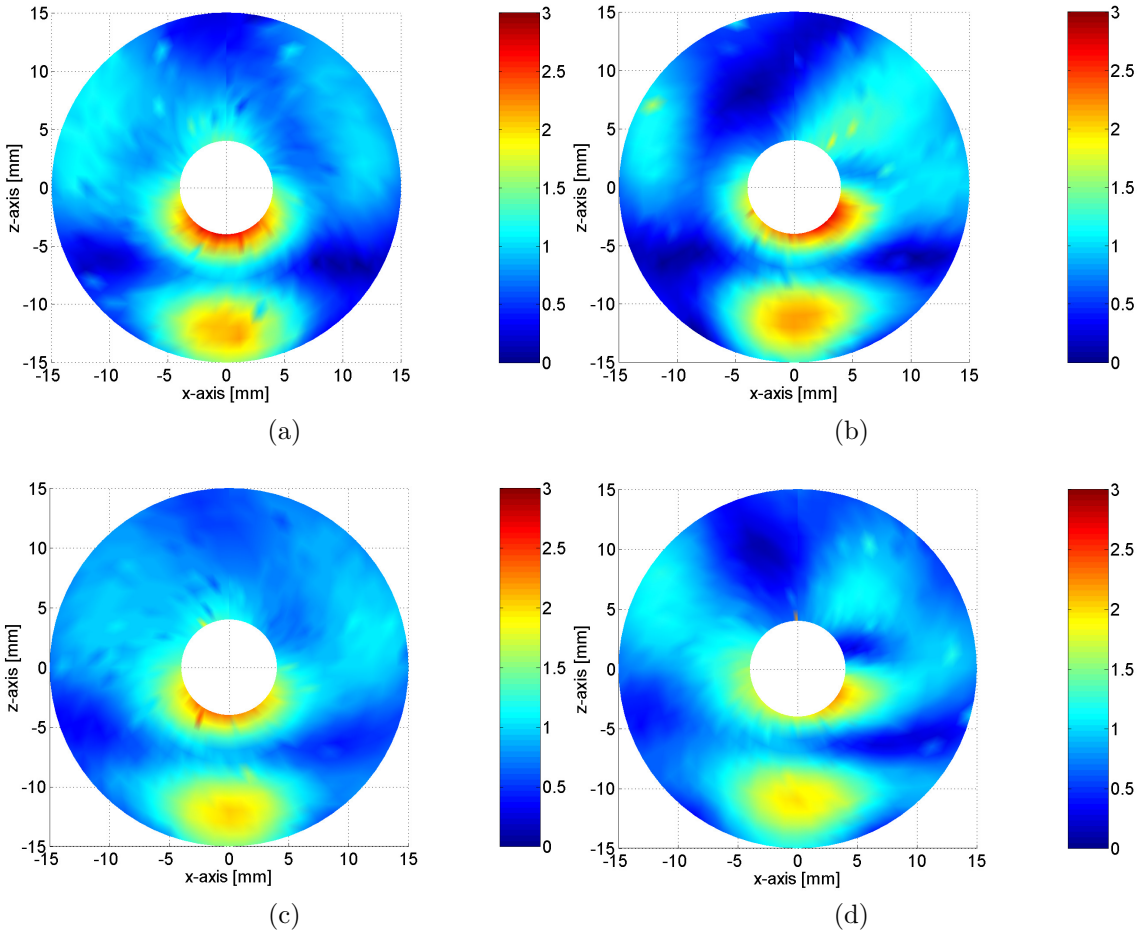

Figure 7.9: Measured amplitude of scattered field around hole (r_o = 3 mm) at centre frequency of 115 kHz: (a) specimen 17, no defect; (b) specimen 17, 6.2 mm crack in bottom layer at right side of hole (z = 0 mm, x = 3 mm); (c) specimen 18, no defect; (d) specimen 18, 6.2 mm long fatigue crack in bottom layer at right side of hole.

large multi-layered plate (section 6.2.3) where it was seen that for defects of similar dimensions no significant amplitude increase is observed.

7.3.3 Influence of a defect on the scattered field around a hole

In order to perform these experiments on specimen 17 the detached PZT disc was replaced with a new one. The influence of a fatigue crack on the scattered field was then studied on specimens 17 and 18. The results for the two specimens (figure 7.9a, 7.9c) show the scattered field around the fastener hole without a crack with a similar

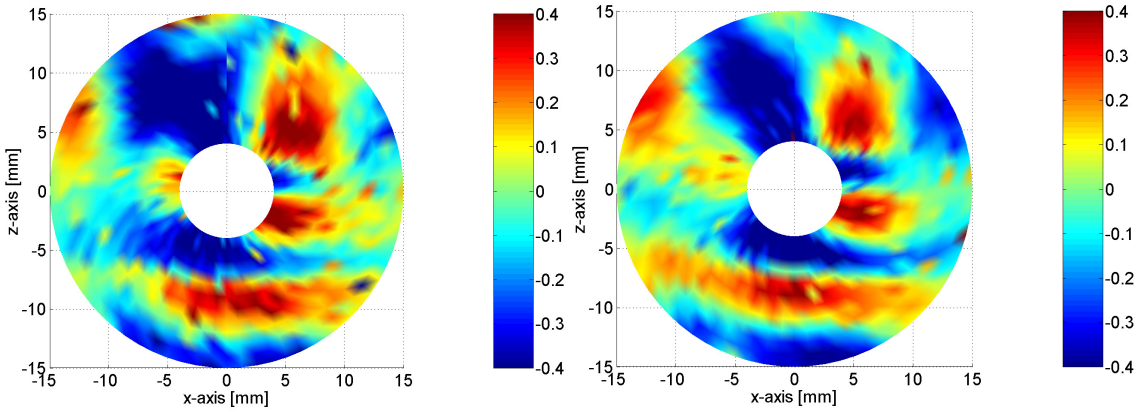

(a) (b)

Figure 7.10: Difference in amplitude (115 kHz) between the scattered field around a fastener hole (r_o = 3 mm) and at a hole with a 6.2 mm long crack at the right boundary of the hole in one of the layers; (a) specimen 17; (b) specimen 18.

overall amplitude pattern. Studying these two figures in more detail it is possible to see that figure 7.9a is slightly more symmetric than figure 7.9c. This is most probably due to the fact that the incident wave field was more symmetric (figure 5.22). Figures 7.9b and 7.9d show the scattered fields around the fastener hole for specimen 17 and 18 respectively with the presence of a fatigue crack (about 6 mm long). The amplitude patterns in these two figures show an overall good agreement. Similar to what was observed for specimens 8 and 10, specimens 17 and 18 show an amplitude increase in front of the defect (z = -3 mm, x = 3 mm in figure 7.9b and 7.9d). The predicted amplitude increase due to the presence of the crack looks larger for specimen 17. Results from the investigation performed on the previous tensile specimens predicted a shift of the scattered field due to the presence of the defect. This can also be seen in figures 7.9b and 7.9d where the amplitude patterns are shifted clockwise. The shift and increase in amplitude can better be seen in figure 7.10 where the difference between the scattered fields due to the crack has been taken for the two specimens. In figure 7.10a where the amplitude change due to the defect in specimen 17 is shown, it can now clearly be seen that the amplitude pattern is shifted due to the presence of the crack. It is also seen that the amplitude increases by about 35 % in front of the crack. Similar shift and amplitude increase in front of the defect can be seen for specimen 18 (figure 7.10b). These amplitude

patterns and the corresponding largest amplitude increase (in front of a $\sim$ 6 mm long defect) are similar as for specimen 10, specimen 13 and for the large multi-layered plate (figure 6.13a).

7.4 Summary

This chapter investigated the possibility of monitoring fatigue crack growth in only one layer of a multi-layered structure using low frequency guided ultrasonic waves monitored on the opposite, undamaged, layer. In the first set of experiments it was found that waves excited at 40 kHz (centre frequency) gave a significant amplitude change (15 %) for crack lengths of about 10 mm which would have been detected with this setup. For crack lengths below 5 mm the amplitude change was in the order of typical noise levels ($\sim$ 4 %) observed during these investigations. Therefore the excitation setup was changed and the excitation frequency increased to 115 kHz. For these measurements a 4.8 mm long fatigue crack gave a significant amplitude change (about four times the noise level) of about 18 % and would thus be detected. The presence of this defect resulted in a significant change of the scattered field amplitude pattern. The observed change was slightly larger in the experiments than predicted from the FE simulations. One possible reason is that the incident wave field is different in the experiments and the FE simulations. The overall change in the amplitude patterns due to a defect was quite similar for experiments and FE simulations.

For the second set of experiments guided waves excited at 115 kHz were employed for the monitoring of fatigue crack growth. The measured and (FE) predicted amplitude increase for different crack lengths agreed very well with each other. From these measurements it was seen that a fatigue crack through one of the layers and with a typical surface length of 5 mm produced a repeatable and significant amplitude change ($\sim$ 18 %) for three specimens and would thus be detected. Part through cracks with a length of about 2 mm and below did not give any significant amplitude

increase (~ 5 %). This was in good agreement with the first set of fatigue experiments and the measurements on the large multi-layered plate for similar defect dimensions (2.25 mm long notch). The observed overall change due to the defect (6 mm long crack) on the overall scattered field amplitude patterns was quite similar to the FE simulations. This overall change and the average increase (in front of the defect) was also very similar to the observed changes in the large multi-layered plate for a similar defect.

In the last set of experiments the excitation was performed this time from a single layer (opposite to defect layer), simulating one-sided access for hidden defect detection. The monitoring of fatigue crack growth was performed on the same layer as the excitation. From these experiments the noise level (~ 4 %) was quantified from one specimen. The observed increase in amplitude for increasing crack length was in the same range as in the previous set of experiments. From this set of experiments a defect with a length of 5 mm resulted as before in a significant amplitude increase (12 %). This increase is three times larger than the noise level and could thus be detected. On the other hand quarter-elliptical cracks with a length of 2 mm and below would not be detected here. This is in good agreement with the previous experiments and with the measurements on the large multi-layered plate. The change in the amplitude pattern due to a defect (~ 6 mm long crack) was very similar to previous measurements on multi-layered tensile specimens and the large multi-layered plate for similar defects.

7.5 Conclusion

Because of the similarities seen in the wave propagation and the scattering with the presence of fatigue defects between the tensile specimen studied here and the large multi-layered plates from the previous chapter, it is possible to draw some general conclusions from the results presented in chapter 6 and 7.

Relating the results presented here to the previous chapter (6.2.3), where a part

through notch in a large multi-layered plate was studied, it can be concluded that fatigue cracks part through one of the layers and with a typical length and depth below 2 mm would most probably not be detected in these structures using this setup. For defects over 2 mm and below 3 mm part through one of the layers it was seen that they produce some change in the measured signal, but that this change is just slightly larger than the noise levels in the experiments. For defects of this size it is difficult to draw any conclusion related to their detection sensitivity. For defects which are through the thickness of one layer and 3 to 5 mm long the experiments and FE simulations here show a significant repeatable change in amplitude and could probably be detected with the setup used here. Finally it was seen in this chapter that a fatigue crack through one of the layers and with a typical length of 5 mm would be detected in the tensile specimens by monitoring the undamaged layer. Similar results were found in chapter 6 for a 5.25 mm long notch through one of the layers of a large multi-layered plate. This leads to the conclusion that fatigue cracks of this size and through one of the layers can be detected in these structures by monitoring the opposite undamaged layer.

Chapter 8

Conclusions and outlook

8.1 Overview of thesis

The main aim of this chapter is to review the work done during the PhD and to relate that to the aim of this project, which was was to study the sensitivity of low frequency guided ultrasonic waves to real fatigue cracks in the sub-layer of multi-layered aircraft structure. The first part of this chapter presents a review and conclusions from the studies on the propagation and excitation of guided ultrasonic waves in multi-layered plates and tensile specimens. Main conclusions are presented from the studies on the scattering of these waves at fastener holes with and without defects in multi-layered structures. Conclusions are also presented and analysed for the fatigue experiments. In the following section the work presented in this thesis is analysed critically and improvements are suggested. The last part of this chapter gives some suggestions of future work.

8.2 Wave propagation in multi-layered plates and tensile specimen

The characteristics of the low frequency guided waves propagating in the structures had to be understood as a first step. A general review of these results and their

implications for defect detection is given in chapter 4. Initially in this chapter dispersion curves for guided waves propagating in infinite single and multi-layered plates (total thickness: 6.2 mm) are presented. By comparing the dispersion curves and mode shapes for guided waves propagating in infinite single and multi-layered plates it was shown that for low frequencies (20 kHz) the dispersion curve and mode shape of the lowest flexural (A_0-like) mode in a multi-layered plate is similar to the A_0 mode in a single layer plate with the same thickness. For high frequencies ($\sim$ 500 kHz, frequency thickness: $\sim$ 3 MHz mm) the dispersion curves and mode shapes (in the adherents) of the A_0-like mode are similar to a single layer plate with the same thickness as one of the adherents. In the frequency range used in this thesis (35 kHz - 115 kHz) the A_0-like mode is more similar to the A_0 mode in a single layer plate with the same thickness as the multi-layered plate. This result indicates that a similar scattering behaviour at a fastener hole can be expected in these two structures at the working frequency range.

Dispersion curves in a single layer plate strip were calculated using a SAFE code. The SAFE calculations showed that due to the finite width of the plate strips multiple width modes can propagate. The lowest flexural mode (Fx) showed a relative constant amplitude across the width with slightly higher amplitude at the edges. The constant amplitude of the lowest flexural mode makes it a suitable candidate for fatigue crack growth monitoring. As predicted by literature, the dispersion curve of this mode agrees well with the dispersion curve of the A_0 mode in a large single layer plate. Higher order bending width modes ($Fx1$, $Fx2$) have an amplitude variation across the width.

Similar investigations were performed on multi-layered tensile specimens. A very important result from these studies on the wave propagation in plate strips, is that the thickness mode shapes for the lowest flexural mode (Fx) and the first two higher order width modes ($Fx1$, $Fx2$) in this structure agree well with the thickness mode shape of the lowest anti-symmetric mode in an infinite plate. This suggests that these flexural modes in the multi-layered tensile specimens should have similar sensitivity

for defects as the A_0-like mode, which can be used for the detection of fatigue cracks in large multi-layered structures, e.g., in aircrafts. Studies investigating the influence of the specimen width on the wave propagation showed that more modes propagate with increasing width, as predicted in literature.

8.3 Excitation of flexural waves in tensile specimen

Three techniques were presented and discussed in chapter 5 for exciting flexural modes in the tensile specimen. Two of the techniques tried to approximate the uniform width mode shape of the Fx mode across the width by placing a PZT plate and later multiple PZT discs across the width. Another technique was tried for low frequencies (35 kHz) were a limited number of flexural modes can propagate. The idea behind this technique (mode suppression technique) was instead of approximating the mode shape of Fx across the width, to try and suppress the first higher order mode ($Fx1$). These techniques excite mostly the flexural modes and only to a smaller extent torsional and longitudinal modes. The wave propagation was studied experimentally by investigating the wave propagation and especially the interference between the two flexural modes, Fx and $Fx1$. These results were compared to FE simulations. Similar investigations were done on the multi-layered tensile specimen which used the mode suppression technique to obtain a repeatable and relative constant incident wave field. The amplitude at the location of the fastener hole were compared between these specimens.

Using a PZT plate as excitation in a single layer tensile specimen (35 kHz), it was not possible to isolate the lowest flexural mode. Results from these measurements showed an amplitude variation across the width and length of the specimens. This variation was caused by the interference of the two flexural modes that can propagate at this frequency (Fx and $Fx1$). The methodology developed to estimate their

amplitude ratio ($Fx/Fx1$) studies this interference. This excitation setup excited mostly the $Fx1$ mode (amplitude ratio below one), resulting in a non uniform incident field with large amplitude variations across and along the specimen. The reason for this is that the force exerted by the PZT plate on the structure is not uniform across the width, exciting in this way more the first higher order mode ($Fx1$).

Different to the results from the FE simulations where an increase in amplitude ratio ($Fx/Fx1$) for an increasing number of PZT discs was predicted, the measured amplitude ratios for the method using multiple PZT discs resulted in similar amplitude ratios for one, three and five discs. The measured amplitude ratios (below one) were of the same order of magnitude as for the PZT plate. By increasing the number of discs it was also seen that it was more likely to excite a torsional mode. The mode suppression technique which used only two discs, resulted in a four times higher amplitude ratio compared to the two previous techniques, but did not manage to isolate the Fx mode. FE simulations which modelled the PZT discs as point forces, predicted a much higher amplitude ratio (~ 20). Possible reasons for the large difference between the FE simulations and the experiments are the position accuracy of the PZT discs and the extra added mass due to the discs which was not modelled. The influence of the position accuracy was studied and it can be concluded that this cannot explain this difference, thus the most probable reasons are the extra added mass of the discs and the interaction between the guided waves and the discs.

Since it was not possible to isolate the Fx mode in the more simple single layer structure the mode suppression technique was used to try and excite the $Fx1$ mode in the multi-layered tensile specimen instead. The mode suppression technique used here did not excite a single mode ($Fx1$) as intended, but excited multiple flexural modes causing an amplitude variation. Due to time constraints it was decided to move ahead with this excitation setup. The resulting incident wave field amplitude was repeatable at a location where the fastener hole was located, showing a high and relatively constant amplitude for all of the specimens investigated. Locally around the fastener hole, scattering similar to that of an A_0-like flexural mode in a large

plate can be expected, as the mode shapes through the thickness are similar. For the last specimens which were fatigued the excitation was performed from a single side. This excitation was used in order to prove the concept of hidden fatigue damage detection by single sided access. Good repeatability was observed between the two specimens, producing an area of high amplitude at the centre of the specimens. The measured amplitude patterns looked very similar to the amplitude patterns obtained with the previous excitation setup which used three PZT discs.

The studies on the wave propagation in the multi-layered tensile specimen and large plates helps to understand the waves in these structures. A method combining different measurements of the interference pattern at different width locations was used for measuring the relative amplitude ratios between the propagating modes in the tensile specimens. Using this methodology it was seen that PZT plates and multiple PZT discs are not very useful for isolating a single mode at low frequencies. The used technique of mode suppression gave a better wave propagation compared to these methods.

8.4 Scattering and defect detection in large plates

Chapter 6 presented results from studies performed on the scattering of flexural waves at a fastener hole with and without defects in single (notch through the thickness) and multi-layered plates (notch through and part through one layer). Preliminary experiments and FE simulations were carried out on a single layer plate. The theoretical scattering calculation at a fastener hole in a single layer plate was compared against FE simulations for the scattering in a multi-layered plate at the working frequency (115 kHz). Experiments for the scattering of the A_0-like mode at a fastener hole with and without a defect were performed and compared with FE simulations. The obtained results from the FE simulations for a large multi-layered plate were also compared to the scattering in a multi-layered tensile specimen.

From the measurements of the scattering and defect detection at a fastener hole

in a single layer plate it was seen that the amplitude pattern was shifted with larger shifts for larger defects in single layer plates. The experimental results showed a good agreement to FE simulations.

The scattering at a fastener hole in a single layer plate obtained by theory was compared against the FE results for the scattering in a multi-layered plate with the same total thickness as the single layer plate. From this comparison a good general agreement was found between the two cases. This verifies the initial hypothesis for the similarities in the scattering between these two structures.

Experiments for the scattering of the A_0 like-mode ($f = 115$ kHz, $\lambda = 15.8$ mm) at a fastener hole in the multi-layered plate showed good agreement with FE simulations used for these investigations, thus verifying the FE model. Results from experiments and FE simulations for a 2.25 mm long rectangular notch approximately $\frac{2}{3}$ through one of the layers (3 mm thick) showed a very small amplitude change (opposite layer) due to the defect, suggesting that this size of defects ($\sim \frac{\lambda}{7}$) cannot be detected by monitoring the undamaged opposite layer. For a rectangular notch through one of the layers and with a length of almost one third of the wavelength (5.25 mm) experiments and FE simulations agree well with each other, both showing a significant ($\sim$ 25 %) amplitude increase in front of the defect on the opposite (undamaged) layer. Similar studies were performed for real fatigue cracks in multi-layered tensile specimens. Comparing the results from the scattering in a large multi-layered plate to the scattering in a multi-layered tensile specimen with the presence of a fatigue crack (6 mm long and through one layer) a good overall agreement was observed between them, but with the tensile specimen predicting a slightly larger influence of the defect on the scattered field amplitude. This suggests that similar sensitivity to this type of defects can be expected in these two structures.

These studies of the scattering of low frequency guided anti-symmetric waves at fastener holes in multi-layered plates contributed to the understanding of this phenomena. This type of investigation on multi-layered structure has not been carried out to a large extent before. The presented results helped also to understand

the scattering in a multi-layered tensile specimen. The results for the tensile specimen can be used to predict the sensitivity to defects in a large multi-layered plate. In this chapter the FE code was verified for the scattering in single and multi-layered structure. Finally, a detection limit for the multi-layered plates was proposed.

8.5 Fatigue crack growth monitoring

Results from the fatigue crack growth monitoring in multi-layered specimens using guided ultrasonic waves were presented in chapter 7. Three sets of experiments were performed during these investigations. The first set of experiments included three multi-layered specimens, but only two were fatigued successfully. From these experiments it was seen that low frequency guided ultrasonic waves (40 kHz) were not sensitive enough to detect fatigue cracks. Increasing the frequency to 115 kHz the guided waves showed greater sensitivity to fatigue cracks. In this case the measured and predicted (FE) amplitude of the ultrasonic wave field on the undamaged layer (behind the location of the crack), decreases almost linearly for increasing crack lengths. Reasonably good agreement was found between the amplitude decrease predicted from the FE simulations for a 5 mm long through notch and the drop in amplitude for a 4.8 mm long fatigue crack. The observed change of the scattered field amplitude pattern due to this defect was slightly larger in the experiments than the FE simulations. This is believed to have been caused by the difference in the incident wave.

For the second set of fatigue experiments, three multi-layered specimens were fatigued successfully. The on-line fatigue crack growth for all of the investigated specimens showed a similar increase in the monitored amplitude for different crack lengths, making it possible to detect fatigue cracks. The average amplitude increase for the three specimens was about 18 % for a 5 mm long crack (through one layer) and a 16% change in the FE simulations. This defect produces a change larger than the noise level ($\sim$ 4 %) and would have been detected. For crack lengths smaller

than 2 mm no significant amplitude change was observed. The measured influence of the defect on the overall scattered field was similar to the predictions from the FE simulations.

In the third set of fatigue experiments four more specimen were manufactured. A single sided access was used for the excitation and measurement. From these four specimens only one was fatigued and monitored successfully. For this specimen the monitored amplitude showed a similar increase for increasing crack lengths as in the second set of fatigue experiments, validating the single sided access for fatigue crack detection. The amplitude increase for a 5 mm long crack (through one layer) was in this case about 12 %. This increase was in the same range as for the second set of fatigue experiments for a similar defect. From this experiment an estimate of the noise levels was obtained. The noise level in this experiment ($\sim$ 4 %) was seen to be about three times lower than the increase in amplitude due to a crack of detectable size (5 mm long).

From the fatigue experiments on the tensile specimens and the scattering calculations on the large multi-layered plates, it is possible to draw some general conclusions. It can be concluded that fatigue cracks part through one of the layers and with a typical length and depth below 2 mm (115 kHz, $\sim \frac{\lambda}{7}$) would most probably not be detected in these structures with the experimental setup used here. On the other hand a fatigue crack through one of the layers and with a typical length of about 5 mm (115 kHz, $\sim \frac{\lambda}{3}$) produces a change in the scattered field amplitude which is about four times larger than the estimated noise level. This defect can be detected in the tensile specimens by monitoring the opposite (undamaged) layer. This thesis showed that the flexural guided wave modes in multi-layered tensile specimen are very similar to the lowest anti-symmetric mode, used for defect detection in a large plate. Because of this and the fact that the influence of a fatigue crack on the scattered field in the tensile specimens showed a good overall agreement with a large plate for similar defects, it can be concluded that similar sensitivity to fatigue cracks can be expected in these two structures.

8.6 Critical review

Before proposing any future investigations that might be undertaken after this work it is useful to address some points in this thesis and to propose ways in which the investigations could have been improved.

The investigations which looked in to the excitation of the lowest A_0 mode in the tensile specimen took a significant time to perform. Taking this into account and the fact that it was not possible to isolate this mode needs some explanation. The initial idea was to use PZT plates for the excitation of the guided waves. During the course of this work it was seen that this was not possible. Further investigations using SAFE were therefore undertaken in order to understand the waves in these structures which were excited by the PZT plates. Another method using multiple PZT discs did not manage either to excite and isolate a single mode. The measurements performed for these studies did not agree with the FE simulations. Similar to what has been observed by other authors the difference is most probably caused by the interaction between the guided waves and the PZT discs and the extra added mass (disc) which is not taken into account in the FE simulations. Due to the difficulties in the modelling of PZT material and time constraints, the PZT discs were not modelled here. Nevertheless the excitation setup used in the fatigue experiments managed to generate a repeatable incident wave field which was fairly well understood.

A problem encountered during these investigations was the actual manufacturing of the multi-layered structures. This was mainly due to the limitation of the equipment available for bonding plates together. Usually an autoclave and an adhesive film would have been used to bond the plates together. Despite not using an autoclave the adhesive layers in the multi-layered tensile specimens were acceptable. The large multi-layered plate showed a larger variation, thus using an adhesive film would have improved the quality of the adhesive layer.

In the investigations presented here the A_0-like mode was used for the detection of sub-layer fatigue cracks. The choice of this particular mode was based on the

fact that it was easy to excite and measure with the available equipment, but also because of the experience within the research group which utilizes this type of mode for defect detection. In these studies no investigations were made in order to quantify the effect of damping in these structures. It has been shown that the attenuation is frequency dependent in these structures increasing for higher frequencies. The guided waves employed here were used at low frequencies in order to obtain only a small damping. The employed mode is not the only mode which could have been used in the studies presented here. Another possible mode which could be used at low frequencies and which has good sensitivity to defects in single layer plates is the S_0 mode. To detect smaller defects than those detected here, guided ultrasonic waves at higher frequencies should be used. In this case the damping has to be taken into consideration.

To exclude reflections from the boundaries the FE geometry had to be made quite large. In order to reduce the size of the FE models and thus reduce computational time, absorbing boundary conditions could have been used. It must be said that the points mentioned would most unlikely have altered the results and main conclusions in a significant way.

8.7 Future work

8.7.1 Excitation of guided waves in tensile specimen

Since these specimens are used in various kind of fatigue experiments which involve damage detection using guided waves, it would be interesting to obtain an excitation which can isolate the lowest guided wave modes making the interrogation much easier. The excitation using a PZT plate could be used to isolate a single mode, but further studies (FE and experiments) need to be done in order to understand its vibration characteristics. FE simulations of the wave propagation in tensile specimen using PZT plates or multiple discs should model the PZT itself and the bond layer.

Other type of transducers which could be investigated for this purpose are EMATS, laser line sources or wedge transducers which can prescribe the wavelength as for higher frequency guided waves.

8.7.2 Scattering

The scattering of the A_0-like mode (low frequencies) at a fastener hole with and without defects was quite well understood. Other modes such as the S_0-like mode, or higher frequencies could be investigated in the future for the detection of defects in multi-layered structure. Further studies could be deployed to investigate the possibility of detecting sub-layer defects in multi-layered structure when the adhesive is missing at the fastener hole, a common problem in the inspection of aircrafts. These studies could focus on understanding the scattering under these conditions.

8.7.3 Fatigue crack growth monitoring

As mentioned higher frequency guided waves could be used for the detection of smaller fatigue cracks. To study the sensitivity of these waves to sub-layer defects similar fatigue experiments to those presented here could be performed. For this type of experiments it should also be easier to find appropriate excitation which is crucial for obtaining repeatable results. This could be e.g. done by a commercial variable angle wedge transducers, which also allows for selecting appropriate modes.

8.7.4 SHM in aircrafts

From this work it was seen that the methodology which used low frequency guided ultrasonic waves proved to be sensitive to defects through one layer (5.25 mm long $\sim \frac{\lambda}{3}$). In the future it would be interesting to investigate the possibility of high frequency guided ultrasonic waves for detecting and sizing smaller defects in real aircraft structures. Obviously a disadvantage with this could be the attenuation which could make the monitoring of large areas difficult. Nevertheless high frequency waves could be used for inspecting fatigue damage at fastener holes or be part of a

short-range SHM system which monitors structurally important sub-structures of aircrafts.

In the beginning of this thesis it was mentioned that the aircraft industry is currently investigating the possibility of integrating a SHM system in aircrafts. In order for the work here to have a more practical relevance to this industry, fatigue crack monitoring experiments would need to be conducted on more complex multi-layered structures as those found in aircrafts.

Bibliography

[1] P. Fromme, *Defect detection in plates using guided waves*, PhD thesis, Diss. ETH No. 14397 (2001)

[2] H. Speckmann, R. Henrich, *Structural Health Monitoring - Overview on technologies under development*, Proc. of the World Conference in NDT, Volume 9, No 11, (2004)

[3] S. G. Sampath, *Aging combat aircraft fleets-long term applications*, (Neuilly-sur Seine/France: AGARD LS-206), (1996)

[4] R. Radhakrishnan, *Damage Characterization*, Joint FAA/Delta 8th Quarterly Meeting, Destructive evaluation and extended fatigue testing of a retired passenger aircraft, Atlanta, (2004).

[5] C. Boller, *Next generation Structural Health Monitoring and its integration into aircraft design*, Int. J. Sys. Sci., Volume 31, No 11, 1333-49 (2000)

[6] I. N. Komsky, *Modular dry-coupled ultrasonic probes for field inspections of multi-layered aircraft structures*, Proc. SPIE, Volume 5768, 176 (2005)

[7] H. J. Schmidt and B. Schmidt-Brandecker, *Structure design and maintenance benefits from health monitoring systems*, Proc. 3^{rd} Int, Workshop on Structural Health Monitoring, Stanford, USA, 80-101 (2001)

[8] C. Boller, *Ways and options for aircraft structural health management*, Smart. Mater. Struct., Volume 10, 432-40 (2001)

[9] S. G. LaRiviere, J. Thompson, *Development of reliable NDI procedures for airframe inspection*, Proc. 10: Airframe inspection reliability under field/depot conditions, paper 7, (1998)

[10] C. D. Smith, *Federal aviation administration aircraft inspection research and development program*, Proc. of SPIE, Volume 2945, 200-209 (1996)

[11] D. J. Griffiths, *Introduction to electrodynamics*, 3rd edition, Upper Saddle River, New Jersey: Prentice Hall, ISBN 0-13-805326-x

[12] E. Lindgren, J. S. Knopp, J. C. Aldrin, G. J. Steffes and C. F. Buynak, *Aging aircraft NDE: capabilities, challenges and opportunities*, in Review of progress in Quantitative Nondestructive Evaluation, Volume 26, ed. by D.O. Thompson and D.E. Chimenti, AIP Conference Proceedings Volume 894, 1731-1738 (2007)

[13] J. S. Knopp, J. C. Aldrin and P. Misra, *Considerations in the validation and application of models for eddy current inspection of cracks around fastener holes*, J. Nondestr. Eval., Volume 25, No 3, 123-137, (2006)

[14] T. Dogaru, C. H. Smith, R. W. Schneider and S. T. Smith, *Deep crack detection around fastener holes in airplane multi-layered structures using GMR based eddy current probes*, in Review of Progress in Quantitative Nondestructive Evaluation, Volume 23, ed. by D. O. Thompson and D. E. Chimenti, AIP Conference Proceedings Volume 615, 398-405 (2004)

[15] W. F. Avrin, *Eddy-current measurements with magnetoresistive sensors: third-layer flaw detection in a wing-splice structure 25 mm thick*, in NDE of Aging Aircraft and Aerospace Hardware IV, ed. by M. K. Ajit, Proc. of SPIE, Volume 3994, (2000)

[16] J. Krautkramer and S. Krautkramer, *Ultrasonic testing of materials*, Springer-Verlag Berlin and Heidelberg GmbH & Co. KG, ISBN-10: 3540512314

[17] E. Lindgren, D. Judd, M. Concordia, J. Mandeville, J. C. Aldrin, F. Spencer, D. Fritz, E. Pratt, R. Waldbusser and R. T. Mullis, *Validation and deployment of automated ultrasonic inspections for the C-130 center wing*, ASIP Conference, Savannah, Georgia, (2004)

[18] I. N. Komsky and J. D. Achenbach, *Application of a self-calibrating ultrasonic technique to the detection of fatigue cracks by the use of Lamb waves*, in Review of Progress in Quantitative Nondestructive Evaluation, Volume 12B, ed. by D.O. Thompson and D.E. Chimenti, Plenum Press (NY), 2167-2174 (1993)

[19] R. A. Smith, D. Edgards, L. D. Jones and D. M. Percivall, *An ultrasonic solution for second-layer crack detection*, Insight, Volume 47, Issue 2, 81-84 (2005)

[20] J. L. Rose, *Recent advances in guided wave NDE*, IEEE Ultrasonics Symposium Proceedings, Volume 1, 761-770 (1995)

[21] S. I. Rokhlin, M. Hefets and M. Rosen, *An ultrasonic interface-wave method for predicting the strength of adhesive bonds*, J. Appl. Phys., Issue 52, 2847 (1981)

[22] A. Pilarski, *Ultrasonic evaluation of the adhesion degree in layered joints*, Mater. Eval., Volume 43, Issue 6, 765-770 (1985)

[23] P. B. Nagy and L. Adler, *Nondestructive evaluation of adhesive joints by guided-waves*, J. Appl. Phys., Volume 66, Issue 10, 4658-4663 (1989)

[24] M. J. S. Lowe and P. Cawley, *The applicability of plate wave techniques for the inspection of adhesive and diffusion bonded joints*, J. Nondestr. Eval., Volume 13, No 4, 185-200 (1994)

[25] M. J. Quarry, *Guided wave inspection of multi-layered structures*, in Review of progress in Quantitative Nondestructive Evaluation, Volume 23, ed. by D.O. Thompson and D.E. Chimenti, AIP Conference Proceedings Volume 700, 246-253 (2004)

[26] E. Lindgren, J. C. Aldrin, K. Jata, B. Scholes and J. Knopp, *Ultrasonic plate waves for fatigue crack detection in multi-layered metallic structures*, Health Monitoring of Structural and Biological Systems 2007, ed. by T. Kundu, Proc. of SPIE, Volume 6532, (2007)

[27] R. P. Dalton, P. Cawley and M. J. S. Lowe, *The potential of guided waves for monitoring large areas of metallic aircraft fuselage structure*, J. Nondestr. Eval., Volume 20, Issue 1, 29-46 (2001)

[28] D. N. Alleyne and P. Cawley, *Optimazation of Lamb wave inspection techniques*, NDT & E Int., Volume 25, Issue 1, 11-22 (1992)

[29] ABAQUS V. 6.7.1, Simulia, Dassault Systemes

[30] J. H. Goodbread, *Mechanical properties of spongy bone at low ultrasonic frequencies*, PhD Thesis, Diss. ETH No. 5856, (1976)

[31] W. A. Grandia and C. M. Fortunko, *NDE applications of air-coupled ultrasonic transducers*, 1995 IEEE Ultrasonic Symposium, Proceedings, Volume 1, 697-709, ISSN 1051-0117

[32] http://www.mtpinc-exporter.com/chemicals/tds/Hysol%20EA%209394.2.pdf Specifications for Hysol 9394-EA epoxy paste adhesive

[33] M. V. Predoi, M. Castaings, B. Hosten and C. Bacon, *Wave propagation along transversely periodic structures*, J. Acoust. Soc. Am, Volume 121, Issue 4, 1935-1944 (2007)

[34] R. D. Cook, *Finite Element Modeling for stress analysis*, J. Wiley & Sons, New York, 1995, ISBN 0-471-10774-3

[35] D. N. Alleyne, M. J. S. Lowe and P. Cawley, *The reflection of guided waves from circumferential notches in pipes*, J. Appl. Mech., Volume 65, Issue 3, 635-641 (1998)

[36] O. Diligent and M. J. S. Lowe, *Reflection of the S_0 Lamb mode from a flat bottom circular hole*, J. Acoust. Soc. Am., Volume 118, No. 5, 2869-2879 (2005)

[37] R. W. Morse, *Dispersion of compressional waves in isotropic rods of rectangular cross section*, J. Acoust. Soc. Am., Volume 20, Issue 6, 833-838 (1960)

[38] R. D. Mindlin and E. A. Fox, *Vibrations and waves in elastic bars of rectangular cross section*, J. Appl. Mech., Issue 27, 152-158 (1960)

[39] N. J. Nigro, *Steady-state wave propagation in infinite bars of non circular cross section*, J. Acoust. Soc. Am., Issue 40, 1501-1508 (1966)

[40] B. Aalami, *Waves in prismatic guides of arbitrary cross section*, J. Appl. Mech., Issue 40, 1067-1072 (1973)

[41] Y. K. Cheung, *The finite strip element method in structural analysis*, Pergamon Press (1976), ISBN 0080183085

[42] H. Taweel, S. B. Dong and M. Kazic, *Wave reflection from the free end of a cylinder with an arbitrary cross-section*, Int. J. Solids Struct., Volume 37, Issue 12, 1701-1726 (2000)

[43] T. Hayashi and J. L. Rose, *Guided wave simulation and visualization by a Semi-Analytical Finite-Element Method*, Mater. Eval., Volume 61, Issue 1, 75-79 (2003)

[44] O. M. Mukdadi, Y. M. Desai, S. K. Datta, A. H. Shah and A. J. Niklasson, *Elastic guided-waves in a layered plate with rectangular cross section*, J. Acoust. Soc. Am., Volume 112, Issue 6, 1766-1779 (2002)

[45] L. Pochhammer, *On the propagation velocities of small oscillations in an unlimited isotropic circular cylinder*, Journal für die reine und angewandte Mathematik, Volume 81, (1876)

[46] Lord Rayleigh, *On the Free Vibrations of an Infinite Plate of Homogeneous Elastic Matter*, Proc. of the London Mathematical Society, Volume 20, 225-234 (1889)

[47] H. Lamb, *On waves in an elastic plate*, Proc. of the Royal Society of London, Series A, Containing Papers of a Mathematical and Physical Character, Volume 93, 114-128 (1917)

[48] W. T. Thomson, *Transmission of elastic waves through a stratified solid medium*, J. Appl. Phys., Volume 21, 89-93 (1950)

[49] L. Knopoff, *A matrix method for elastic wave problems*, Bull. Seism. Soc. Am., Volume 54, 431-438 (1964)

[50] M. J. S. Lowe, *Matrix techniques for modeling ultrasonic waves in multi-layered media*, IEEE T. Ultrason. Ferr., Volume 42, 525-542 (1995)

[51] J. L. Rose, *Ultrasonic waves in solid media*, Cambrdige University press, ISBN 0 521 64043 1

[52] B. N. Pavlakovic, M. J. S. Lowe, D. N. Alleyne and P. Cawley, *Disperse: A general purpose program for creating dispersion curves*, in Review of Progress in Quantitative Non Destructive Evaluation, Volume 16, ed. by D.O. Thompson and D.E. Chimenti, Plenum Press (NY), 185-192 (1997)

[53] R. D. Mindlin, *Influence of rotary inertia and shear on flexural motions of isotropic, elastic plates*, J. Appl. Mech., Volume 18, Issue 31, 31-38 (1951)

[54] R. Seifried, L. J. Jacobs and J. M. Qu, *Propagation of guided waves in adhesive bonded components*, NDT & E Int., Volume 35, 317-328 (2002)

[55] K. L. J. Fong, *A study of curvature effects on guided elastic waves*, PhD thesis, Imperial College London, (2005)

[56] P. Wilcox, M. J. S. Lowe and P. Cawley, *Lamb and SH wave transducer arrays for the inspection of large areas of thick plates*, in Review of Progress in Quantitative Nondestructive Evaluation, Volume 19, ed. by D. O. Thompson and D. E. Chimenti, AIP Conference Proceedings, Volume 509, 1049-1056 (2000)

[57] B. A. Auld, *Acoustic fields and waves in solids*, Vol II, ISBN: 0-89874-783-X

[58] D. N. Alleyne and P. Cawley, *Optimization of lamb wave inspection techniques*, NDT & E Int., Volume 25, Issue 1, 11-22 (1992)

[59] P. Belanger, *Feasibility of thickness mapping using ultrasonic guided waves*, PhD thesis, Imperial College London, (2009)

[60] Y. -H. Pao and C. C. Chao, *Diffraction of flexural waves by a cavity in an elastic plate*, J. AIAA, Volume 2, Issue 11, 2004-2010 (1964)

[61] A. N. Norris and C. Vemula, *Scattering of flexural waves on thin plates*, J. Sound Vib., Volume 181, Issue 1, 115-125 (1995)

[62] P. Fromme and M. B. Sayir, *Measurement of the scattering of a Lamb wave by a through hole in a plate*, J. Acoust. Soc. Am., Volume 111, Issue 3, 1165-1170 (2002)

[63] O. Diligent, T. Grahn, A. Boström and P. Cawley, *The low-frequency reflection and scattering of the S_0 Lamb mode from a circular through-thickness hole in a plate: Finite Element, analytical and experimental studies*, J. Acoust. Soc. Am., Volume 112, Issue 6, 2589-2601 (2002)

[64] D. N. Alleyne and P. Cawley, *The interaction of Lamb waves with defects*, IEEE Trans. Ultrasonics, Ferroelectrics, and Frequency Control, Volume 39, 381-397 (1992)

[65] M. J. S. Lowe and O. Diligent, *Low-frequency reflection characteristics of the S_0 Lamb wave from a rectangular notch in a plate*, J. Acoust. Soc. Am., Volume 111, Issue 1, 64-74 (2002)

[66] P. Fromme and M. B. Sayir, *Detection of cracks at rivet holes using guided waves*, Ultrasonics, Volume 40, Issues 1-8, 199-203 (2002)

[67] Z. Chang and A. Mal, *Scattering of Lamb waves from a rivet hole with edge cracks*, Mech. Mater., Volume 31, Issue 3, 197-204, (1999)

[68] P. Fromme and M. B. Sayir, *Monitoring fatigue crack growth at fastener holes using guided ultrasonic waves*, in Review of Progress in Quantitative Nondestructive Evaluation, Volume 21, ed. by D. O. Thompson and D. E. Chimenti, AIP Conference Proceedings, Volume 615, 247-252 (2002)

[69] P. Fromme, B. Masserey and M. B. Sayir, *On the detectability of fatigue crack growth at fastener holes using guided waves*, in Review of Progress in Quantitative Nondestructive Evaluation, Volume 22, ed. by D. O. Thompson and D. E. Chimenti, Volume 615, 187-195 (2003)

[70] B. Masserey and P. Fromme, *In-situ monitoring of fatigue crack growth at fastener holes using Rayleigh-like waves*, in Review of Progress in Quantitative Nondestructive Evaluation, Volume 27, ed. by D. O. Thompson and D. E. Chimenti, AIP Conference Proceedings, Volume 975, 1484-1491 (2008)

[71] J. E. Michaels, T. E. Michaels, B. Mi, A. C. Cobb and D. M. Stobbe, *Self-calibrating ultrasonic methods for in-situ monitoring of fatigue crack progression*, in Review of Progress in Quantitative Nondestructive Evaluation, Volume 24, ed. by D. O. Thompson and D. E. Chimenti, AIP Conference Proceedings, Volume 760, 1765-1772 (2005)

[72] J. E. Michaels, T. E. Michaels and B. Mi, *An ultrasonic angle beam method for in situ sizing of fastener hole cracks*, J. Nondestr. Eval., Volume 25, 3-16 (2006)

[73] B. Mi, J. E. Michaels and T. E. Michaels, *An ultrasonic method for dynamic monitoring of fatigue crack initiation and growth*, J. Acoust. Soc. Am., Volume 119, Issue 1, 74-85 (2006)